T.C.
ONDOKUZ MAYIS ÜNİVERSİTESİ
FEN BİLİMLERİ ENSTİTÜSÜ

MASTER THESIS

RADIO FREQUENCY ENERGY HARVESTING METHOD TO SPPLY WIRELESS SENSORS

ASMA DIDI

DEPARTMENT OF ELECTRICAL AND ELECTRONIC ENGINEERING

SAMSUN
2018

ETHICAL DECLARATION

I declare that all the information in this thesis prepared in accordance with the thesis writing rules of Ondokuz Mayis University Institute of Science is accurate and complete, i acted according to the information at the stage of production of scientific ethics, refering to all sources that I have used as a reference.

12/06/2018

Asma Didi

ÖZET

Yüksek Lisans

KABLOSUZ ALGILACILAR İÇİN RF ENERJI HASAT YÖNTEMİ

Asma Didi

Ondokuz Mayıs Üniversitesi Fen
Bilimleri Enstitüsü Elektrik
Elektronik Mühendisliği
Anabilim Dalı

Danışman: Prof. Dr. Okan ÖZGÖNENEL

Akıllı kontrol sistemleri güç tüketimindeki son gelişmelerden olan Kablosuz Algılayıcı Ağları ve Nesnelerin İnternetinden yararlanmaktadırlar. Aküler, bu sistemlerin otonom hale getirilerek geliştirilmesini sağlamaktadırlar. Bununla birlikte bu besleme yöntemi modern uygulamalar için uygun olmamaktadır. Bu sensörleri beslemek için çevrelerinde mevcut olan termal enerjiyi, mekanik titreşimleri, ışık dalgalarını veya radyo frekanslarını kullanmak alternatif bir çözüm olmaktadır.
Bu tez, özellikle Radyo Frekanslarının dalgalarını kullanarak, enerjide otonom bir sensör ağı oluşturmayı amaçlayan yenilikçi çözümlerin geliştirilmesine katkıda bulunmayı önermektedir. Sensörler, gelen güç yoğunluklarının hâkim olmadığı ve genellikle düşük olduğu bir ortama yerleştirilmektedirler.

İlk olarak, mekanik, termal, kimyasal, ışık dalgası enerjisi ve Radyo Frekansı gibi farklı enerji toplama teknikleri ve kaynakları incelenmiştir. Bu çalışma, Radyo Frekansı dalgalarının enerji hasat sistemlerini diğer çalışmalarda yapılan sistemlere göre konumlandırmayı mümkün kılmıştır.
Geniş bir frekans bandında enerji toplamanın yararını gösterdikten sonra, kentsel ortamda ve kırsal alanda mevcut olan RF güç yoğunluğunun değerlendirilmesi üzerinde istatistiksel bir çalışma yapılmıştır. Sensörün ortamı, seçilen mimarinin enerji depolama hücresinin eklenmesi veya bir dc-dc dönüştürücünün kullanılması gibi seçimlerini içerir.
Çeşitli çok bantlı RF hasat sistemleri, çeşitli frekans bandında enerji hasat edebilecek kapasitede tasarlanmıştır. Ayrıca bu koşullar altında, birden fazla RF kaynağı mevcut olduğunda, sistem geniş bir frekans bandı üzerinden çalışacak şekilde tasarlandığında hasat edilen enerji miktarı arttırılabilir.

Haziran 2018, 110 sayfa

Anahtar Kelimeler: Enerji hasatı; Rectenna; Radyo frekansı; Sensör ağı; Empedans eşleştirme ağı.

ABSTRACT

Master's Thesis

RADIO FREQUENCY ENERGY HARVESTING METHOD TO SUPPLY WIRELESS SENSORS

Asma Didi

Ondokuz Mayıs University
Graduate School of Sciences
Department of Electric and
Electronic Engineering

Supervisor: Prof. Dr. Okan ÖZGÖNENEL

Wireless Sensor Networks (WSN) and the Internet of Things (IOT) are benefiting from recent advances in power consumption for intelligent control entities. Batteries have enabled the development of these systems by making autonomous. Nevertheless, this supplying method is unsuitable for modern applications. An alternative solution to supply these sensors is to use the energy available in their environment, such as thermal guards, mechanical vibrations, light waves or Radio Frequencies.
This thesis proposes to contribute to the development of innovative solutions aiming to make a network of sensors autonomous in energy by exploiting in particular the waves of Radio Frequencies [RF]. The sensors are placed in an environment for which the power densities incident are not mastered and are generally low.
Firstly, different sources and techniques of energy harvesting were studied such as mechanical, thermal, chemical, light wave energy and Radio Frequency. This study has made it possible to position the energy harvesting systems of Radio Frequency waves compared to other systems.
After demonstrating the interest of collecting energy over a wide frequency band, a statistical study was carried out on the evaluation of the RF power density present in the urban environment and in the countryside. The environment of the sensor involves choices of the chosen architecture, such as for example the addition of energy storage cell or the use of a dc-dc converter.
Several mutli-band RF harvester systems have been designed capable of harvesting energy in several frequency bands. Also, under these conditions, when multiple RF sources are available, the amount of energy harvested can be increased when the system is designed to operate over a wide frequency band.

June 2018, 110 pages

Key Words: Energy harvesting; Rectenna; Radio frequency; Sensor network; Impedance matching network.

ACKNOWLEDGEMENT

Firstly, I would like to express my sincere gratitude to my advisor Prof. Dr. Okan ÖZGÖNENEL for the continuous support of my Master study and related research, for his patience, motivation, and immense knowledge. His guidance helped me in all the time of research and writing of this thesis. I could not have imagined having a better advisor and mentor for my Master study.

Last but not the least, I would like to thank my family: my parents and to my brothers and sisters for supporting me spiritually throughout writing this thesis and my life in general. I humbly extend my thanks to my close friends who have helped me get through this years. All because of them, I have amazing and embarrassing memories that I will take with me.

June 2018 , Samsun

Asma Didi

LIST OF CONTENTS

Page

ABBREVIATIONS

AC	: Alternative Current
ADS	: Advanced Design System
DC	: Direct Current
FM	: Frequency Modulation
GSM	: Global System for Mobile Communications
HB	: Harmonic Balance
HFSS	: High Frequency Structural Simulator
RF	: Radio Frequency
UMTS	: Universal Mobile Telecommunications System

LIST OF FIGURES

Page

LIST OF TABLES

Page

1. INTRODUCTION

Nowadays, the need to be able to control the environment in which we find ourselves is more and more important and this allows us to anticipate our actions. A very used example is the weather forecast. A sensor is a small, self-contained device that can perform simple measurements on its immediate environment. It allows to observe and control many physical phenomena such as temperature, pressure, brightness, etc., which is essential for many industrial and scientific applications. The role of a sensor is to transform a physical quantity into an exploitable electrical quantity; for example a digital signal usable by a computer. The interface can be made by a wired link or, as has been the case for a few years, by radio waves which has given rise to wireless sensors.

On the other hand, the progress made in recent decades in the fields of microelectronics and micromechanics has made it possible to produce, with a reasonable cost, components of a few cubic millimeters of volume and therefore of little space, Micro sensors, they are real embedded systems. The deployment of several of them for the purpose of collecting and transmitting environmental data to one or more collection points in an autonomous manner forms a wireless sensor network (WSN).

A traditional way to power these sensors is to use a battery or battery that stores a fixed amount of energy. These storage devices have a limited life which then requires their replacement when empty. This maintenance related to the change of the battery can be expensive in the case of sensors located in locations difficult to access.

It appears obvious that for a large number of distributed sensors would require that they be provided with a power supply with a term the longest possible life for limited maintenance which, moreover, is impossible under certain conditions. This question of energy autonomy has been accompanied in recent years by the appearance of a new field of activity, namely the recovery of the ambient energy present in the immediate environment of the system to be supplied. This work is then part of the context of the recovery of ambient energy, a field of re1search better known under its name energy harvesting.

This thesis proposes to contribute to the development of innovative solutions aiming to make sensors autonomous in energy by exploiting in particular the electromagnetic energy of radio-frequency waves. Previous work on RF energy harvesting system has focused mainly on the issue of harvesting energy at a single operating frequency. But in an urban environment, the frequencies and the level of RF power density are not controlled. It is therefore wise to develop systems capable of harvesting energy in several frequency bands. Also, under these conditions, when multiple RF sources are available, the amount of energy harvested can be increased if the system is designed to operate over a wide frequency band. This further consolidates our interest in Radio-Frequency power sources.

2. LITERATURE REVIEW

2.1. Energy harvesting: basics

2.1.1. Architecture of an energy harvesting unit

An energy harvesting system for powering a sensor is composed of five distinct blocks as shown in Figure 2.1.

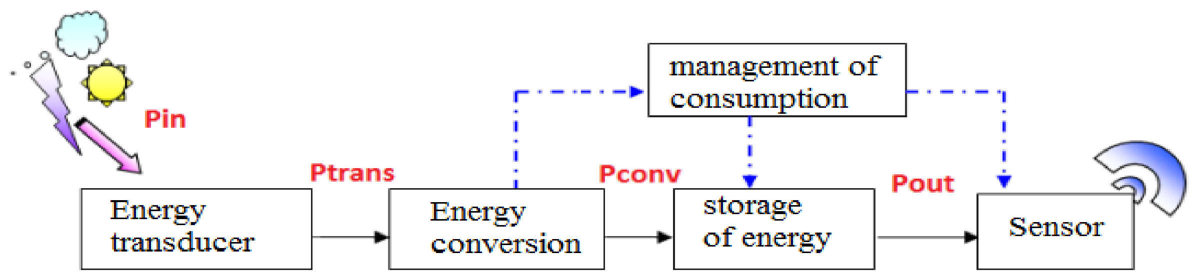

Figure 2.1 Block Diagram of energy harvesting unit for power supply an autonomous sensor

The first part of the complete system is the energy transducer. This provides as an output signal, a physical quantity which can be used in response to another specific physical quantity as an input signal. The principles of this transduction are based on the existence of various physical or chemical effects. There are six main classes of signals: thermal, mechanical, optical, magnetic, electrical or chemical (Harb, 2011).

Then, the second part allows the conversion of the energy. The energy received at the output of the transducer is converted into continuous electrical power. This part may consist of rectifiers, converters or charge pumps. The choice depends among other things on the input transducer. Indeed, the transducers can be listed in two groups. The energy transducers of the mechanical vibrations or those of the electromagnetic waves generate an alternating voltage. In this case, the energy converter will be a voltage rectifier. As for the photovoltaic or thermal energy transducers, dc-dc converters will ensure the conversion since the output voltage of the transducers is a DC voltage. The major challenge of this part is to ensure the highest possible conversion efficiency between the transducer and the sensor to be powered (Han vd, 2006).

The third part is a cell for storing converted energy. This can be electric capacitors, supercapacitors or rechargeable batteries. This cell is used to accumulate received energy and to supply it to the sensor according to the energy requirement (Wang vd, 2013).

Finally, the fourth part of this system is that of consumption management. It is composed of microprocessors and converters incorporating algorithms which allow the energy received either to the storage cell or to the sensor to be transmitted as required (Raghunathan and Chou, 2006). In the scientific literature, when referring to the management of consumption, very often the term "Power Management" is used. This term is also used when it is necessary to adapt the impedance of a generator to maximize its power generally called MPPT (Maximum Power Point Tracking), or simply to insert a step-up converter between the generator and the element storage only to raise the voltage of the latter. The search for the maximum harvestable power of an energy source is a subject very widespread in the scientific literature. For example, Aman Kansal (Kansal vd,2007) and Vijay Raghunathan (Raghunathan and Chou, 2006) of the University of California have been working on the supply of communicating sensors networks and especially taking into account that the harvested energy evolves over time and is not the same for each node of the network. Their real-time consumption management algorithm determines, at each time step, the operating cycle of the load, as a function of available energy (known thanks to an energy prediction algorithm). Thus, the study of consumption management for self-powered sensors results in the development of algorithms to better manage the load by adapting its consumption to available resources.

2.1.2. Efficiency of the energy harvesting unit

It is important to correctly determine the efficiency of an energy harvesting unit to avoid confusion when reading the manuscript. In some articles of the bibliography, the energy harvesting efficiency is actually the efficiency of energy conversion and not the overall efficiency. To do this, we will strive to make the difference between them.

The definition of the efficiency of conversion of an energy harvesting unit,η_{conv}, is the ratio of the output power dc at the output of the conversion circuit P_{conv} to the input power present at the output of the energy transducer P_{trans} :

$$\eta_{conv} = \frac{P_{conv}}{P_{trans}} \tag{2.1}$$

With η expressed in %, P_{conv} and P_{trans} in Watt.

And the overall efficiency of energy harvesting unit, which will be called η_{all} , counts the efficiency of the transducer (with P_{in} the incident power at the transducer) and that of the storage cell (see Figure 2.1). Thus, η_{all} is defined by:

$$\eta_{all} = \frac{P_{trans}}{P_{in}} \frac{P_{conv}}{P_{trans}} \frac{P_{out}}{P_{conv}} \tag{2.2}$$

With η expressed in %, P_{conv} and P_{trans} in Watt.

With η expressed in%, P_{conv} , P_{trans} , P_{out} and P_{in} in Watt. We note that these two efficiencies will be expressed in%.

2.2. Autonomous sensor: energy requirement

The technological advances made in the field of wireless networks, micro-fabrication of microprocessors have allowed the development of a new generation of sensor networks adapted to a wide range of applications. These sensors are small, wireless, autonomous electronic devices capable of communicating either to each other or to a master entity. They form a network of wireless sensors capable of giving and transmitting useful information about a region or an area of interest. Thanks to their computing capabilities, these wireless communicating sensors make it possible to envisage many applications that were not yet feasible a few years ago. Today, these small and inexpensive sensors can be, for example, placed along roadsides or in buildings that can thus detect a variety of physical phenomena. Many fields of application are envisaged such as environmental control, building, agriculture, industrial machinery or urban traffic surveillance, health, or sport. These sensors include the physical layer of the internet of things, a domain in full expansion. "The Internet of things is a network of networks that allows, through standardized, unified electronic identification systems and mobile wireless devices, to directly and unambiguously identify digital entities and physical objects and thus to be able to retrieve, store, transfer and process, without discontinuity between the physical and virtual worlds, the related data"(Benghozi and Bureau,2012). Deployed on a large scale, wireless sensor networks are often placed in resource-constrained environments such as limiting processing, storage, and above all energy.

The maintenance of the sensor nodes is a significant cost in terms of maintenance and replacement of the batteries used. Energy limitation is an essential issue in the design of wireless sensor networks because it directly affects the lifetime of a network.

2.2.1. Consumption by blocks

Figure 2.2 shows the basic architecture of an autonomous energy sensor which can be divided into two parts. The first deals with energy management and the other measures, processes and sends data. The first part is thus composed of a generator which allows the conversion of the energy collected by a transducer into electrical power, which is then shaped by a converter (ac-dc or dc-dc) and transmitted to a cell of energy storage. The measurement and communication part consists of measuring with various sensors, processing the information (filtering, compression, conversions) and transmitting them with the transmitter - receiver.

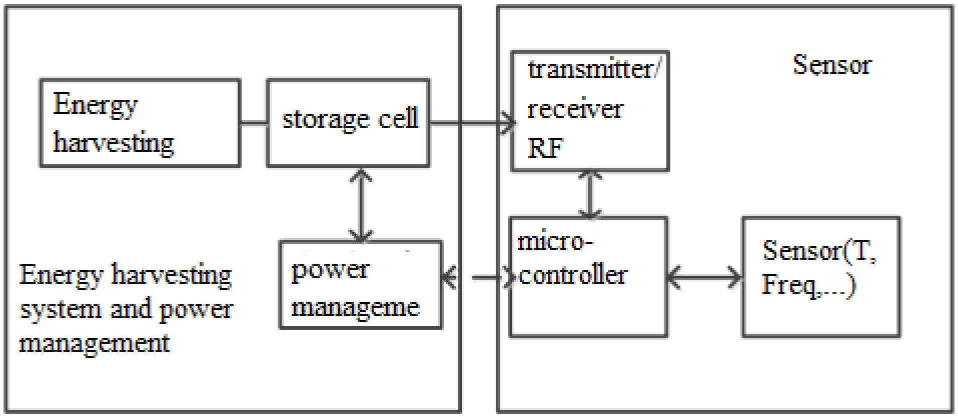

Figure 2.2 Diagram of a self-powered sensor.

Compound of the transmitter-receiver., the radio communication part is responsible for communication between the sensor and the external world. The consumption of this block depends on the distance on which the sensor will communicate and the distance depends on the architecture of the network in which the sensor is located. There are three main communication architectures: Infrastructure mode with one or more base stations, ad hoc mode without base station and mixed mode with one or more base stations. One of the very active lines of research today is trying to minimize the energy consumption of these protocols. An example of architecture to save energy is the CSEM (Swiss Electronics and Microelectronics) Wise NET project. The module consumes an average of 25µW by communicating a packet of 56 bytes every 100 seconds, which is 100 times less than a standard S-MAC or T-MAC protocol (El-Hoiydi etc, 2004).

2.2.2. Consumption of the complete sensor

It is possible to estimate the energy required for the operation of a sensor, being made up of the blocks described above, by analyzing the various electronic components that constitute it. In Table 2.1 we have selected several components that can be used in a wireless sensor.

The sequencing for the functioning of the sensor is as follows:

microcontroller (power consumption (in Ws), C_{micro}= 2.7 µW x 1.5 s), measurement sensor wake-up (C_{SenMes}= 0.675 mW x 30 µs), data processing (C_{data}= 0.677mW x 2 ms) standby of the sensor ($C_{stanby1}$= 100 µW x 30 µs) and then wake up of the transceiver part (C_{radio}= 100 µW x 1.6 ms) and send the data ($C_{delivery}$= 100 µW x 350 µs) and then finally switch off the microcontroller and the transmitter-receiver part ($C_{standby2}$= 2.7 µW x 1 ms).

Table 2.1 Consumption of several components constituting a sensor

Components	Consumption in active mode	Standbyb power consumption	Operating Time	References
Radio communication nRF24L01	$52\mu\ A$ @1.9V	900nA@1.9V	350 μs	(Nodilo,2000)
Microcontroller EM6607	$1.8\mu\ A$ @1.5V	100nA@1.5V	1.5 s	(Em,2007)
Humidity sensor AD7814	$250\mu\ A$ @2.7V	0.43μA@2.7V	30 μs	(TMP35,2007)

Thereafter, the energy consumed during a period of activity is defined as this equation:

$$E_{conso}= C_{micro} + C_{senMes} + C_{data} + C_{standby1} + C_{radio} + C_{delievery} + C_{standby2} = \mathbf{6}\mu J \quad \textbf{(2.3)}$$

With η expressed in %, P_{conv} and P_{trans} in Watt.

If the various action times described above are added, the total duration of operation of the sensor is 2 s. It is therefore possible to calculate the average power consumed by the sensor:

$$P_{averge}=\frac{6\mu J}{2s}= 3\mu W \quad \textbf{(2.4)}$$

$$\eta_{conv} = \frac{P_{conv}}{P_{trans}} \quad \textbf{(2.5)}$$

With η expressed in %, P_{conv} and P_{trans} in Watt.

Thus, depending on the components chosen, the sensor designed can reach energy consumption of the order of microwatt as presented in the example above.

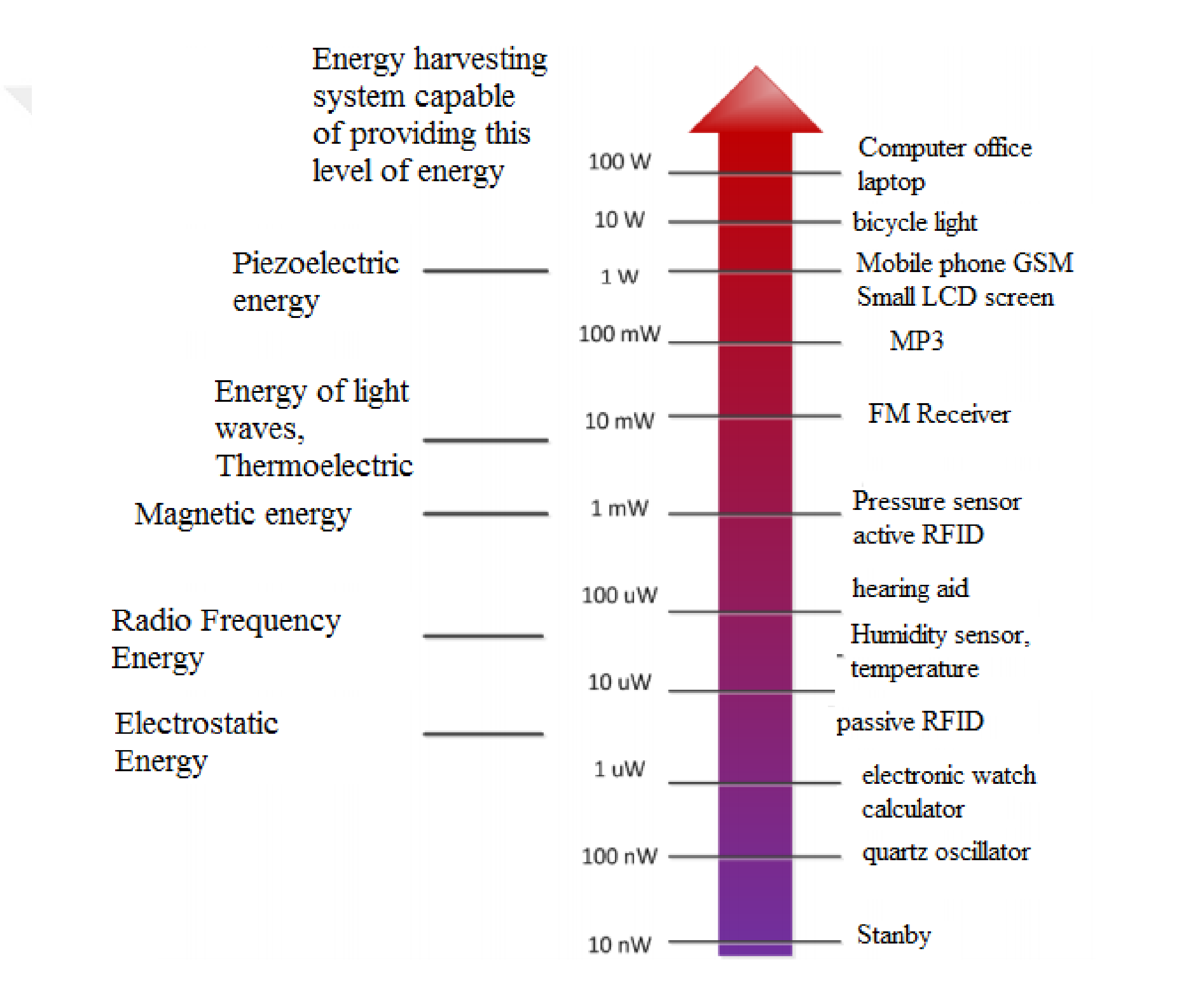

Figure 2.3. Power Requirements Scale for Electronic Devices and Energy Harvesting Associated with Power Levels (Belleville,2009).

In order to give a few orders of magnitude, Figure 2.3 gives an estimate of the powers required for the operation of several sensors and electronic devices. The different types of energy recovery are also listed and listed in this figure depending on their ability to provide these energy levels. The range of sensors for which we will concentrate in this paper is that of volume systems of the order of cm^3 and consumption of the order of the milliwatt maximum.

Thus, due to the congestion of the systems, several energies will not be considered here as for example wind, geothermal or hydroelectricity.

2.3. The Different Sources and Techniques of Energy Harvesting System

As explained above, only energy sources with harvesting systems of the order of cm^3 are considered. The sources studied in this chapter are grouped into several categories: the energy of mechanical vibrations (piezoelectric, magnetic and electrostatic), thermal, chemical and the energy of radiation (light waves and Radio Frequencies).

2.3.1. Energy of mechanical vibrations

Mechanical vibrations are widely present in our environment. These can come from human body movements, natural or voluntary, but also vibrations due to existing machines (washing machine, motor ...). This section presents the existing mechanical sources and techniques for transforming mechanical energy from the surrounding environment into electrical energy.

2.3.1.1. Transducers for the energy of mechanical vibrations

2.3.1.1.1. Structure of transducers

There are three transducers to harvest energy from mechanical vibrations: magnetic, piezoelectric and electrostatic. They are all based on the same principle. A simplified model of this transducer has been demonstrated by William and Yates (Roundy etc, 2003) and is shown in Figure 2.4.

The maximum energy available in this transducer is calculated from the following differential equation:

$$m\ddot{z}(t) + d\dot{z}(t) + kz(t) = -A(t) \tag{2.6}$$

This equation connects the displacement z (t) of the seismic mass m with respect to the case to the excitation vibrations characterized by the acceleration: A (t) = ÿ (t) (with k the stiffness of the spring and d damping viscous).

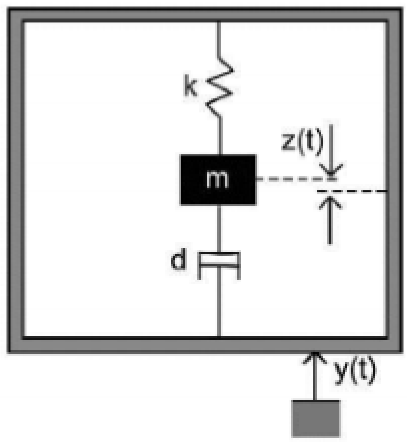

Figure 2.4 Models of William and Yates (Roundy etc, 2003)

2.3.1.1.2. Magnetic transducer

A magnetic transducer consists of one or more magnets creating a field magnetic field, and a coil immersed in this field. A recessed beam (Figure 2.5) with a spring allows generating a relative displacement z (t) between the magnet and the coil when the system is excited by a vibration y (t).

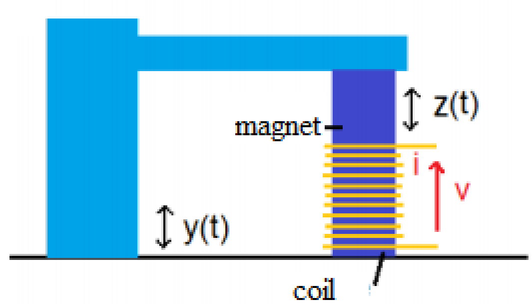

Figure 2.5 Example of Magnetic Transducer Structure (Williams and Yates, 1995)

The change over time of the magnetic flux through the surface surrounded by the coil creates a voltage V proportional to the speed of change of the magnetic flux Φ and the number of revolutions N of the coil, according to the Faraday law, expressed Equation (2.7).

$$V = -N\frac{d\phi}{dt} \quad \textbf{(2.7)}$$

The efficiency of this type of transducer can reach 30%. They are however difficult to miniaturize, firstly because the density of energy decreases with the size of the system, and secondly because it is difficult to have a stable system with strong magnetic fields.

In spite of everything, different structures have been manufactured using microelectronics (Beeby etc, 1995) (Figure 2.6). These structures have been etched on a silicon wafer and therefore contain either micro-manufactured copper coils or magnets. The volume of this structure is $0.1cm^3$. Figure 2.7 shows an example of a structure with copper coils. This allows generating 586 nW at 60 Hz for an ambient vibration acceleration of $8.829m.s^{-2}$. The voltage generated is very low, however, of the order of 10 mV on a load of 170 Ω.

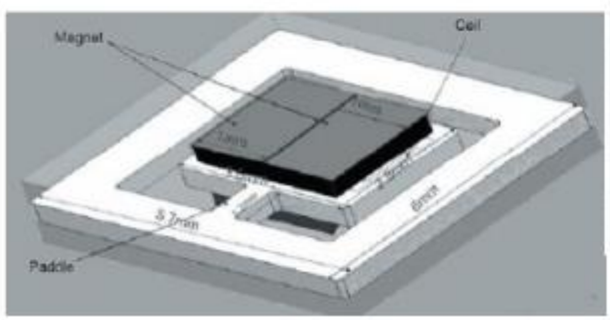

Figure 2.6 Diagram of the micro-generator (Beeby etc, 1995)

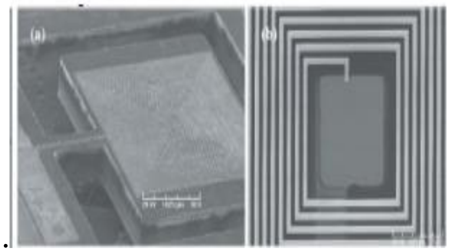

Figure 2.7 Two coil architectures (Beeby etc, 1995)

Systems operating at low frequencies are quite voluminous, which correlates well with the definition of the resonance pulsation of the system (which depends on the mass used according to equation (2.7)). Moreover, the generated voltages are low, which can cause problems for the rectification of this voltage. It should be noted that the output voltage of a magnetic transducer is alternative, which induces the use of an ac-dc converter. We can note that the frequencies involved are less than 100Hz. The coils then tend to be more resistant than inductive, resulting in losses by Joule effect.

Another problem raised by the integration of this system on the same chip an electronic circuit is the presence of strong magnetic fields, which can disrupt the operation of the neighboring electronics and create malfunctions.

Thus, systems for harvesting magnetic energy make it possible to generate high current levels to the detriment of low voltages. These systems are also well adapted for vibrations of low frequencies and high amplitude, such as those related to the movements of the human body. The integration is nevertheless more difficult, due to the low performances of the magnets and the planar coils of Nano metric size.

2.3.1.1.3. Piezoelectric transducer

Piezoelectric transducers use non-conductive materials whose property is to electrically bias under the action of a mechanical stress, and conversely to deform mechanically under the application of an electric field. In the case of energy recovery, the direct piezoelectric effect is generally exploited. The mechanical structure is in most cases an embedded beam, on which one or more PZT ceramics are bonded (Figure 2.8). The vibrations of the beam induce a deformation of the piezoelectric material, thus creating its polarization.

Unlike magnetic systems, piezoelectric systems produce high voltages for lower currents and are adapted to higher vibration frequencies. However, because of their structure in beams, these systems are generally not very compatible with the recovery of ambient energy when they are to be integrated. Indeed, reducing the size of the system leads to an increase in the resonant frequency which is difficult to make fall.

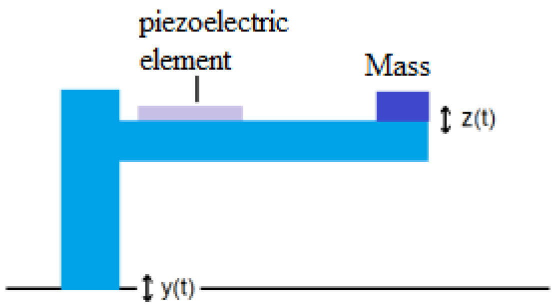

Figure 2.8 Example of piezoelectric transducer structure (Roundy, 2003).

Many systems using this energy harvesting technique exist as prototypes. In 2003, a generator with a volume of 1 cm3, illustrated in Figure (2.9), harvests 375 μW for an acceleration vibration of 2.5ms^{-2} at 120 Hz (Roundy, 2003). It is shown that this generator can power a 1.5 GHz radio transmitter.

The energy of the human body can also be a useful source for piezoelectric energy harvesting. For example, piezoelectric shoes developed at the University of Cambridge, which generate an average power of 2 mW when the bead strikes the ground at a frequency of about 1 Hz (Brown etc, 1969). It is also possible to find in the literature a flexible generator based on a piezoelectric polymer recovering 0.21 mW mounted on a folding and folding finger at a frequency of 3 Hz (Sark etc, 2007), or even piezoelectric nanowires developed at the University of Georgia (Sark etc, 2007) (Yang etc, 2009), which are integrated on textile fibers could eventually generate a power density of 20 to 80 mW per m3 (Figure 2.10).

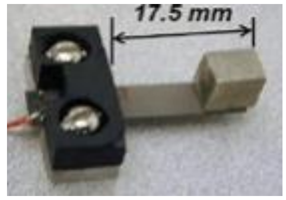

Figure 2.9 Beam device (Roundy ,2003).

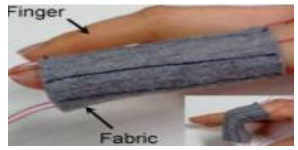

Figure 2.10 Finger surrounded by a piezoelectric polymer (Yang etc ,2009).

The characteristics of several piezoelectric generators in the literature are summarized in Table 2.2. From this table, it can be seen that for low-frequency operation, the energy harvester must have a large volume.

Table 2.2 Vibration energy harvesting: piezoelectric systems

References	Power (uW)	Surface (mm^2)	Volume (mm^3)	Voltage (V)	Acceleration (m/s^2)	Frequency (Hz)	Mass (g)
(Roundy ,2003)	375	100	1000	11	2.5	120	
(Marzenki ,2007)	0.0263	5	5	2	4	196	
(Elfrink etc ,2009)	67.9		27		10	419	
(Kwon etc ,2010)	17		28.7		6.4	353	
(Kanno etc ,2010)	5.3	100		2.5	5	126	

(Defosseux etc ,2011)	4000	156	1560		10	277	6.87
(Wright etc ,2002)	0.62		3	2.2	9.8	214	0.17

A piezoelectric energy harvesting system can be used, if there is suitability between its frequency of resonance and the frequency of the peak of the vibrations from which it is desired to harvest the energy. Indeed, the piezoelectric generators only function correctly very close to their resonant frequency. Thus, since the spectrum of vibrations is mostly a spectrum of lines, it is necessary to calibrate the resonant frequency of the energy harvesting system on a vibration line. Micro-fabrication is a non-negligible parameter that comes into play in the complexity of this system. Indeed, this makes it very difficult to obtain a precise resonant frequency which can change during operation. There is still no ideal system for solving this problem of frequency adaptation. The miniaturization and the correct functioning of these systems in real load range remains to be proved.

2.3.1.1.4. Electrostatic transducer

Electrostatic transducers produce electrical energy by varying the capacitance of a capacitor. The principle is as follows: one of the two plates separated by a dielectric is mobile, and by moving the capacity of the device is varied. If this capacitor is powered by a generator, then the variation of this capacitor makes it possible to multiply the energy of the power source, and therefore to produce it. This device implies that a first source of energy is available. The energy produced can be expressed as follows:

$$E= \frac{1}{2} V_{in}^{2}(C_{max} - C_{min}) \frac{C_{max}}{C_{min}} \quad \textbf{(2.8)}$$

E represents the energy produced, V_{in} the supply voltage, C_{max} and C_{min} the maximum and minimum capacities

There are three different electrostatic transducers (Figure 2.11). These three architectures rely on the use of interdigitated combs which allows increasing the total capacity of the system. The two electric plates are insulated from each other and pre-charged. Under the effect of external vibrations, the latter have a relative displacement with respect to each other. If the voltage generator operates at constant load, the decrease in capacitance induced by the variation of the distance between the two plates will increase the voltage of the generator and thus increase the energy stored in the capacitor. Also, if the voltage is fixed, the movement of the plates will produce a current due to the movement of the loads. In 2002, these three structures are compared and it is deduced that the "in plane gap closing" structure (Figure 2.11b) allows the highest power density. For a vibration acceleration of 2.25 ms^{-2} at 120 Hz a power density of 116 μW/cm^3 is obtained (Wright etc ,2002).

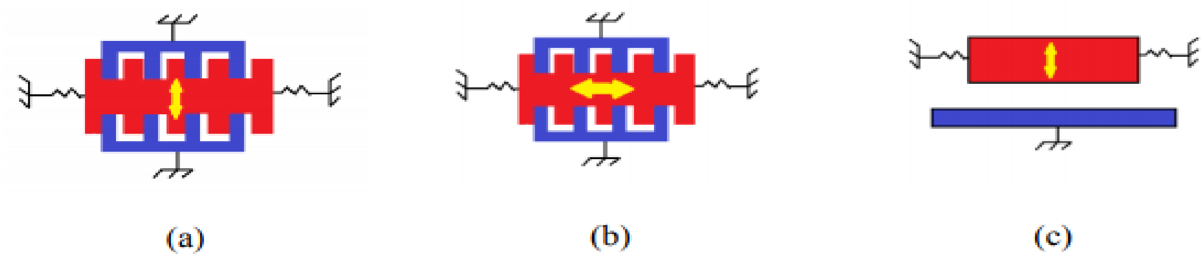

Figure 2.11 Three electrostatic transducers: (a) In-plane gap overlay, (b) In-plane Gap closing (c) Out-of-plane Gap closing (Mitcheson etc, 2004).

To overcome this polarization source fault, it is possible to use electrets. Electret is an electrically charged dielectric capable of retaining its charge for years. It acts as an electric dipole can ensure a permanent polarization of the variable capacity. An interesting application is the development of an electrostatic energy harvesting system using as a source the movements of the heart. This system was developed by the CEA-Leti to design a stand-alone pacemaker (Lefeuvre, 2011). The energy collector of the pacemaker has dimensions of 18 mm x 9 mm x 3 mm and operates at a resonance frequency of 20 Hz. It is capable of recovering about 40 μW, sufficient power to power the pacemaker.

Table 2.3 Vibration energy harvesting

References	**Power (uW)**	**Surface (mm^2)**	**Volume (mm^3)**	**Voltage (V)**	**Acceleration (m/s^2)**	**Frequency (Hz)**	**Mass (g)**

(Roundy ,2003)	11	100	100		2.3	100	
(Mitcheson etc ,2004)	24	784	1568	2300	4	10	
(Despesse etc ,2007)	1000	1800	18000	3	3	50	100
(Kansal vd,2007)	0.061	66	66		2.5	250	0.05

Electrostatic Systems As shown above, the current transducers rely on the use of interdigitated combs. This technique leads to better integration. Indeed, if the air gap is divided by a factor k^2, the electric fields are increased by a factor k^2 (Wood etc, 2011). Moreover, it is possible to produce these transducers with MEMS technologies which would allow them to be integrated on the same chip with the associated electronics. Indeed, several electrostatic transducers made using MEMS technology exist in the scientific literature such as the one carried out in 2014 within ESIEE Paris and has a total volume of less than 100 mm^3 (Guil etc ,2012). The device is capable of recovering 2.3 μW at 260 Hz for acceleration of 1 g and at a pressure of 0.15 Torr when the system is precharged with a voltage of 10 V. However, the fault of this system occurs if the two the capacitor armatures touch each other, there is no power generated and the two plates are likely to remain glued. Therefore, mechanical stoppers must be integrated. Consequently, this addition makes the manufacturing process more complex and limits the integration possibilities of the system.

2.3.2.Thermal energy

2.3.2.1. Source of thermal energy

The transfer of thermal energy is a transmission of this energy from a region to another, under the influence of a temperature difference. Heat, which is itself a form of heat energy transfer, comes from different forms of energy, such as sunlight, electricity (movement of electrons along a conductor), and human body.

2.3.2.2. Thermal transducer

Thermal transducers use a temperature gradient to produce electrical energy by Seebeck effect. This phenomenon, highlighted in 1822 by Thomas Seebeck, evokes the appearance of a potential difference at the junction of two materials subjected to a temperature gradient. Conversely, the Peltier effect shows that the circulation of a current in a couple of distinct materials induces a temperature difference between the two ends of the conductors.

These transducers are based on the use of thermocouples: most of the time, two N and P type semiconductor bars are connected by a conductive material (Figure 2.12 and Figure 2.13). One of the most widely used semiconductors is Bismuth Telluride (Bi2Te3), which is one of the materials with the highest yield at temperatures below 450K. Silicon-germanium (SiGe) alloys are often used at high temperatures up to 1300 K. (Mag etc, 2010).

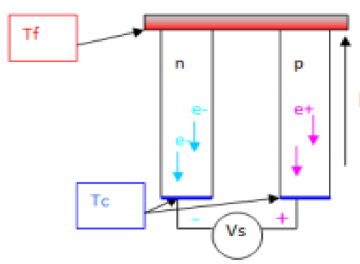

Figure 2.12 Thermocouple (Dashevsky etc ,1998)

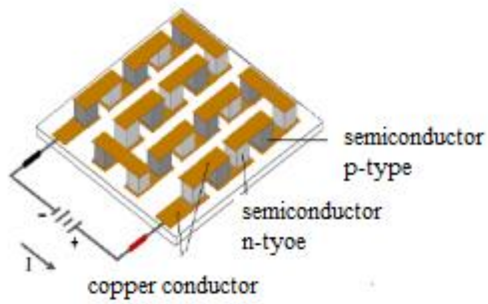

Figure 2.13 Thermocouple in series (Lossec etc, 2010).

A heat flux induces a displacement of the holes and electrons in the thermocouples and the appearance of an electric current. The higher the temperature gradient, the more energy harvested is important as shown by the following equation:

$$\frac{P}{S} = h\,\Delta T \qquad \textbf{(2.9)}$$

With P the output power, S the surface, ΔT the temperature gradient and h power density per ° C and per m² of the converter.

Using equation (2.9), it appears possible with a temperature differential 37 ° C / 20°C, for example a device positioned on the human body, to produce 13.6mW / cm² (Torfs etc ,2008). In practice, in order to increase the contact surface and thus the harvested power, the thermocouples are electrically connected in series (Figure 2.13) and in parallel from a thermal point of view, ie each element is subjected to the same thermal gradient.

Table 2.4 summarizes the properties of several thermocouples found in the literature. Several thermocouples have been marketed among others by Thermolife (Thermolife, 2000), Micropelt (Micropelt,, 2000) (Figure 2.14). With a volume of 0.2 cm³, Thermolife has marketed a system capable of producing up to 30 μW with a temperature gradient of 5 ° K. Seiko has also developed a watch (Figure 2.15) fed entirely by a thermoelectric module using the temperature difference between the wrist and the ambient air.

Figure 2.14 Thermocouples: (a) Thermolife (Thermolife, 2000), (b) Micropelt (Micropelt,, 2000).

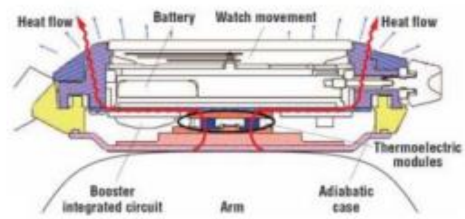

Figure 2.15 Seiko watch (Kishi etc, 1991).

Table 2.4 Performance of multiple thermocouples

References	Thermocouples	Surface	Power generated
(Vullers etc ,2009)	MicroPelt company	2.5 x 3.5 mm^2	1.7 mW.K^{-1} ($\Delta t = 5K$)
	Nextreme company	1.6 x 3.2 mm^2	25 mW. K^{-1} ($\Delta t = 70K$)
(Chennault etc ,2008)	BiTe(158 Thermocouples)	0.101 cm^2	0.16μW.K^{-1} ($\Delta t = 5K$)
	PbTe(58 Thermocouples)	0.04 cm^2	10 mW. K^{-1} ($\Delta t = 220K$)

This made it possible to obtain a power of 22 µW (Kishi etc ,1991). It was also possible to feed a communicating oximeter (Torfs etc, 2008) plated on the arm. The latter system is able to recover 200 µW for an ambient temperature of 22 °C. In order for these systems to be as efficient as possible, it is generally necessary to have high temperature gradients as well as high heat flux. To channel the heat flow between the two thermocouple armatures, a radiator must be placed on one of the two faces of the module. Figure 2.16 and Figure 2.17 show prototypes with radiators. The size of these radiators is not insignificant compared to the size of the heat recovery unit.

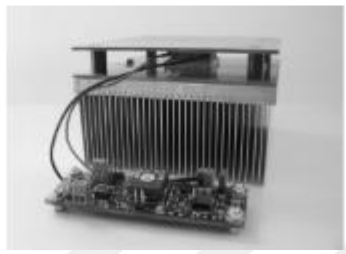

Figure 2.16 Prototype L.Mateu (Mateu etc, 2006)

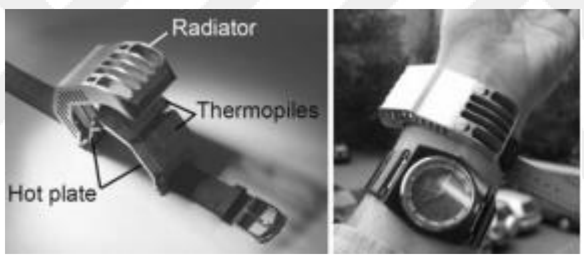

Figure 2.17 Watch (Leonov and Vullers, 2011).

Another disadvantage of thermal energy recovery is its low efficiency. Indeed, despite the improvements made to the materials used, the efficiency of a system is generally less than 10% for heat transfers from 200 ° C. to 20 ° C. (Δ ° K = 180) and less than 1% for heat transfers from 40 ° C to 20 ° C (Δ ° K = 20).

2.3.3. Biochemical energy

The available energy can also be in biochemical form. Transforming chemical energy into electrical energy is the concept of biofuel. The difference with respect to a fuel cell is the catalyst which is in this case biological. Bio-piles can be classified into two classes depending on the biocatalyst used: micro-organisms or enzymes. Micro organic bio-batteries have long lifetimes of up to 5 years, whereas enzymatic bio-batteries typically live for about 30 days due to the fragile nature of the enzymes (Kim etc, 2006). However, a major advantage of using enzymes is that it is possible to get rid of the ion exchange membrane and considerably reduce the size of the system. Only the principle of enzymatic bio-batteries will be detailed here. A description of the micro organic bio-batteries is detailed in (Du etc, 2007).

Enzymatic bio-batteries involve enzymes such as biocatalysts and more precisely redox enzymes. Figure 2.18 shows how it works. Two electrodes ensure the functioning of the generator: an anode, place of the oxidation of a fuel (glucose for example), and a cathode, place of the reduction of the oxidizer (generally the oxygen). The electrodes collect the electrons between the electrodes and thus allow the generation of an electric current. These electrode reactions require catalysts. In the case of the enzymatic bio-batteries, the microorganism which ensures the redox reaction and the electron transfer is replaced by a biological catalyst, the enzymes. A particular class of enzymes, called oxidoreductase, has as a function the catalysis of redox reactions. The use of these enzymes connected to electrodes allows the construction of enzymatic bio-batteries. To ensure their functioning, it is necessary to immobilize the enzymes in order to maintain the stability of the catalyst and the efficiency of its connection. This connection between the enzyme and the electrode may require the intervention of a mediator which ensures the electronic transfer between these two parts. The choice of the mediator then becomes paramount for the efficiency of the bio-batteries. Given the different electrochemical potentials of these two electrodes, an electrical current flow between the cathode and the anode.

We can give the example of the functioning of the bio pile glucose / dioxygen. At the anode, glucose (C6H12O6) is oxidized by the enzyme glucose oxidase to gluconolactone (C6H10O6). It then loses two electrons and two H + ions. The electrons are transferred to the anode via the redox mediator which is oxidized by the anode. The H + ions pass through a selective membrane that only passes these ions. The redox mediator is used to accelerate the transfer of electrons. It is possible, for example, to use potassium ferricyanide or ubiquinone which accepts electrons and transfers them to the electrode. At the cathode, is reduced to water using the enzyme laccase and the mediator ABTS which is reduced at the level of the electrode by recovering an electron. H + ions and electrons "pick up" the oxygen atoms to form water. This system generates an electric current (circulation of the electrons between the anode and the cathode).

The most efficient bio-batteries to date generate about 1.5 mW.cm^{-2}. A bio battery using a glucose dehydrogenase / diaphorase couple at the anode and a bilirubin oxidase at the cathode was developed by Sony in 2009 (Sony). The element is a 39 mm side cube (Figure 2.18) operating on glucose and capable of generating 50mW. The combination of 4 cubes in series allows the power supply of an MP3 player. The major shortcoming of these systems is the limited lifetime of enzymes.

Figure 2.18 Bio-batteries developed by Sony (Sony)

2.3.4. Energy of electromagnetic radiation

In this section, we are interested in systems that can recover energy in the form of radiation: light waves and Radio-Frequencies.

2.3.4.1. Energy of light waves

The source of the light waves can be the sun or artificial lights (desk lamps, streetlights, etc.).The harvesting of energy from the radiation of light waves is possible thanks to the use of photovoltaic cells made from silicon wafers in the majority of cases. When converting light directly into electrical energy, we speak of the photovoltaic effect for which the energy of the photon is used to excite an electron from its ground state to an excited state. Figure 2.19 illustrates a photovoltaic cell. There are three stages in the process of recovering photovoltaic energy. First, a photon arrives at the semiconductor with sufficient energy. This will excite an electron-hole pair that will leave its ground state from an energy point of view. At this level of excitation, the photon dissociates the electron-hole pair. The electrons are directed towards the n - doped layer (which becomes the pole -) and the holes towards the doped layer P (becoming the + pole). Obtained in this way an electric generator of which the open circuit voltage is about 0.6V.

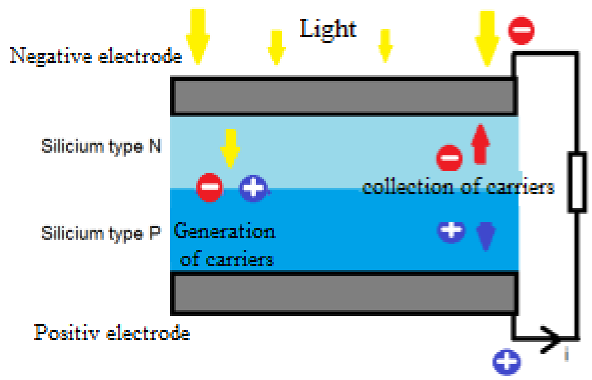

Figure 2.19 Diagram of a photovoltaic cell (Unio, 2012).

There are different types of materials used in the manufacture of photovoltaic cells. Monocrystalline silicon (c-Si) and polycrystalline silicon (mc-Si) cell technology is the most widely represented category with 85% of the photovoltaic market and is mainly used in outdoor environments. However, this technology has a high cost, due to the use of expensive substrates (silicon wafers). Amorphous silicon (a-Si) cells are also widely used and are mainly used for indoor applications. Tellurium Cadmium (CdTe) cells, and Indium Gallium and Selenium Copper (CIGS) cells are in full growth. This second category of technology has a low cost, thanks to the use of cheap substrates (glass, metal, plastic). Table 2.5 shows the recoverable power density, efficiency, and cost for several technologies.

Photovoltaic panels are systems that are well known today and are marketed for the production of energy at high volume in sunny areas spread over several m² of surface. This method of harvesting energy for the supply of low-power electronic objects is also found. For example, the French company Solems developed in 1981 a calculator powered by a cell of 3 to 4 cm² in Si-Amorphe (Fong vb , 2010). The calculator consumes only a few micro amps under 1.5V. Citizen also produces watches powered by solar energy (Nodilo, 2000). Also, Power Plus produces a clock radio with solar panel and dynamo. One hour of recharging by solar panel offers 20-30 minutes of music (Lynx, 2012). However, it should be noted that all these devices must be placed in the light for a long time (a few hours to a few days) for a short time use.

Table 2.5 Properties of photovoltaic cell technologies

Technology	Performance under the sunlight 1000w.m^2(commercial cells)	Power density under fluorescent lamp a 100 lux (uW.cm^2)	Substrate	Cost
c-Si	12.16% (Module~ 1m^2)	~20-60 uW/cm^2 (Cell. ~100cm62)	c-Si	High
Mc-Si	12.16% (Module~ 1m^2)	~20-60 uW/cm^2 (Cell. ~100cm62)	mc-Si	High
a-Si	5-7% (Module~ 1m^2)	~35 uW/cm^2 (Module ~1 m^2)	glass	Reliable
CdTe	10-11% (Module~ 1m^2)		glass	Reliable
CIGS	8-13% (Module~ 1m^2)	~35 uW/cm^2 (Module ~1 m^2)	Glass Metal Plastic	Reliable
Triple junction GaInP/GaAs/Ge	25-30% (Module~ 1m^2)		C-Ge	Very high
Organic	1.5% (Module~ 1m^2)	~10 (Module ~1 m^2)	Plastic	Reliable
Dye cells	1.5% (Module~ 100cm^2)	~10 (Module ~100cm^2)	Plastic	Reliable

Table 2.5 summarizes the characteristics of various photovoltaic energy harvesters found in the scientific literature and intended for the supply of sensors or electronic

devices. The efficiency of the photovoltaic cell used and the efficiency of the dc-dc circuit designed to optimize the transfer of power between the cell and the load were distinguished.

The energy harvesters summarized in Table 2.6 have reasonable sizes, ie. below the cm². Under optimum sunshine conditions, on the order of 100 mW / cm², these systems can supply sensors that can consume up to several tens of milliwatts.

Table 2.6 Summary of various photovoltaic energy harvesting systems existing

References	Cell Type	Device Size	Cell Efficiency	Circuit Efficiency	Power Recovered
(Sark etc ,2007)	a-SI on computer mouse	28 cm^2	14%	50%	10 mW
(Sark etc ,2007)	Si	112 cm^2	10%	70%	50 mW
(Gula ect,2011)	Poly-Si	45x76 mm	11.84%	90%	400 mW
(Gula ect,2011)	a-Si	45x46 mm	4.57%	90%	86.4 mW
(Gula ect,2011)	CIGS	5 cm^2	N/A	82%	30 uW (very low sunshine)

The main limitation of systems for harvesting of photovoltaic energy is of course related to the very high sensitivity of this type of device to the lighting conditions. By way of example, the energy harvested by a photovoltaic cell is reduced by a factor of 100 in the case of a cloudy sky and by a factor of 2500 if it is placed inside (Roundy and Wright, 2004).

2.3.4.2. Energy of radio-frequency waves

2.3.4.2.1. Source of RF waves

Radio-Frequency (RF) waves emitted by cellular base stations or wireless local area networks can serve as a potential source of energy harvesting. The available frequency range is from 3 kHz to 300 GHz.

The available RF power density explained below is defined in far field. In this zone, the electromagnetic field has essentially the shape of a plane wave, the electric field and the magnetic field are in phase and the ratio of their amplitudes is constant. Under these conditions, the intensity of the electric field can be converted into an incident power density according to the following equation:

$$S= \frac{E^2}{Z_0} \quad \textbf{(2.10)}$$

Where S is the incident power density expressed in W / m², E is the electric field expressed in V / m and z_0 is the free space characteristic impedance of the order of 377 Ω.

The power density depends on the distance between the source and the receiver, since the field E varies as a function of this. It is thus possible to quantify the power received at the output of the antenna as a function of the incident power and the distance between a transmitter and a receiver thanks to the telecommunications equation, also called the Friis equation, given by:

$$P_r = P_t G_t G_r \left(\frac{\lambda}{4\pi d}\right)^2 \quad \textbf{(2.11)}$$

Where P_r is the received power (watts), P_t is the transmitted power (watts), G_r and G_t are the gain of the transmitting and receiving antenna (in dBi), λ is the wavelength of the frequency (meters), and d is the distance between the two antennas (meters).

Equation (2.11) assumes that this is a line exposed in visibility between transmitting and receiving antennas, Because of the health risks associated with human exposure to radiation safety guidelines have been proposed by the ICNIRP (International Commission on Non-Ionizing Radiation Protection) (Intet, 1998) on the maximum permissible exposure (MEP) for the general public. This has led to a number of studies on the level of power density in various locations, which can be used as a reference point for the harvesting of RF energy. Visser et al. (Visser ect, 2008) collected power density measurements on GSM base stations in several European countries (Bergqvist etc., 2001). Their data are based on measurements taken between 935 and 960 MHz (frequency band for GSM 900 in Down Link mode) and between 1805 and 1880 MHz (frequency band for GSM 1800 in Down Link mode). The measurements were carried out in several places (in town, industrial zone, small town, rural area, and countryside) with different characteristics of the site (eg measurements on the ground, on the roof or on the balcony or indoors or outside). At distances between 25 and 100 m from a GSM base station, the RF power density is between 1 and 0.01 mW / cm². Another study was carried out by Burch et al. (Burch ect, 2006) to quantify RF exposure levels in a residential neighborhood near Denver, Colorado. The study area contained 15 antennas of radio and television broadcasts, operating at frequencies of 55 to 687 MHz RF power density measurements were performed inside and outside the 161 houses within 3 km of the antenna group. The indoor and outdoor RF power densities average between 0.8 and 2.6 mW / cm².

Thus, these results on the RF power density level suggest that the distance between the transmitter and the receiver is an important parameter to be taken into account in the study of RF energy harvesting.

2.3.4.2.2. RF Energy transducer

The purpose of an RF energy harvesting is to convert the energy of the electromagnetic waves contained in the ambient RF sources into a DC electrical voltage. This system, also called rectifying antenna or rectenna is shown in Figure 2.20. A typical rectenna consists of a receiving antenna followed by an impedance matching network, a rectifier, a dc filter and a load representing the equivalent impedance of the sensor to be supplied.

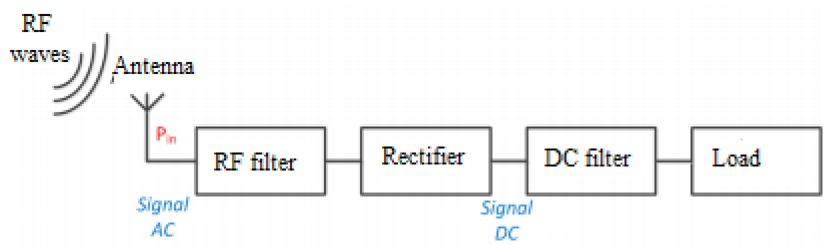

Figure 2.20 Diagram of an RF energy harvesting.

The first works on wireless transmission date from the 1894 with Marconi which demonstrated the feasibility over a distance of 2.85 km. In 1896, Tesla shows it for a distance of 48 km. In 1969, William Brown filed a patent on the architecture of a Radio Frequency Energy Harvester (Brown ect, 1996) and in 1977, he improved his design with thin film technology.

In 1992, in Japan, an aircraft was powered by the power emitted by Radio-Frequency waves (frequency set at 2.411 GHz). Placed on a ground vehicle, a phased array antenna array was used to steer the microwave beam on the aircraft (Figure 2.21) (Matsumoto, 2002).

In the 2000s, work was carried out to power by the energy of the waves the village of Grand-Bassin located in a canyon difficult to access on the island of Reunion. The electricity supplied by the EDF power reaches the top of the canyon by a high voltage line, and is then transformed using magneton in radio frequency signal sent by a horn antenna for a distance of 700 m in the direction of the town. The power emitted was 800 W at 2.45 GHz and 65 W was harvested at the output of the rectenna designed which represents an efficiency of 5% (Celeste, 2004).

Figure 2.21 Piloting an Airplane Powered by RF Energy (Freq = 2.411 GHz) (Matsumoto, 2002)

The deployment of telecommunication networks (GSM, UMTS), ISM and Wi-Fi bands has led to a strong interest in the development of rectenna that can operate at low incident power levels. Consequently, since the 2000s many devices for the harvesting of RF energy have been presented in the scientific literature. The RF-dc conversion efficiencies of the most recent prototypes are higher and can reach up to 75% for an incident power of -10 dBm (Agrawal etc. , 2014).

An example of work on the harvesting of ambient RF is that of Sample and Smith (Sample and Smith, 2009) from Intel. They attempted to harvest energy from a television transmission tower, which delivers 960kW at 674-680 MHz, to power a thermometer / hygrometer. Their system, as shown in Figure 2.22, consists of a periodic log antenna and an RF-dc conversion circuit. The device is placed outside a balcony at a distance of 4.1 km from the transmitting tower. A maximum power of 60 μW (0.7 V across an 8 kΩ load) was measured. This example shows the feasibility of powering sensors with the surrounding RF energy. Table 2.7 summarizes the results of several prototypes found in the scientific literature.

Figure 2.22 Harvesting of ambient RF energy for supplying a thermometer (Sample and Smith, 2009).

Table 2.7 Summaries of various radio frequency energy harvesters

Reference	Source	Frequency	Dimensions Prototype	Distance source of emission	Power harvested	Intended application
(intanavongsa ect , 2012)	No indication	915 MHz	~7 cm^2	…..	37 μW	Powering microcontroller

(Nimo, 2012)	1GHz P_t=0.03 W	1 GHz	50 mm x 52 mm	3.3 m	1 μW	
(Ancey, 2005)	Phone P_t=2 W	900 MHz	….	1m 2m	1.9 mW 500 μW	
(AFEIT, 2009)	Urban environment Power density : 0.04 mW/m^2	1.8 GHz	~few cm^2		400 pW	
(Visser ect, 2008)	Phone P_t=1 W	1.8 GHz	~few cm^2	20 cm		Electronic thermometer supply
(Sample and Smith , 2009)	TV antenna	674-680 MHz	Antenna 20 cm^3	4 km	60 μW	Electronic thermometer supply
(Fong vb , 2010)	P_t=100 mW	4 GHz	3mm x 3mm	7 cm	0.5 μW	Powering printed circuit
(Vullers etc ,2009)	No indications	920 MHz	1 mm x 0.8mm	~1.2 m	2 μW	RFID
(Nasab vb , 2010)	Urban environment	940-960 MHz	~cm^2	500 m		Powering a diode

From this bibliographic study on the harvesting of radiofrequency energy, the distance between an RF transmitter and the rectenna appears to be a sensitive point. This sensitivity is explained by the Friis equation (equation (2.11)), because the incident power at the level of the rectenna is inversely proportional to the square of the distance.

It should be noted that this principle is now widespread in the industrial environment, with the generalization of RFID tags (Figure 2.23). The principle of these chips is to harvest the energy of electromagnetic sources placed in the vicinity (of the order of the meter) in order to be able to send their identification code, as described in

(Finkenzeller , 2010) (Figure 2.24). RFID is used for identification, tracking and inventory management (Zuo , 2010). NXP designs RFID tags such as the UCODE G2XM (NXP , 2013). The power emitted by the reader is 2 W for a frequency between 868.5 and 867.6 MHz. Under these conditions, this tag can operate at a distance of 7 m thanks to its sensitivity of -15 dBm.

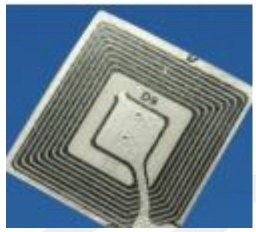

Figure 2.23 RFID Tag (Nodi ect, 2000).

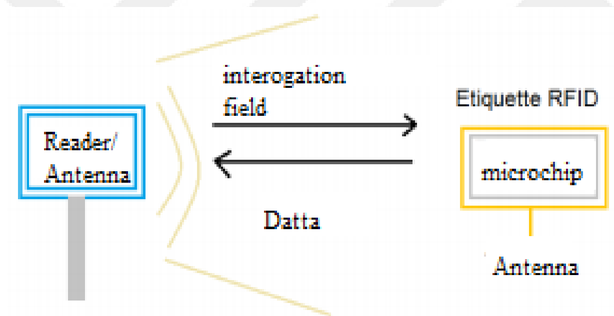

Figure 2.24 Schematic diagram of RFID.

2.4. Review of Available Sources

In this section, as a result of this state, we draw up the assessment on potential energy sources to supply sensors.

2.4.1. Advantages and disadvantages of different sources

Table 2.8 summarizes the advantages and disadvantages of different sources in this chapter. One possibility to compare sources in an equivalent way is to look at their power density levels. Obviously, photovoltaic energy is the one with the highest power density by far. However, the major disadvantage of this source lies in its non-regularity. From this point of view, considering all these sources, Radio-Frequency waves appear to be the only ones to be omnipresent in our daily lives. Thus, despite its low power density on average, the energy of the RF waves is an interesting source.

Table 2.8 Summary of advantages and disadvantages for multiple sources energy

Energy source	Average power density/Energy	Advantages inconvenience
Thermoelectric	$50\mu W/cm^2$ 0.5v@ΔT=1℃	++fixed and sustainable system --Low performance --Low output voltage →Energy with low temperature gradients
Vibration: Piezoelectric	100 µW/cm^3 10 µW/g mass	++No source of voltage required ++High output power and voltage (2.10 V) - -Mobile part - -Fragile materials - -Aging problem →Integration →Coupling and strength of fine films
Vibration: Electrostatic	100 µW/cm^3 10 µW/g mass	++ Techno Compatible Silicon -- Mobile Parts --Complex management electronics -- Very high voltages - -Voltage source required →Mechanical stability
Vibration: Electromagnetic	100 µW/cm^3 10 µW/g mass	++ No source of voltage required ++ No "intelligent" materials - -Mobile Parts - -Output voltage low (0.1 to 0.2V) - -Integrated systems

		- -Difficulties in manufacturing the coil →Integration coil and magnet
Radiation: Photovoltaic	Outside 15000 μW /cm^3 (in broad daylight) 150 μW /cm^3 (Cloudy) Inside 6 μW /cm^3	++ Fixed / Reliable System ++ Technology at the point / Easy to integrate / inexpensive --Power depends on sunshine conditions (brightness, angle of incidence) - -Sensitivity to pollutants (dust) Fragility of cells →Recover sufficient energy
Radiation: Waves Radio Frequencies	RFID 2.5 GHz: 10 μW /cm^3@ 1m GSM900: Transmitter/receiver 50 m→ 1.2 mW / m² 200 m→ 0.26 mW / m	++ Omnipresent in everyday life. (TV / Radio, Wi-Fi, mobile phone, etc.) --Difficulty in evaluating the energy harvested in a real environment --Depends on the distance between the transmitter and the measuring point, the physical characteristics of the propagation medium and the frequency of the signal. Improved Conversion Systems →RF / DC. Antenna optimization and choice of the most suitable frequency ranges

2.4.2. Scientific positioning: RF energy harvesting

The state-of-the-art report on energy sources highlighted the interest of the source of Radio-Frequency waves. Unlike most other sources, the energy of RF waves in urban areas is continuously available thanks to the different RF transmitters present. Although the average RF power density is relatively low compared to other energy sources, it is nevertheless close to 1 mW / m² in urban areas. In addition, wireless communication standards have led to the proliferation of radio transmitters over a wide range of frequencies, such as GSM 900 and 1800, UMTS 2100, and Wi-Fi

Previous work on rectenna has focused mainly on the issue of energy harvested at a single operating frequency. However, in an urban environment, the frequencies and the level of RF power density are not controlled. It is therefore advisable to develop systems capable of harvesting energy over several frequency bands. Also, under these conditions, when multiple RF sources are available, the amount of harvested energy can be increased if the system is designed to operate over a wide band of frequencies. This further strengthens our interest in Radio Frequency energy sources.

2.5. Conclusion

In this chapter, several sources and techniques of energy harvesting for the energy autonomy of communicating sensors have been studied. Only the sources allowing an integration of systems of the order of cm^2 were chosen. Techniques to harvest energy from mechanical vibrations (piezoelectric, magnetic and electrostatic), thermal, chemical and radiation energy (light waves and Radio Frequencies) were studied. The advantages and disadvantages of each were summarized, which enabled us to take an overview. With a power density of the order of 100 mW / m^2, the solar energy source appears to be the highest. However, RF energy is omnipresent in our urban environment, and the efficiency of RF energy conversion systems is far superior to that achieved with photovoltaic energy retrievers. For these reasons, the energy source of the Radio-Frequency waves emerges from this balance sheet as a promising source for the supply of sensors. After illustrating the principle of an energy harvesting of radiofrequency waves by some prototypes found in the scientific literature in this first chapter, we will concentrate the rest of our study on the architecture of an RF energy harvester. From this analysis, we will identify the key points of the design of a rectenna. This will enable us to design a system for harvesting RF energy in a high stress environment ie having low levels of RF power density and in the case where the presence of one or more frequency bands is uncertain.

3. MATERIALS AND METHODS

3.1. Introduction

As we have shown in the first chapter, the energy conveyed by Radio Frequency waves can be harvested in order to be converted into continuous electrical power for the sensor supply. The device allowing this conversion is called rectenna.

The first part of this chapter is devoted to rectenna architectures. Its basic principle is first exposed. We will see later that a rectenna can be designed to harvest energy over several RF frequency bands. The different architectures possible for these multiband transducers will then be detailed. Then, in the case where the sensors are placed in environments for which the power density level is relatively low, we will show the interest of adding an energy storage cell or a dc-dc converter to the following the RF energy harvester.

The second part of this chapter details the issues related to the design of a rectenna. It will first be shown that it is important beforehand to evaluate the RF power density present in the sensor environment. Then, the rectifier, the impedance matching network, the load and the receiving antenna will be explained in detail. Each of these parts requires a reflection as to the choice of the most appropriate architecture because these induce an impact on the output DC voltage as well as on the overall efficiency of the circuit. Thus, we will try to identify the properties of each and the associated locks.

3.2. Radio Frequency Harvesting Systems

In this section, the principle of an RF energy harvesting is detailed: architecture and its characteristics. In view of the multitude of frequency bands present in our environment, it is interesting to harvest several frequencies. In these cases, there are several rectenna architectures and these are also presented in this part.

3.2.1. Overview of an RF energy harvesting unit

An RF energy harvesting system is composed of several elements. As seen in Figure 3.1, a radiation source, such as, for example, an RF transmitter or a GSM base station is used to broadcast an RF signal. This emitted electromagnetic signal is collected by a receiving antenna and is converted into a continuous electrical power usable by means of an RF-dc conversion circuit. Then, the continuous electrical power can directly power the load. The latter can also be placed in a storage element if, for example, the harvested power is greater than the power required for powering the load. Finally, if the output voltage of the RF energy harvester is not sufficient or fluctuating, a dc-dc converter may be interposed between the output of the harvester and the load. In the following sections, each of these blocks is examined in detail.

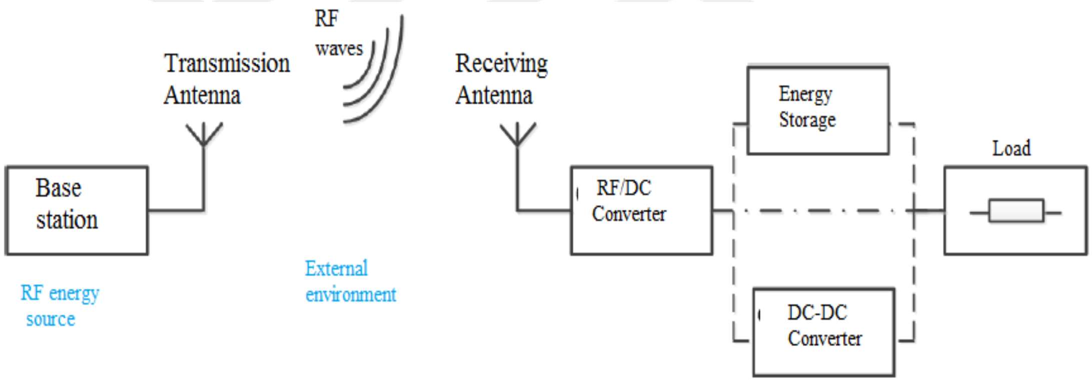

Figure 3.1 Schematic diagram of an RF energy harvester in its environment.

3.2.2. Basic architecture of a rectenna

The purpose of an RF energy harvester, also called rectifying antenna or rectenna, consists in converting the electromagnetic energy contained in the sources into a continuous electrical voltage dc. A typical rectenna consists of a receiving antenna followed by an impedance matching network, a rectifier, a dc filter and a load representing the equivalent impedance of the sensor to be powered (Figure 3.2).

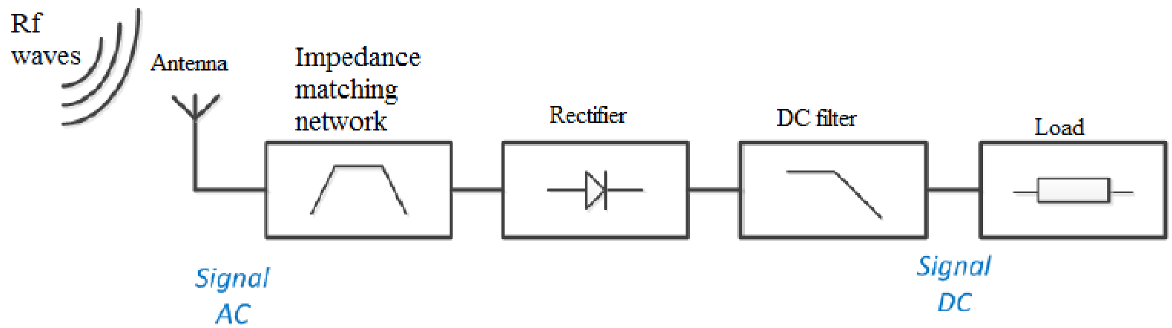

Figure 3.2 Structure of a rectenna.

The impedance matching network has the function of performing an impedance matching between the receiving antenna and the rectifier at the selected frequency and for a given incident RF power.

The rectifier performs the conversion of the ac signal received at the output of the impedance matching network into a continuous signal DC. It is generally made up of diodes and capacitors.

The output filter dc is used to filter the HF harmonics and to allow only the DC component to pass through. It can also carry out an adaptation of impedances between the rectifying circuit and the load for a given power dc.

3.2.3. Single-band and multi-band architectures

Numerous studies on harvesting of RF energy have been presented in the scientific literature. The first harvesters were designed to harvest only one RF tone (Huang ect, 2013), (Mikeka ect, 2012), (Olgun ect, 2012), (Tentzeris and Kawahara, 2008). The functionality of these systems is considerably degraded if the frequency of the electromagnetic wave to be harvested differs from the resonant frequency for which they were designed. Moreover, in the ambient environment of the sensor, the frequency bands present are not controlled. To use under such conditions a rectenna adapted to a single frequency for the supply of a sensor does not seem judicious.

Other works have rectennas that are capable of harvesting several signals at different frequencies. Thus, the energy of several RF frequency bands is accumulated and a greater amount of energy is harvested (Collado and Georgiadis, 2013), (Nimo and Reindl, 2012), (Pavone ect, 2012), (Pinuelae ect, 2013), (Sun ect, 2013).

To do this, several architectures are envisaged and the main difference between each is the design of the network of adaptation of impedances. This network corresponds to the output impedance of the antenna with the conjugate impedance of the input of the rectifier. It should be noted that the input impedance of the rectifier varies as a function of the frequency and the incident power. Similarly, the impedance of the antenna may vary depending on the frequency. As a result, it is easier to adapt these impedances to a single frequency for a given incident power. From this observation, the adaptation of impedances on multiple RF bands induces two kinds of losses: those due to the mismatch of impedances and those related to the constituent elements of the adaptation network.

(Collado and Georgiadis, 2013) and (Nimo and Reindl, 2012) show losses due to difficulties in adapting the impedance over a large bandwidth. The architecture of Figure 3.3 is that used in (Collado and Georgiadis, 2013) and (Nimo and Reindl, 2012). The designed adaptation network encompasses the signals to be recovered over a wide frequency band. However, due to antenna and rectifier variations as a function of frequency, an RF band of a few hundred MHz induces an impedance mismatch and a decrease in the RF-dc conversion efficiency. To illustrate this, we can study (Collado and Georgiadis, 2013) and (Nimo and Reindl, 2012). In (Collado and Georgiadis, 2013), the RF-dc conversion efficiency is 8% on an RF band of 1550 MHz for an incident power of -20 dBm whereas in (Nimo and Reindl, 2012) this efficiency is doubled and increases to 15% for the same incidental power. On the other hand, the bandwidth of the rectenna in (Nimo and Reindl, 2012) is 300 MHz or 1200 MHz less than (Collado and Georgiadis, 2013). Due to the variation in the input impedance of the rectifier and the antenna as a function of frequency, losses due to mismatch are much higher on 1500 MHz than on 300 MHz, effectiveness of conversion of the two examples. Therefore, it is better to recover RF energy on several small RF bands than on a single broader one.

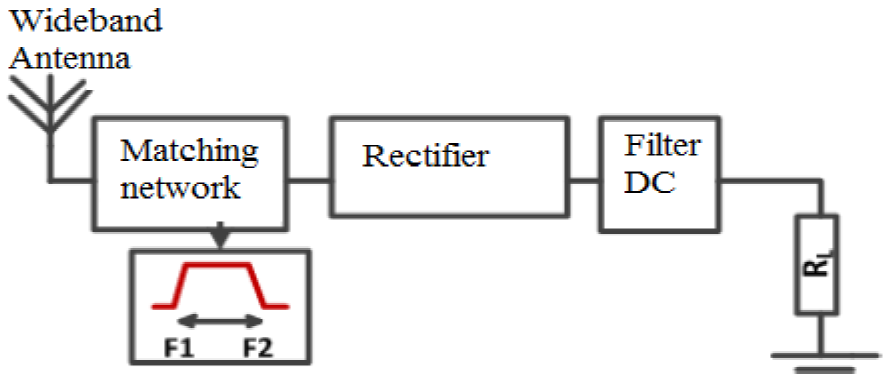

Figure 3.3 Wideband Rectenna with an impedance matching network of band-pass type.

From the work done in (Masotti ect, 2013) and (Suh ect, 2002), we can explain how the losses related to the impedance matching network components affect the conversion efficiency of a rectenna. As shown in figure 3.3, the objective is to achieve an adaptation for several distinct frequencies (and not on frequency bands as for the previous architecture). For an incident power of -10 dBm, the (Suh ect, 2002) rectenna reaches a conversion efficiency of 40% for two frequencies at 1.8 GHz and 2.1 GHz. This result is obtained by means of a complex network composed of an architecture based on an L-shaped network and three T-networks. The majority of the multi-frequency rectennas based on the architecture of figure 3.3 is designed to two frequencies (Mikeka ect, 2012), (Supercapacitor, 2015) and presents the same results as (Suh ect, 2002). In (Masotti ect, 2013), Diego Masotti and Al, attempted to harvest four distinct frequencies (900 MHz, 1750 MHz, 2150 MHz and 2450 MHz).

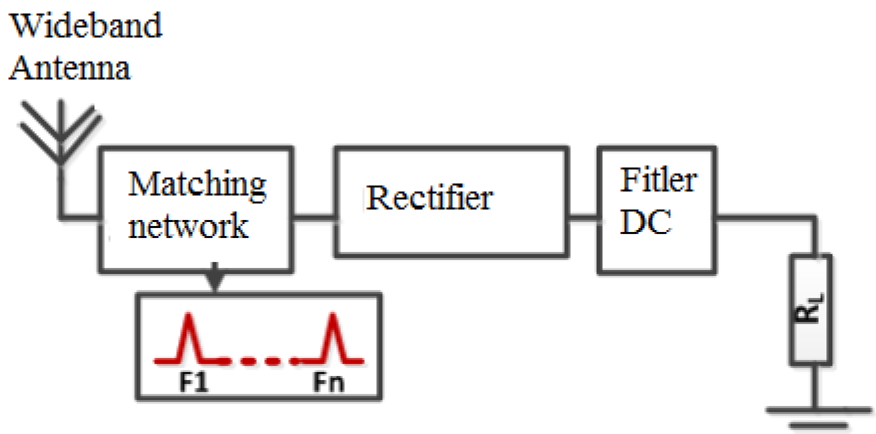

Figure 3.4 Multi-frequency Rectenna with multi-frequency impedance matching network.

Their network is shown in Figure 3.4 and the reflection coefficient at the input of the network, shown in Figure 3.6, confirms that the system could not be adapted for the four selected frequencies. Masotti explains this result because of losses in the rectifier components that have not been modeled. In addition, searching for the optimal network for one of the frequencies can seriously degrade the performance of the rectenna for another frequency of operation. In (Collado and Georgiadis, 2013), it is also shown by simulation that the conversion efficiency RF-dc decreases drastically as a function of the increase in the number of frequencies for which the system is adapted. To our knowledge, there are no rectennas designed to operate at five or more frequencies with this type of architecture.

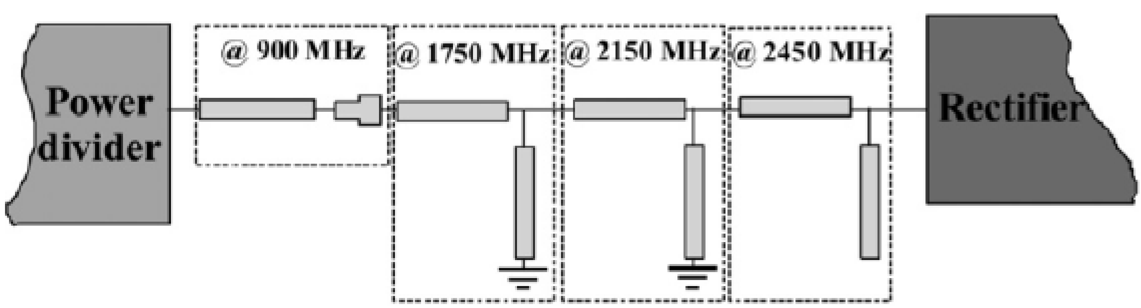

Figure 3.5 Matching network designed by (Masotti ect, 2013).

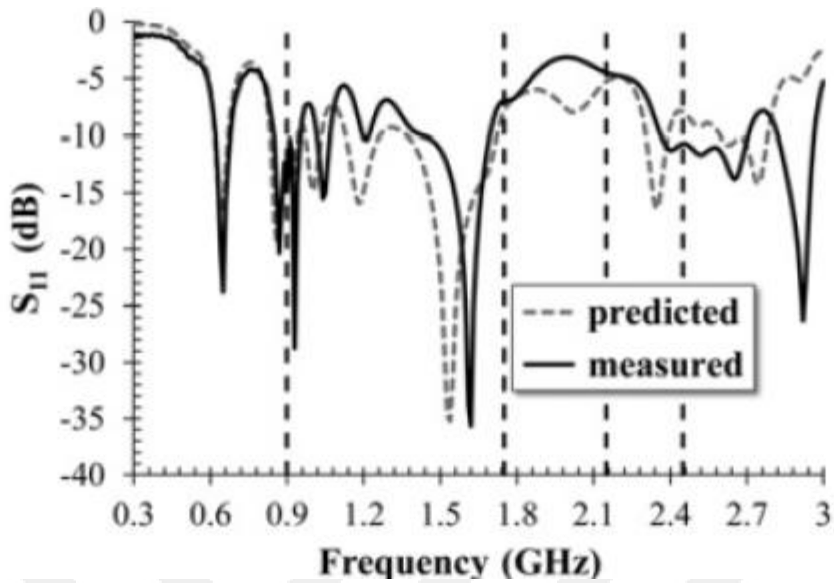

Figure 3.6 Input reflection coefficient of the matching network (Masotti ect, 2013).

Consequently, due to the losses inherent to the components and the non-linear behavior of the rectenna, it is difficult to obtain a rectenna having the same conversion efficiency over several frequencies with this architecture. In addition to the limitation of the number of adaptation frequencies, another disadvantage of this architecture is the drastic degradation of the conversion efficiency if the frequencies present in the environment of the rectenna are different from the optimum adaptation frequencies.

Another solution for harvesting the energy on several RF bands is to stack several rectennas as shown Figure 3.7. In this case, the impedance matching networks are designed to select a specific frequency and the output voltages dc of each rectenna is added; the resulting dc voltage is applied to the load (Pinuelae ect, 2013), (Kim etc ,2006). In (Kim etc ,2006), an RF energy harvester is designed to operate at three frequencies 0.9, 1.8 and 2.45 GHz. For an incident power of -15 dBm per frequency, a RF-dc conversion efficiency of 45% is obtained at 0.9 GHz and 1.8 GHz and 25% at 2.45 GHz. Despite these interesting results, the cumulative effectiveness is not given, ie. If two or three RF tones are present. Indeed, the evaluation of the quality of the combination of each output voltage dc is not taken into account. This is an important parameter to take into account as interference between each branch can occur and degrade the overall efficiency of the circuit. Moreover, no energy is harvested outside the selected frequencies. Finally, this architecture may not be suitable for applications with compactness requirements due to the number of antennas to be used.

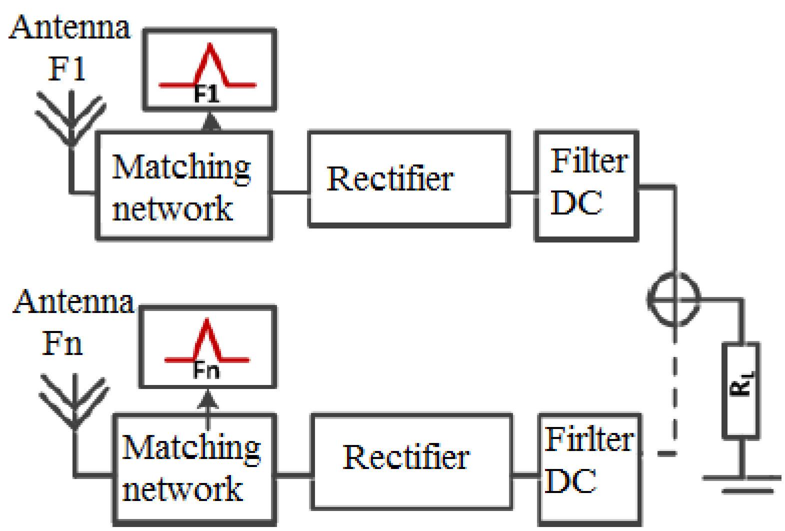

Figure 3.7 Rectenna multi-frequency: stacking several rectennas.

3.2.4. Optional blocks: energy storage and DC-DC converter

3.2.4.1. Energy storage

In practice, an RF energy harvesting system can integrate an energy storage cell. Indeed, the peak current demanded by certain sensors can go beyond what the RF energy harvester can provide. In this case, it is necessary to use an energy storage system to accumulate the energy harvested by the rectenna and to supply the sensor when the stored energy is sufficient to supply the sensor.

The choice of a storage cell depends on several factors, such as sensor demand, cell storage capacity, discharge rate, size and cost. There are currently two main energy storage technologies: supercapacitors (Freitas ect, 2013) and rechargeable batteries (Kawahara ect, 2009).

A supercapacitor is a solution for storing energy. It is an electrochemical capacitor that has an exceptional energy storage capacity compared to traditional capacitors. The supercapacitor is achieved by depositing activated carbon on an aluminum film. The two electrodes thus formed are immersed in an aqueous or organic electrolyte. The electrical charges are stored at the electrode / electrolyte interface. The value of the capacity is proportional to the surface of its reinforcements, and to the nature of the constituent material.

If the batteries have a long lead time in the range of energy density (3.5 Wh / kg for a supercapacitor versus 30-40 Wh / kg for a battery) compared to the supercapacitors, they are recharging much faster and have incomparable durability. Thus, a supercapacitor can support more than one million recharge cycles when a battery is often limited to 400 cycles and sometimes up to 4000 recharge cycles for the best ones (Supercapacitor, 2015).

Recently, these capacitors have been explored for use in energy harvesting systems because they have a long lifetime in terms of charge-discharge cycles (Wang ect, 2013). Nevertheless, they suffer from large leakage currents, which limits their use for long-term energy storage. If the ambient RF energy is only available for a small part of the day, a supercapacitor with a high self-discharge rate is therefore not the most suitable for sensor supply (Camara ect, 2010).

On the other hand, three types of rechargeable battery can be used: Nickel Cadmium (NiCad), nickel-metal hydride (NiMH) and Lithium-Ion (Li-Ion) (Battery, 2010). Ni-Cd batteries are now relatively outdated in terms of autonomy and are no longer sold in the European Union, following the ban on the use of cadmium in portable batteries. The selection between the NiMH and Li-Ion batteries involves several compromises. Li-Ion batteries can store more energy than NiMH batteries because they offer a higher energy density than their mass and volume. In addition, Li-Ion batteries have a lower self-discharge rate (5-10% per month) than most NiMH batteries (20-30% per month). On the other hand, Li-Ion batteries are generally more expensive than NiMH batteries for a similar capacity because of the materials used. Although Lithium is abundant on Earth, sites where it is easy to extract are scarce, which in turn increases prices. In addition, Lithium batteries have a high operating voltage, typically about 3.6 V, which is three times that of NiMH batteries. To power them, it would probably be necessary to use a dc-dc converter. Recently, LSD (Low Self Discharge) NiMH batteries have emerged on the market. These were developed by Sanyo in 2005 (Sanyo, 2012) and have been marketed for a few years. Although they are more expensive than NiMH, they retain up to 85% capacity per year and charge faster than other batteries (Supercapacitor, 2015).

3.2.4.2. The DC-DC converter

As explained above, the position of the sensors with respect to the emission sources is not necessarily known and may change over time. The variation of this distance induces a fluctuation of the power captured by the receiving antenna (Friis equation) and by the same of the voltage variations at the output of the rectifier, leading to instability of the supply voltage. For this reason, a voltage regulator, also called dc-dc converter, can be used to provide a more stable DC supply voltage. A voltage regulator maintains at its output, within certain limits, a constant output voltage regardless of the load or input voltage. Two types of regulators can be considered: Linear regulators (Figure 3.8) and SMPS switched mode power supplies (Figure 3.8). SMPS is the acronym for Switch Mode Power Supply. It corresponds to power supplies which use the principle of switching to control the transfer of energy with theoretical unit efficiency.

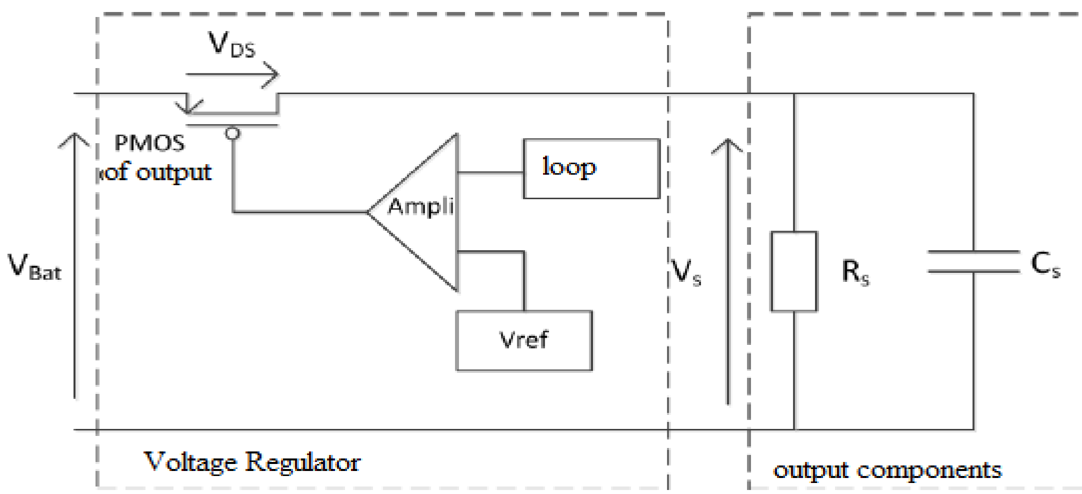

Figure 3.8 Linear Regulator (Yan ect , 2008)].

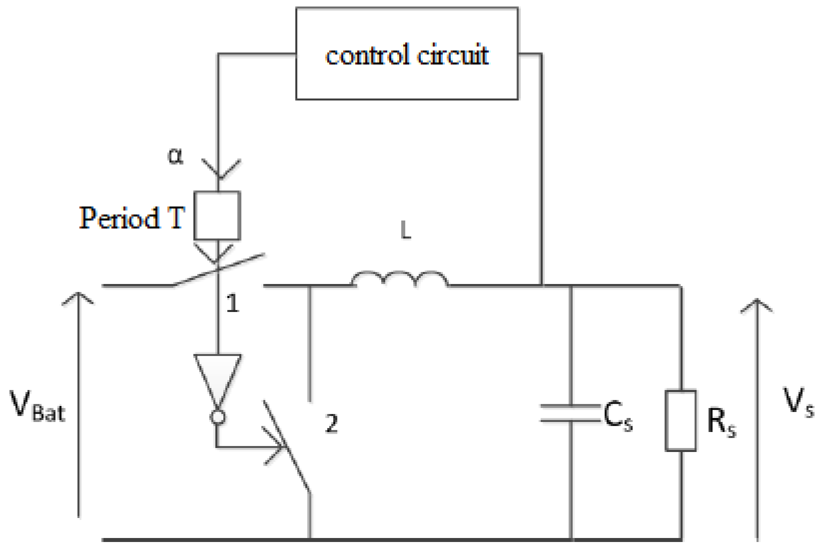

Figure 3.9 Functional Principle of a Switch Mode Power Supply (SMPS): Case of a Buck Chopper (Yang ect, 2005).

The linear regulator supplies a fixed voltage regardless of its supply voltage (V_{Bat}) and its output current. The comparison between the output voltage V_s and the reference voltage V_{ref} makes it possible to control the output transistor and thus to adjust the voltage V_s. The term "linear regulation" is used because the power element is controlled continuously. Indeed, any variation in the supply potential V_{Bat} or the output current and therefore in the load R_s, results in a variation in the output voltage V_s which is transmitted by the feedback loop to the input of the amplifier. When the regulator is operating correctly, the potential change of this input causes the return of the potential V_s to its nominal value. The voltage V_s is thus regulated. Figure 3.9 shows that the output voltage V_s is always less than the battery voltage by a value equal to the voltage V_{ds} of the output transistor. Thus, linear regulators operate only as a step-down device. In this category of regulators, there are still LDO (Low Drop Output) type regulators which make it possible to obtain a regulated voltage V_s very close to their supply voltage V_{Bat} (Supercapacitor, 2015).

The choppers operate on the principle of cutting. During a part of the working period, the battery supplies energy to a storage element (inductor or capacitor). During the remaining time, the stored energy is transferred to the controller output. There are multiple configurations that enable the output voltage to be lowered, raised or reversed with respect to the input voltage. Figure 3.9 shows the principle of a series chopper to lower the voltage. During a fraction α of the period T, the switch 1 is closed and the 2 is open. During the remainder of the period T, the switch 2 is closed and the 1 is open. The battery then supplies power to the inductance L and to the load R_S. The voltage V_S is adjusted by acting on the duty cycle α. The control circuit makes it possible to generate α from a comparison between the output voltage V_S and a reference voltage. One of the advantages of these SMPS is that it is possible, depending on their configuration, to lower, raise or reverse the voltage. Moreover, they have, in theory, a high efficiency of the order of 90% (Yang ect, 2005).

A rectenna is presented in (Lee ect , 2008) integrating a step-up converter at the output of the rectifier. The output voltage of the controller allows a 4.15V lithium battery to be charged. This converter is designed to act as an active resistor whose value adapts to match the optimum load resistance of the RF energy harvester. Nevertheless, the proposed technique requires an initial characterization of the rectenna. It is necessary to obtain the output power curves dc over a range of incident power densities and for several load resistors. The value required for the optimum resistance is determined from the curves. The system is able to recover from 8 to 420 µW from a 6 cm x 6 cm rectenna with an incident power ranging from 30 µW / cm2 to 70 µW / cm2 respectively, at 2.4 GHz. The overall efficiency of the system (integrating the converter) is 16.7% for a power density of 70 µW / cm2. This relatively low value is impacted by the addition of the dc-dc converter. Indeed, according to Figure 3.10, the overall efficiency (in %) is defined by:

$$\eta_{global} = \eta_{Rect} . \eta_{Conv} \quad \textbf{(3.1)}$$

with the efficiency of the RF-dc conversion circuit,

$$\eta_{Rect} = \frac{P_{Rect\_out}}{P_{RF\_incident}} \quad \textbf{(3.2)}$$

And the efficiency of the converter,

$$\eta_{Conv} = \frac{P_{Conv\_out}}{P_{Rect\_out}} \quad \textbf{(2.3)}$$

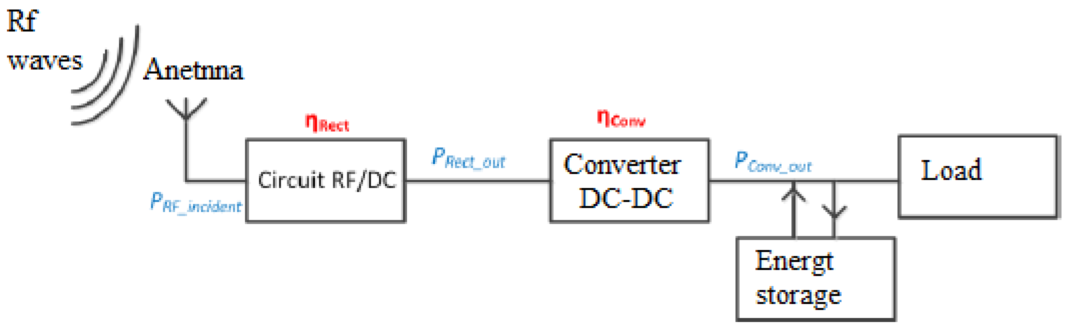

Figure 3.10 Diagram of an RF energy harvester with a DC-DC converter and an energy storage cell.

If the data of (Lee ect , 2008) are taken, the efficiency of the rectenna is 24.6% for a power density of 70 µW / cm2 and that of the converter is 77.1%. The overall efficiency is 16.7%, the addition of the converter implies an 8% drop in overall efficiency.

Therefore, the addition of a converter implies a fall in the efficiency of the system. On the other hand, this converter makes it possible to have a stable output voltage whatever the input fluctuations and makes it possible to supply the sensors or the storage cells with their nominal voltage.

3.3. Key Points in The Design of a Rectenna

The performances of a rectenna are generally evaluated in relation to the value of the conversion efficiency RF-dc and the output voltage. For a given rectenna, these two quantities depend on the choice of the load, the rectifier, the receiving antenna and the impedance matching network. In this section, we will detail the characteristics of these constituent blocks and their influence on the performance of the rectenna.

3.3.1. Preliminary remarks on the available radio frequency power density.

The performances of a rectenna are generally evaluated in relation to the value of the conversion efficiency RF-dc and the output voltage. For a given rectenna, these two quantities depend on the choice of the load, the rectifier, the receiving antenna and the impedance matching network. In this section, we will detail the characteristics of these constituent blocks and their influence on the performance of the rectenna.

3.3.2. Preliminary remarks on the available radio frequency power density.

Before starting the design of a rectenna, it is important to evaluate the density of RF power transmitted from the base stations present in the sensor environment. These data are extracted from measurement campaigns usually carried out to evaluate the population's exposure to electromagnetic fields (Kimect , 2011), (Skyworks , 511), (Xie ect , 2009). To complement these reports, raw data provided by the National Frequency Agency (ANFR) were used to calculate the statistical results presented in this section (Schreider ect , 2006).

3.3.2.1. GSM and UMTS networks

In this section, we will only detail mobile networks. The relay antennas permanently emit a signal whose power can be up to 30 Watts depending on the geographical coverage and the type of cell considered. In figure 3.11, the heights of the emission point H_e, and of the reception point H_r, and the distance d between the two points are detailed. It is important to note that the power losses are a function of both the distance d and the difference in height between these two points, Delta, (Kuhnect , 2009).

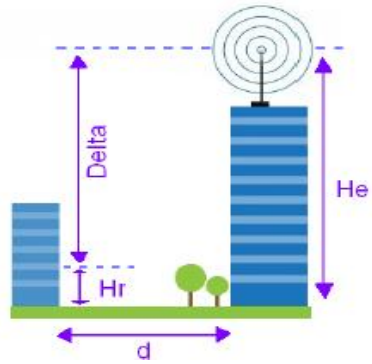

Figure 3.11 Geographical indications of measurements: d distance between transmission and reception points, Delta: difference in height between transmission and reception points.

The three predominant RF bands of all the RF base stations are the GSM900 (935-960 MHz), the GSM1800 (1805 to 1880 MHz) and the UMTS (2110-2170 MHz). The FM band was not selected because the average density recorded in town or in the countryside does not exceed 0.005 mW / m².Whether urban or rural, the GSM900 and GSM1800 base stations emit similar levels of power density. Regardless of the base station, the RF power density is 30% higher in urban than in the countryside. It should be noted that the measurement conditions between those taken in town and in the field are slightly different. This is related to the difference in emitter heights: H_e = 25 m for a microcell and 35 m for a macro cell. The higher standard deviation in the countryside implies a higher dispersion in terms of power density compared to data in urban environments. Thus, an urban environment seems to be more appropriate for the viability of an RF energy harvester. For example, in the Frei study (Hoarau ect , 2008), measurements were taken of 166 volunteers recruited from urban areas around the city of Basel (Switzerland), who carried the dosimeter for one week. The main sources of exposure are the antennas of mobile phone base station, mobile phones and phones wireless DECT.

3.3.2.2. Wi-Fi

Wi-Fi signals also appear as sources available in the environment. In France, the power delivered to the antenna of a Wi-Fi router must not exceed 100 mW (Georgiadisect, 2010). The average power actually emitted by the transmitter is much lower and varies according to the type of exchange, the size of the data to be transmitted, the throughput and the number of simultaneous users. In reality, given the architecture of the protocol, and in particular the times reserved for listening to the connected devices, the maximum average power emitted by a Wi-Fi transmitter cannot exceed half of the maximum authorized power, ie 50 mW . The data is transmitted as packets of radiofrequency signals separated by waiting or response times of the access point or the computer (Dejean ect , 2005).

3.3.2.3. Conclusions

It is possible to compare the power density as a function of the distance for the different frequency bands studied from the maximum emission power data (EIRP) to be exceeded (defined by the ICNIRP) (Georgiadisect, 2010). As Friis also demonstrates, power loss as a function of distance is faster with GSM than Wi-Fi.

The average power density in the urban environment is estimated to be 0.15 mW / m² for the GSM900 and GSM1800 and 0.05 mW / m² for Wi-Fi in buildings, based on the various measurement reports in the scientific literature. As for FM bands, their average power density does not exceed 0.005 mW / m² in urban or rural areas. Therefore, it will be preferable for the RF energy harvesting device to be located at a maximum of 300 m from a GSM station or a few meters from a Wi-Fi router.

Thus, the energy harvesting of several RF bands may be a relevant solution to increase the amount of power harvested.

The selection of a frequency band for the optimal operation of the RF energy harvesting system is crucial because it affects the size of the receiving antennas, the operating range of the system, and the design of the various building blocks. The choice of frequencies is then very important beforehand. This will determine the structure of the rectenna and in particular the design of the impedance matching network as will be seen below.

3.3.3. Impedance matching network

3.3.3.1. Principle of the impedance matching network

It is desired to supply a real load Z_L with an impedance RF generatorZ_0. The principle of maximum power transmission states that the power transfer is optimum if the impedances are adapted, ie if Z_L=Z_0 *. If the impedances are not conjugated then a part of the wave transmitted by the generator is reflected.

We might think that a combination of resistance inserted between the two impedances to be adapted could solve the problem. But most of the transmitted energy would then be dissipated in these added resistances. The solution envisaged is to use reactive components (capacitors and inductors) to limit insertion losses. In the remainder of this section, we will build an impedance matching network, taking into consideration that the rectifier input impedance is less than the impedance of the antenna.

It is desired to transform a resistor R_s into a resistor R_p with R_p>R_s. To do this, it is possible to insert a series inductance,L_s, and a capacitance in parallel, C_p , as shown in Figure 3.12. The network L_s C_p thus formed, also called L-network (Merabet ect , 2009), has been chosen for its simplicity and because it can be the basis of more complex networks.

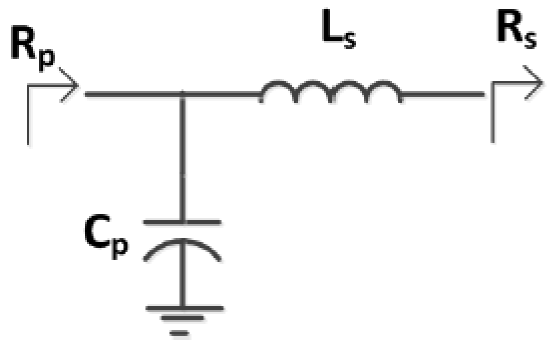

Figure 3.12 Diagram to turn a resistance R_s in a resistanceR_p.

The values of L_s and C_p are determined so as to convert R_s to R_p at the given frequency. To do this, we first calculate the equivalent admittance, Y_{eq} of the association of R_s in series with L_s and in parallel with C_p :

$$Y_{eq}=\frac{1}{R_{s+j\omega L_s}}+j\omega C_p \quad \textbf{(3.4)}$$

For R_s to be transformed intoR_p, the inverse of the real part of Y_{eq} must be equal to R_p and the imaginary part must be zero

$$R_p = \frac{{R_s}^2+\omega {L_s}^2}{R_s} \quad \textbf{(3.5)}$$

$$\frac{\omega\ C_p {R_s}^2+\omega^2 {L_s}^2-\omega L_s}{R_s+\omega^2 L_s}=0 \quad \textbf{(3.6)}$$

From these two expressions, we deduce that:

$$\omega C_p R_p = \frac{\omega L_s}{R_s} \quad \textbf{(3.7)}$$

The quality factor of the series branch, Q_s, is defined as the ratio between the imaginary part, X_s = ωL_s, and real, R_s, of the impedance of the serial branch. Similarly, the quality factor of the parallel branch is the ratio between the real part, R_p, and the imaginary part, X_p = 1 / ωC_p.

$$Q_s = \frac{X_S}{R_S} = \frac{\omega L_S}{R_S} \tag{3.8}$$

$$Q_p = \frac{R_p}{X_p} = \omega R_p C_p \tag{3.9}$$

Thus, we can deduce expressions (3.8) and (3.9) that:

$$Q_s = Q_p \tag{3.10}$$

Therefore, to have a transformation from R_s to R_p, it is necessary that the quality factors of the series and parallel branches be equal. Moreover, thanks to the expressions (3.5) and (3.8), it is possible to write the factor Q_s as a function of R_s and R_p. This factor Q_s is also called the quality factor of the network, Q, and does not depend on the network elements but on the impedances R_s and R_p as shown by equation (3.11).

$$Q_s = Q_p = Q = \sqrt{\frac{R_p}{R_s} - 1} \tag{3.11}$$

The values of the inductance and the capacitance will therefore be chosen so as to have quality factors Q_s and Q_p equal to Q. The L-network has been considered lossless, but in reality the reactive components always have a dissipative part not negligible. This will reduce the power transmission to the load. It is therefore necessary to define the efficiency of the network in order to evaluate the real performance of networks designed for insertion losses.

3.3.3.2. Efficiency of the impedance matching network

(Han,2010) defined the efficiency of a network as the ratio between the power delivered to the load and the incident power in the network. For an L-shaped network, it is possible to demonstrate that this efficiency, η, can be expressed as follows:

$$\eta = \frac{1-\frac{Q}{Q_C}}{1+\frac{Q}{Q_L}} \quad \textbf{(3.12)}$$

With Q_L and Q_C , the quality factors of the inductance and capacitance and Q the quality factor of the network defined in (3.11)

For example, the network L previously studied transformed to 50 Ω 5 Ω has a quality factor Q = 3. If the inductor quality factor Q_L, used is 10 and the capacity is 80, the effectiveness network is equal to 74%.

It is also possible to express the efficiency in the case where the impedances of the source and load are complex as illustrated in Figure 3.13 (Bullardect, 1989).

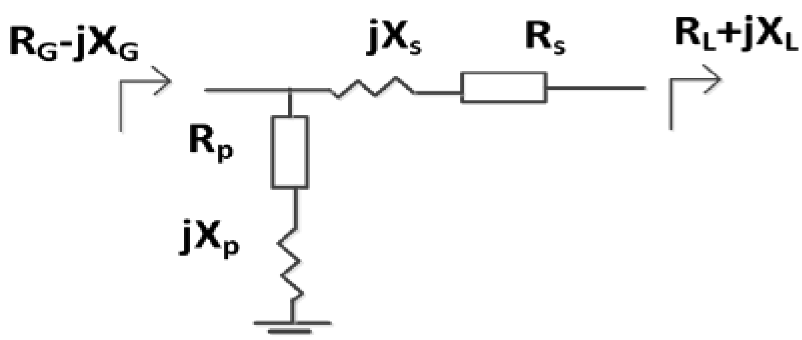

Figure 3.13 L-shaped network for adapting complex impedances.

The effectiveness is expressed as follows:

$$\eta = \frac{1-\frac{Q_p}{Q_{p\_bis}}}{1+\frac{Q_s}{Q_{s\_bis}}} \quad \textbf{(3.13)}$$

With $Q_p = \frac{R_G}{X_p}$, $Q_{p\_bis} = \frac{R_p}{X_p}$, $Q_s = \frac{X_s}{R_L}$, $Q_{s\_bis} = \frac{X_S}{R_S}$.

This expression makes it possible to estimate the efficiency of a network when the impedances are complex. With this expression, we will be able to estimate the insertion losses of the designed network.

3.3.3.3. L-band network bandwidth

The bandwidth of the impedance matching network is the frequency range for which the reflection coefficient satisfies a given criterion. Here, the frequency range considered is that for which S_{11} <-10 dB.

In order to estimate the bandwidth of L network, we simulated the S parameters of the circuit (Figure 3.14) for two values of Q: Q = 1 for a transformation from R_s= 25 Ω to R_p= 50 Ω and Q = 7 for a transformation from R_s = 1 Ω to R_p = 50 Ω. Table 3.5 summarizes the L_S and $C_p$values found for both situations.

As shown in Figure 3.1, the lower the Q factor, the wider the bandwidth. Indeed, it has gone from a bandwidth of 200 MHz to 1 GHz for a value of Q of 7 to 1 respectively. As we have shown in Section 3.2.1, the bandwidth of the L-network is related to the ratio of the input and output impedances of the system to be adapted.

This does not depend on the values of the components L_S and C_p in the case where the components are ideal.

Table 3.1 Value of network components based on Q value

Factor Q value	$R_s(\Omega)$	$R_p(\Omega)$	$L_S(nH)$	$C_p(pF)$
1	25	50	4	3
7	1	50	2.5	10

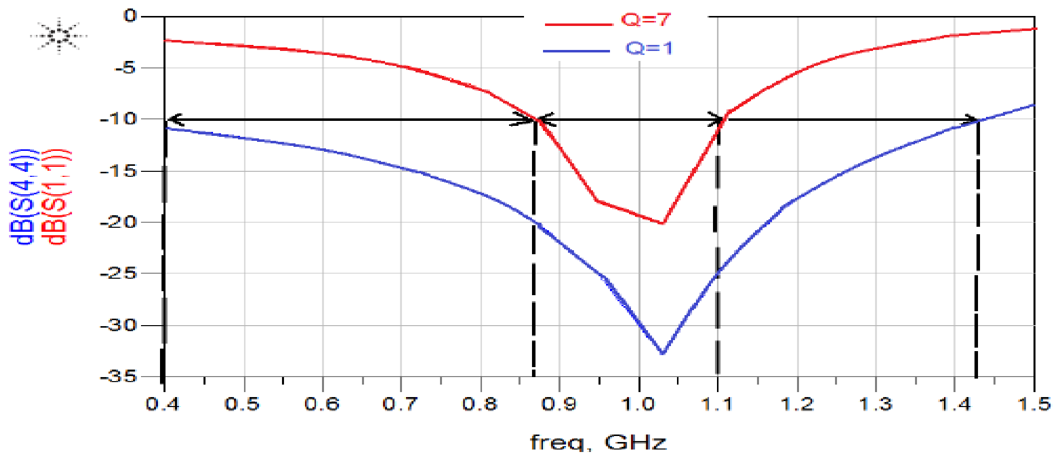

Figure 3.14 S11 as a function of frequency for Q = 1 in blue and Q = 7 in red.

3.3.3.4. Analysis of the main existing network architectures

A simple electrical model of the rectenna including an impedance matching network is shown in Figure 3.15. The antenna is modeled by an alternating voltage source V_s, with an output impedance Z_{ant}= R_s+ jX_{ant}. The X_{ant} reactive part may be capacitive or inductive depending on the design of the antenna. To achieve the maximum power transfer, it is necessary that the network input impedance, Z_{in}, be the conjugate complex of the antenna, ie. Z_{in} = Z_{ant} * = R_s-jX_{ant}. Finally, Z_L represents the complex impedance of the rectifier and of the combined load with $Z_L$and X_L the real and imaginary parts, respectively.

In the general case, adaptation networks are made up of passive elements located or distributed according to technology and frequency of work. The conjugate adaptation of the two impedances is only possible a priori in a single point of frequency.

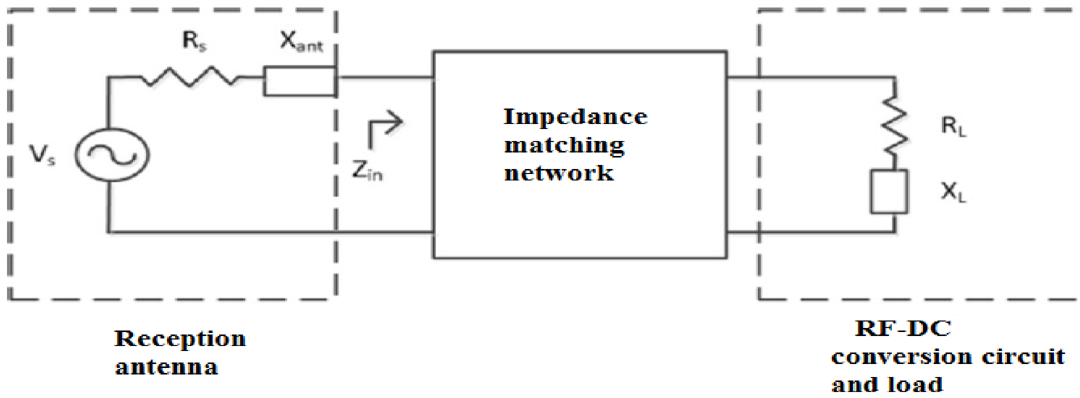

Figure 3.15 Equivalent model of an RF energy harvester.

As discussed in the previous section, one of the most commonly used matching circuits is an L-array (Erickson ect, 2001) that uses two reactive components (inductance and capacitance). Two types of L-arrays are possible: the impedance up-converting and the impedance down-converting. A transformation of a load of impedance equal to Z_L to Z_{in} impedance is considered. If the parallel element is placed on the side Z_L, then Z_{in} is less than Z_L, the network is an impedance is down-converting. On the contrary, if the element in series is placed on the side Z_L, then Z_{in} is greater than Z_L the network is an impedance up-converting. Elements may be capacitors or inductors. Figure 3.16 illustrates the two architectures.

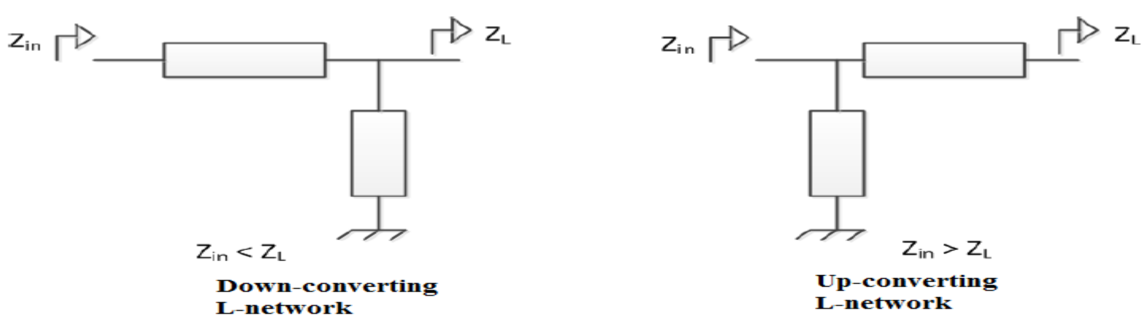

Figure 3.16 Parallel-serial architecture.

Each type of L-network makes it possible to cover part of the Smith chart. The Figure 3.17 shows the maximum impedance coverage (Z_{in}) of the two types of L-network, considering Z_L equal to 50 Ω. (Dieuleveult and Romain, 2008).

On the other hand, not all impedances are generated with the same efficiency. To illustrate this, (Dieuleveult and Romain, 2008) represented on the Smith chart the impedance coverage with an impedance boosting network (with an inductance Ls in series and a capacitor C_p in parallel). With ADS™, he varied Ls from 1 to 30 nH and C_p from 0.5 to 10 pF and he plotted the set of Z_{in} impedances at the input of the network adapted for Z_L = 50 Ω; the frequency is fixed at 2.4 GHz. As shown in Figure 3.17, there is the blue area in Figure 3.18. From the efficiency (3.12), he plotted the insertions losses corresponding to the different impedance networks found (Figure 3.19), these are expressed in dB. The quality factors of both components were set at 30.

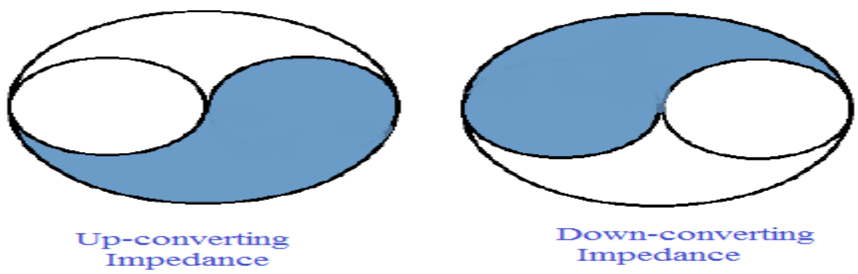

Figure 3.17 Blue zones that can be adapted either by an up-converting impedance or by a down-converting impedance (Dieuleveult and Romain, 2008)

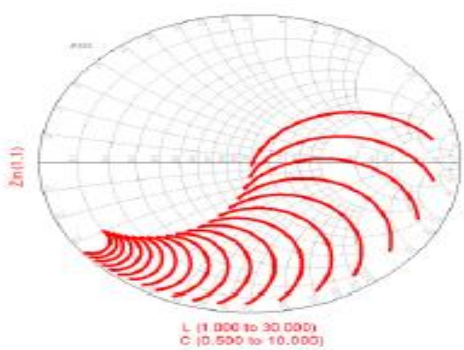

Figure 3.18 Locations of possible Z_(in)impedances with a 2.4 GHz L network (Dieuleveult and Romain, 2008).

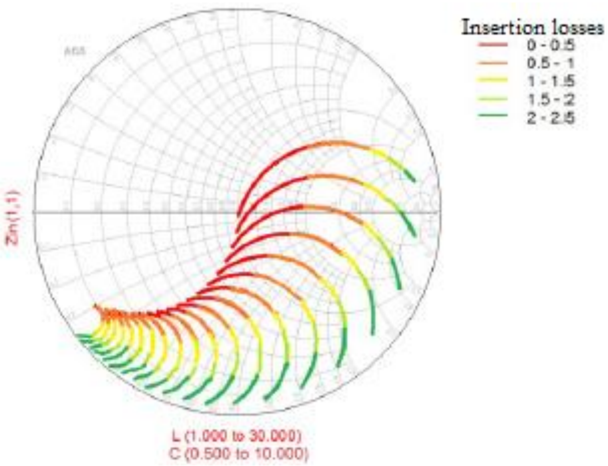

Figure 3.19 Insertion Losses for an L-network at 2.4 GHz.

Note that the network insertion losses are lower for the impedances closest to the center of the Smith chart (50 Ω) and increase when one deviates from the center. However, an L-network has no degree of freedom. As discussed in Section 3.2.2, the Q factor and bandwidth are set by the values of the impedances to be transformed. Thus, the L-network is a bit constraining, especially if you want to change the bandwidth of the network.

Cascading up-converting impedance with down-converting impedance produces the network at Π (Figure 3.20). That of down-converting and up-converting impedance produces the T-network (Figure 3.21).

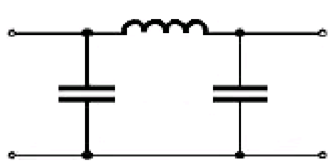

Figure 3.20 Filter in Π.

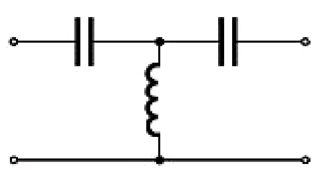

Figure 3.21 Filter in T.

When associating several L networks, the Q factors can be chosen. For example, it is desired to transform an impedance of 5 Ω to 50 Ω. An L- network has a factor Q= 7 (Figure 3.22). If two L-networks are combined in series, it is then possible to perform this transformation in two steps and to change the overall Q-factor by imposing an impedance between the two networks as shown in Figure 3.23. Thus by varying this factor Q, we can play on the bandwidth of the network.

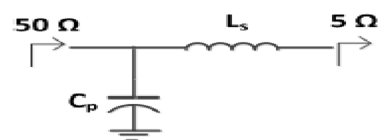

Figure 3.22 Adaptation with an L network

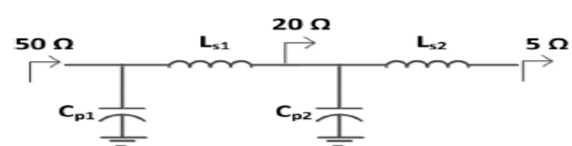

Figure 3.23 Adaptation with two L networks in series.

In addition, as demonstrated in (Hoarau ect , 2008), these networks have the advantage of ideally allowing full coverage of the Smith chart. The impedance transformation path of the adaptation network described in Figure 3.24 explains this result. In a T-network, the Z_L load is always associated with a serial element that will increase its impedance. Then the impedance will decrease again thanks to the impedance step as shown on the chart in Figure 3.24. The designer therefore has more freedom to adapt these impedances.

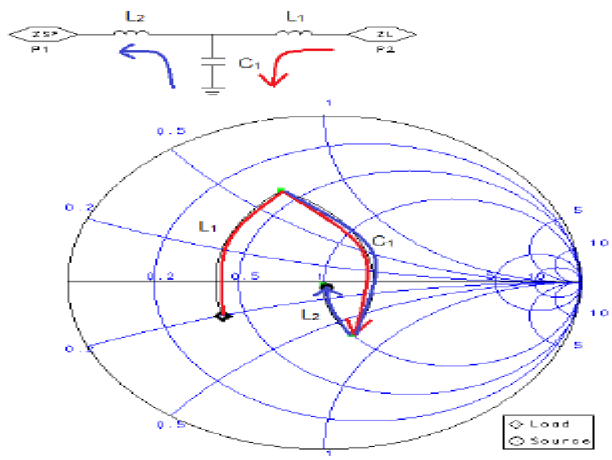

Figure 3.24 Impedance transformation path of a load with a T-network.

Therefore, the T-network (of the same Π) makes it possible to achieve a flexibility of design on the choice of bandwidth. In addition, the insertion losses are lower than for an L network (Bullardect, 1989). That's why we prefer the Π or T networks for rectenna design. The choice between Π and T will be based on the input impedance values of the rectifier.

3.3.4. Different architectures of the rectifier

An RF-dc rectifier converts the energy of the RF electromagnetic wave captured by the antenna into a continuous electrical power. This converter consists essentially of diodes and capacitors. Schottky diodes are generally used for applications whose frequency is between 800 MHz and several GHz. These diodes can also be made based on transistors. In addition, Schottky diodes have a threshold voltage two or three times lower compared to diode junction P-N, which can go down to about 150 mV (Sanyo, 2012). Finally, it is recommended to use diodes with high saturation currents, having a low junction capacitance C_j and a low resistance R_s(Huang ect, 2014).

The main rectifiers of the literature are shown in Figure 3.25. It is possible to classify them into two categories: asymmetric output rectifiers and differential output rectifiers. The first class includes: the series rectifier (Figure 3.25a), the parallel (Figure 3.29b) and the doubler (Figure 3.25c) and in the second class: the Graetz bridge (Figure 3.25d) and Greinacher (Figure 3.25e).

Output voltages and conversion efficiency (defined in section 2.4.2 equation (2.2)) of the different rectifiers were simulated according to the incident power at 0.95 GHz on a load of 11 kΩ. From Figure 3.26 and Figure 3.27, Table 3.3 summarizes the relative performance of these output voltage-based rectifiers, the RF-dc conversion efficiency, and their ability to operate at from a low incident RF power (<-10 dBm).

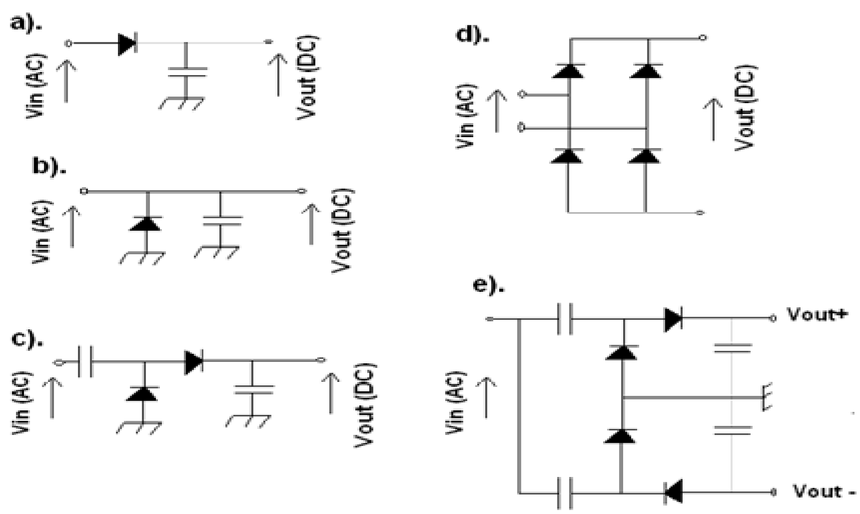

Figure 3.25 Several rectifier architectures: a). series, b). parallel, c).Double of voltage, d). Graetz Bridge e) .Greinacher.

Thus, the series and parallel rectifier are the most suitable for low power incident, ie. below -10 dBm (Haslett, 2008). Other structures such as the voltage doubler or the Greinacher have higher output voltages than the series rectifiers for an incident power greater than 5 dBm. With respect to the Graetz bridge rectifier, it can be noted that it is widely used in low frequency ac-dc converters (Nimo and Reindl, 2012). This rectifier has good power handling provided to use diodes high breakdown voltage. But because of its bridge structure, it is not suitable for low levels of incident power (Wanotayan and Torrungrueng, 2011).

Each presented rectifier has advantages and disadvantages. In the context of ambient RF energy harvesting, the RF power density is relatively low, of the order of mW / m².

Therefore, the rectifier must be able to rectify signals of very small amplitudes. Rectifiers' type series or doubler will be preferred.

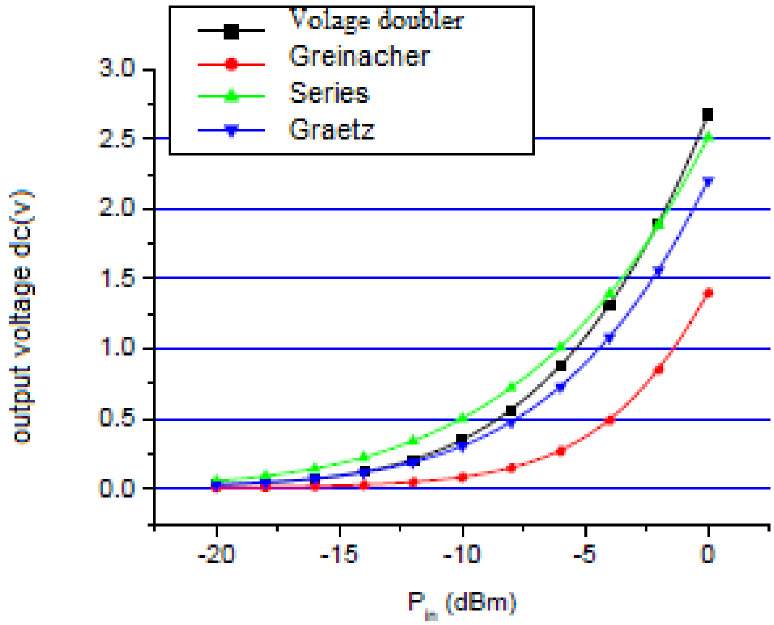

Figure 3.26 Output Voltage vs. Incident Power for 4 rectifiers: voltage doubler, Greinacher, Series and Graetz (Wanotayan and Torrungrueng, 2011).

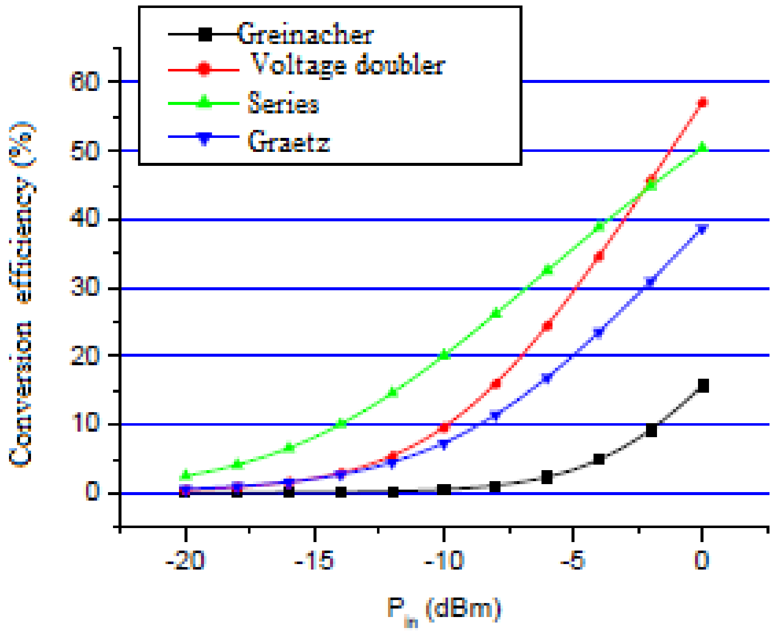

Figure 3.27 Conversion Efficiency for 4 Rectifiers: Voltage Doubler, Greinacher, Series and Graetz (Wanotayan and Torrungrueng, 2011).

Table 3.2 Relative Performance between Several Types of Rectifier.

Rectifier	Amplitude of the output voltage Dc	Starting at low incident RF power levels (<-10dBm)	Conversion efficiency
Series	+	+	++
Graetz Bridge	++	-	-
Parallel	-	+	+
Voltage doubler	++	-	-
Greinacher	++	-	-

3.3.5. Load

The load of the energy harvester represents the equivalent impedance of the sensor to be supplied. The RF-dc conversion efficiency of the rectenna and its output voltage dc vary depending on the value of the load. To illustrate this, a rectenna with a serial rectifier is simulated under ADS. The conversion efficiency is shown in Figure 3.28 as a function of the value of the R_L load. The incident power is set at -10 dBm and the incident frequency at 0.95 GHz. The conversion efficiency is optimal for a given load, here around 4 kΩ. Indeed, the adaptation network has been designed so that the maximum power is transferred for a load of 4 kΩ. Figure 3.29 and Figure 3.30 show the variation of the impedance seen from the rectifier input as a function of the R_L load. The adaptation network has been designed so that the output impedance of the network is equal to the conjugate complex is: 40+ j * 280 Ω.

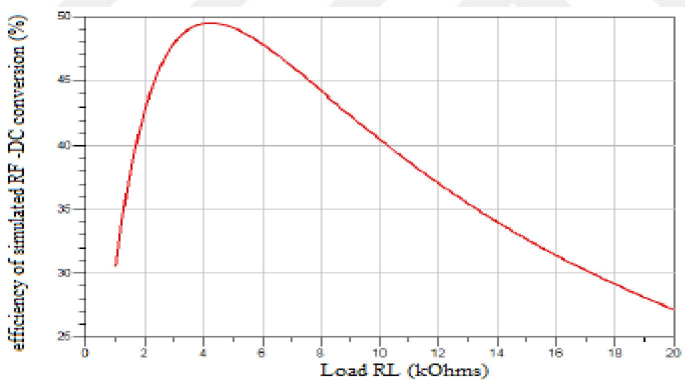

Figure 3.28 Conversion efficiency of simulated rectenna versus load with P_in= -10 dBm and F_req= 0.95 GHz.

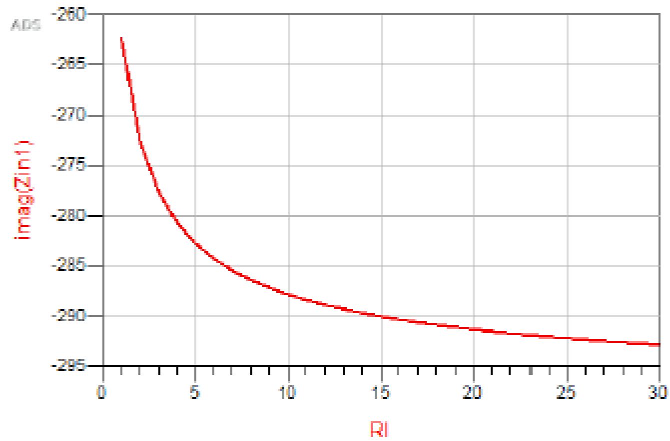

Figure 3.29 Impedance (imaginary part) view of the rectifier input as a function of RL load in kΩ.

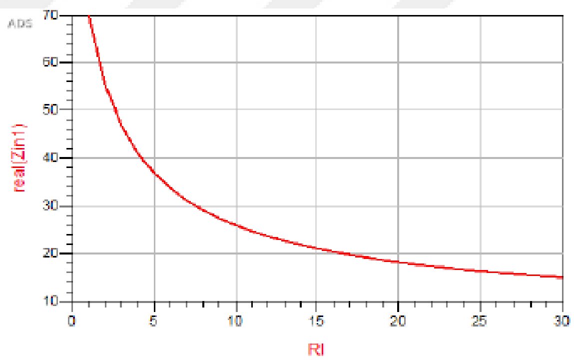

Figure 3.30 Impedance (real part) view of the rectifier input versus RL load in kΩ

In most cases, the goal is to self-power a sensor, the impedance of it is known. This load value is often the starting point for the design of the rectenna. The impedance matching network is then optimized so that the maximum of the conversion efficiency is maximum at this point.

Table 3.3 summarizes the main electrical characteristics (supply voltage, power consumption, and equivalent impedance) of several recent sensors. Note that the evolution of the supply voltage decreases and tends to about 0.3V thanks to technological advances. Their equivalent impedances range from a few ohms to a few tens of kilo ohms, which show a very wide range of values.

Table 3.3 Electrical characteristics of several sensors in the literature

Sensor Information	(Kim ect,2010) ECG	(Yo ect,2008) ECG	(Van ect,2013) Pressure	(Li ect,2013) Temperature	(Chen ect ,2010) Temperature
Supply voltage DC (V)	1.2	1.8	0.8	0.45	0.3
Energy consumption (W)	2.4m	5.8m	15µ	14µ	3.7µ
Equivalent impedance (Ω)	600	620	11k	14k	24.3k

3.3.6. Receiving antenna

In an RF energy harvesting system, the antenna plays an important role because it captures the energy of the incident RF waves. However, the power received by the antenna depends on several factors such as its bandwidth, effective surface, directivity, beam incidence and polarization. Finally, the complete implementation of the antenna must aim to achieve a minimum of losses.

3.3.6.1. Challenges of the antenna

The RF power density study in Section 3.1 has shown that the GMS900, GSM1800, UMTS and Wi-Fi frequency bands are predominant in an urban environment. That is why it is interesting to design an antenna that is able to cover these different frequency bands. In addition, the propagation aspects are to be considered, such as beam incidence on the antenna and low energy levels. Whether in an outdoor or indoor environment, we are forced to multipath phenomena, diffraction or obstruction of the signal by various obstacles such as the walls of buildings. Multiple reflections, when for example the incident signal reflects on several surfaces with an angle of incidence other than normal, can depolarize the signal received at the rectenna. Under these conditions, the use of a polarization diversity antenna would make it possible to overcome these problems (Kawahara ect, 2009).

3.3.6.2. Antennas used in the rectennas

In the case of mono band rectennas, linearly polarized antennas or circular were made (Erickson ect, 2001), (Masotti ect, 2013), (Heikkinen and Kivikoski , 2003), (Phongcharoenpanich ect , 2013).

An interesting example is that of (Olgun ect, 2012) for which a circular patch at 2.45 GHz has been designed with a bandwidth of 200 MHz. As shown in Figure 3.30, two circular slots are placed at an angle of inclination of 45 ° to the vertical diameter of the circular patch. The parameters of the two slots, ie the size and the distance from the center of the disk, are determined so that the larger the size of the two slots, the lower the resonant frequency, and the shorter the distance of the two slots relative to the center of the patch is long, the higher the high resonance frequency.

The designed antenna provides left circular polarization. The minimum of the measured axial ratio is 1.5 dB at 2.455 GHz with a 3 dB bandwidth of 30 MHz and the maximum gain was measured at 3.36 dBi.

Circular polarization allows the antenna to receive the waves in any plane as well as to overcome the problem of depolarization losses that linear polarized waves may encounter. But the implementation of the antenna feed point designed in (Olgun ect, 2012) is a complex realization. This point must be placed at the desired frequency to produce two orthogonal polarizations with the same amplitude, but with a phase difference of 90°.

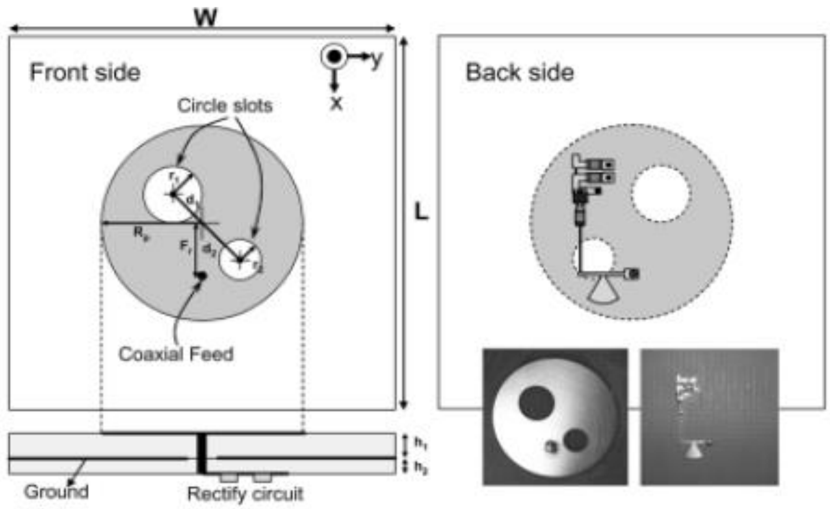

Figure 3.31 Circular patch antenna and rectifier (Olgun ect, 2012).

Another example of a rectenna designed with a circular polarized antenna and adapted this time to two frequencies, 2.45 GHz and 5.8 GHz, is presented in (Heikkinen and Kivikoski , 2003). Two short-circuit-shaped slits are proposed (Figure 3.32). The gain of the simulated antenna is 4.5 dBi at 2.45 GHz and 3.7 dBi at 5.8 GHz. A minimum axial ratio of 2.2 dB at 2.45 GHz and 1.3 dB at 5.6 GHz was measured. A rectifier is associated with each slot and for each frequency, the converted power is recovered separately.

The circular polarization and the two-frequency adaptation of the antenna are two interesting parameters. But the collection of the output power dc on two different branches is much less because the overall prototype is not compact and the combination dc may cause a lot of losses on the final circuit.

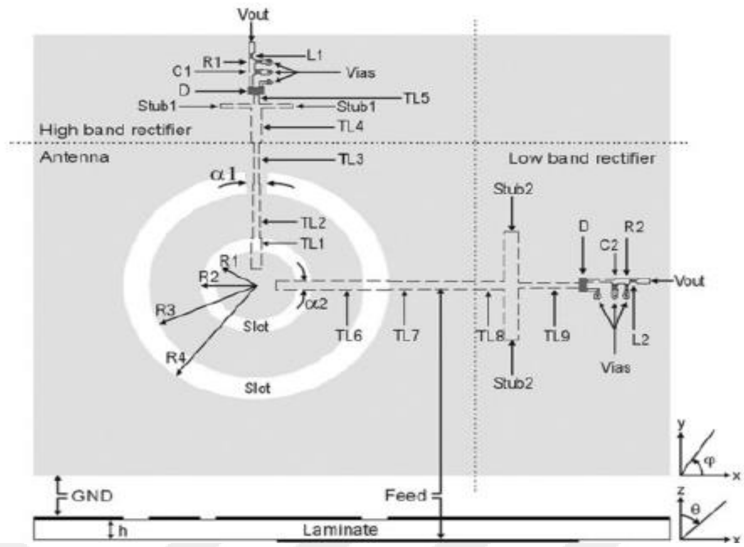

Figure 3.32 Slotted antenna (in the form of a short-circuited loop) and associated rectifier (Heikkinen and Kivikoski , 2003).

3.3.6.3. Circular polarized multi-band antenna

The presence of several communication standards in the urban environment is why we examined multi-band antennas. The idea is to design an antenna operating in the four GSM900, GSM1800, UMTS and Wi-Fi and circularly polarized to overcome the depolarization problems of the incident electromagnetic wave mentioned above. On the other hand, the antenna must have a single output port, in order to simultaneously inject into the conversion circuit, the power recovered in each of the bands. The circular polarization can be generated by exciting two linearly polarized orthogonal waves that are in phase quadrature and have equal amplitudes. Therefore, the power supply of this type of antenna may require a double excitation input or a divider, which increases the size and complexity. For example, a square piece can generate a circularly polarized wave by feeding on two sides of the square, as shown in Figure 3.33a. Another method is to introduce a small perturbation in the antenna which produces two orthogonally polarized elements with the same amplitude and phase shifted by 90 °. An example of this method is to truncate a square or a circular piece, as shown in Figure 3.33b-c. The modifications are implemented on the feeding position by drawing it in a cross shape for example (Figure 3.34). The phase shift of 90 ° is obtained by playing on the lengths of the cross.

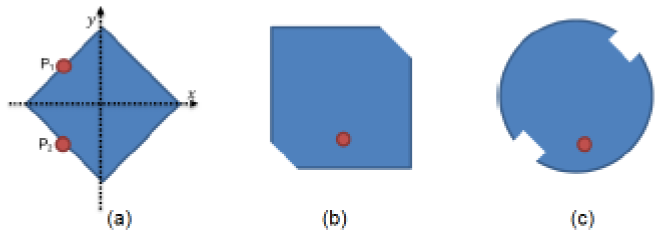

Figure 3.33 Power point on a (a) patch, (b) square, or (c) circular for a circular polarization

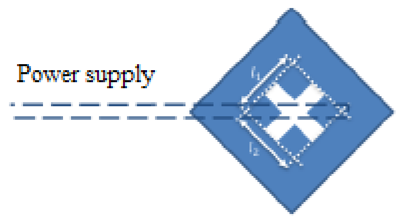

Figure 3.34 Changing the power of a square patch for circular polarization.

Another possible method is to design antennas called non-resonant antennas. These are excited by a current that is constructed by the incident waves and reflected with equal amplitudes and with a phase difference of 180 °. As an example, we can name the helix antennas (Yo ect , 2008), loop (Supelec, 2015) or spiral Archimedes (Collado and Georgiadis, 2013).

These antennas emit circularly polarized waves when the circumference of their wire is of the order of magnitude of the wavelength because the points which are distanced at a quarter wave have a phase difference of 90 ° and the currents are orthogonal with almost equal amplitudes.

Following this analysis and in view of the needs explained at the beginning of this section, we have restricted our field of study for the antenna. It seems that the antenna shaped nested loops is an interesting solution.

3.4. Conclusion

In this chapter, the basic principle of a rectenna has been introduced. Two blocks optional are also detailed: the energy storage cell and the dc-dc converter. Their interest is all the greater as the RF power density present in the environment is weak, of the order of milliwatt per m². Several architectures for the Multi-frequency RF energy harvesting have also been studied.

We then went on to discuss the key points in the design of a rectenna. The study on the levels of the RF power density present in the environment has highlighted the predominant frequency bands such as the GSM900, GSM1800, UMTS and Wi-Fi. From these data, we can conclude that harvesting of energy on several frequencies is an interesting solution. In one environment for which the RF sources are not controlled, have the possibility of harvesting energy over a broadband allows for more flexibility and more probability important to recover the frequency bands present.

In this chapter, we also studied the design of adaptation network impedance. If we wish, as in our case, to obtain an adaptation on a band of Frequency, networks in Π or T are preferred. Moreover, given the impact of the value of the charge on the conversion efficiency, it is better to know at the beginning of the design of the rectenna what is the sensor to feed.

Finally, we explained what could be the most appropriate antenna to be able to capture several frequencies in the urban environment and the circular polarization multi-band antenna seems to be an interesting solution.

After setting up the different points to design our rectenna, we will propose, in chapter 4, innovative solutions explained here and that can harvest the maximum amount of RF energy present and for low levels of RF power density, of the order of 1 mW / m².

4. RESULTS AND DISCUSSION

4.1. Introduction

In the previous chapter, particular attention was paid to each of the blocks constituting the rectenna. Dc voltage and RF-dc conversion efficiency are directly impacted if the architectures are not chosen in a relevant way.

In this chapter, two multiband RF energy harvesters are designed. At first, the architecture and the different parts of the rectenna are chosen and explained. The first rectenna designed to harvest energy on a wideband from 1.8 GHz to 2.6 GHz.

Then, a study on the summation of the different contributions of RF branches of the rectenna will be conducted to improve the RF-dc conversion of a multiband rectenna. Based on the architecture thus found, a second rectenna will be presented. It is adapted to operate on the following four frequency bands: GSM900, GSM1800, UMTS and Wi-Fi.

4.2. Conception of the Rectenna

The different building blocks of the rectenna are detailed in this section: the global architecture, the rectifier and the impedance matching network. The important points of Chapter 2 have been taken into account in the choice of these circuits.

4.2.1. Overall architecture chosen

Figure 4.1 illustrates the architecture of multiband rectenna. The association of Impedance matching network, rectifier and dc filter constitutes an RF branch. The number of RF branches of the rectenna architecture is not limited. The receiving antenna is a broadband antenna and is connected to the input of the circuit. This type of antenna provides a more compact structure than an association of antennas input. In order to improve the RF-dc conversion efficiency, the circuit must take into account the impedance matching constraints of the various components concerned, namely the rectifiers and the receiving antenna. To match each rectifier at the selected frequencies, bandpass impedance matching networks are used. The bandwidth is chosen to cover the entire spectrum of RF power density in a standard RF band such as GSM900, GSM1800, or other. All RF signals are blocked by a low-pass filter to allow only the DC component to pass through the output load. Finally, the outputs of the RF branches are connected together to sum the different continuous contributions.

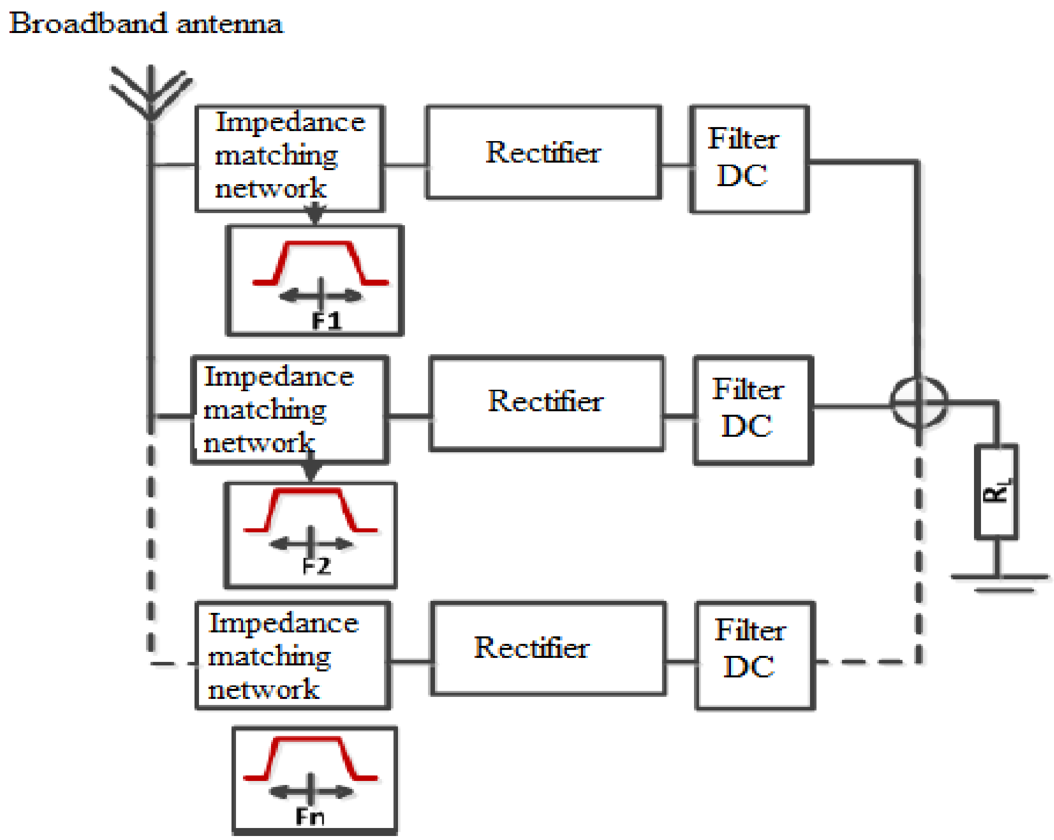

Figure 4.1 Architecture retained for the broadband RF energy harvester.

4.2.2. Choice of rectifier and Schottky diode

It has been studied in chapter 3 section 3.3 that the choice of the rectifier topology involves a compromise between the output voltage level, the incident power and the RF-dc conversion efficiency. In the ambient environment, the level of RF power density is generally low. Thus, the optimal compromise is the series structure (Kuhn ect , 2013). Indeed, the series rectifier has a single threshold that corresponds to that of its single diode.

The choice of the Schottky diode is very important when designing the rectifier. One of the key parameters is its VTH threshold voltage. When only low levels of power are available in the environment, the amplitude of the incident signal may be close to this voltage or even below. Below this voltage value, the diode no longer conducts and losses become predominant (Merabet ect , 2009). One solution to overcome this problem is to use low VTH Schottky diodes, also called "zero bias" diodes. In the literature, many prototypes are designed with the Schottky diode SMS7630 (Sun ect , 2013). This diode has a threshold voltage of 150 mV. Another diode having the same VTH is the MSS20-141 diode and is used in commercial dosimeters. The parameters of the two diodes are given in Table 4.1. We can notice that the internal resistance, Rs, is quite high, of the order of 20 Ω for the two diodes. This value depends mainly on the diode technology, such as the metal used, the N + doping assay or the surface of the diode. The conversion efficiency, η, is defined as:

$$\eta = \frac{P_{dc}}{P_{in}} \qquad \textbf{(4.1)}$$

Where P_{dc} is the output power dc and P_{in} is the RF input power.

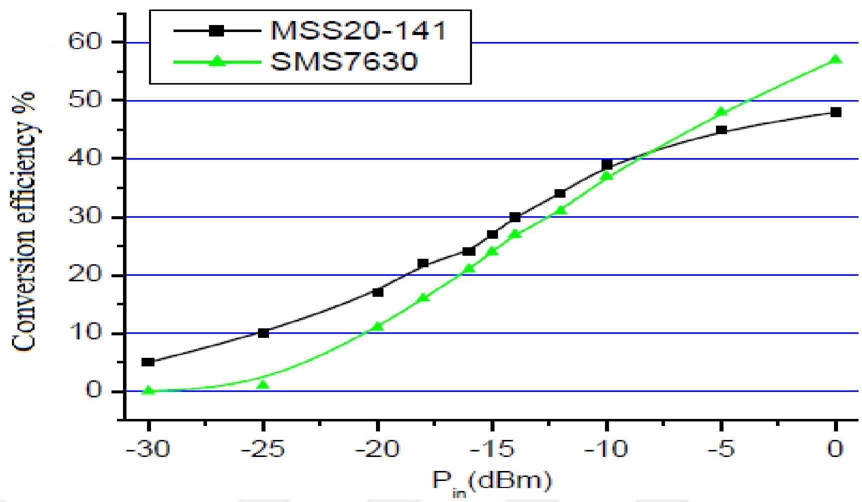

Figure 4.2 Efficiency of conversion Rf-dc simulated as a function of the incident power for two rectifiers comprising either a diode MSS20-141 or SMS7630.

The two most interesting diodes for our case study are Schottky diodes MSS20-141.B10D and SMS7630. The SPICE parameters for each are detailed in Table 4.1. The diode that has been selected for the prototype embodiments is the diode MSS20-141.B01D.

Table 4.1 SPICE model of Schottky diode MSS20-141 and SMS7630

Parameters	Description	SMS7630	MSS20-141	Unit
Bv	Reverse breakdown voltage	2	7.0	v
Cj0	Junction capacitance at zero bias	0.14	0.08	pF

Eg	Band-gap energy	0.069	0.069	eV
Is	Reverse saturation current	5E-6	3.6E-6	A
N	Emission Factor	1.05	1.25	
Rs	Parasitic series resistance	20	20	Ω
Pb(VJ)	Junction potential	0.3	0.15	V
Pt(XTI)	Saturation current temperature exponent	2	2	
M	Junction coefficient of variation	0.4	0.5	

4.2.3. Design method of the impedance matching network

The maximum power is transferred to the load if the complex impedance of the source is equal to the combined complex impedance of the load. As explained in Chapter 3 Section 3.2, this result is achieved by inserting an impedance matching network between the receiving antenna and the rectifier. The most frequently used adaptation networks are the L, Π or T (Boret , 1999) network. We recall that the quality factor, Q which is the ratio between the energy stored in the network and the energy dissipated, is an important parameter. Indeed, a high value of Q means a small amount of dissipated energy but also a narrow bandwidth (chapter 3 section 3.2).An RF branch constituting the rectenna is shown in Figure 4.3. The receiving antenna is modeled by a simple resistor Ra. The rectifier used is the series rectifier associated with an LC filter which acts as a dc filter. A resistor, R_L 430 Ω, models the sensor to power. This value corresponds to average equivalent impedance for several sensors found in the scientific literature (Wong ect, 2008), (Joonsung ect, 2011).

To design the impedance matching network, it is first necessary to determine the input impedance of the rectifier, Z_{rect}.

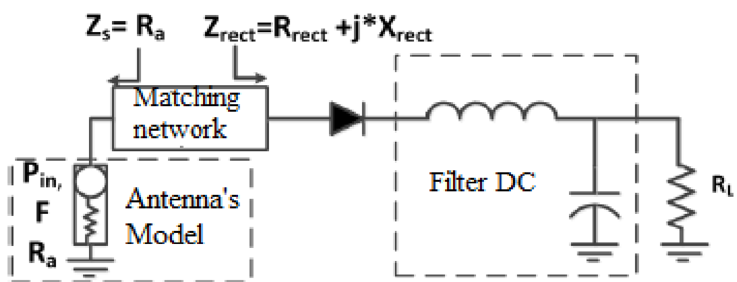

Figure 4.3 An RF Branch of the Modeled RF Energy Harvester.

As discussed in Chapter 3, Section 3.2, en or T networks provide more flexibility for the designer and provide better adaptation over a given frequency band. If it is assumed that the impedance of the antenna is set at 50 Ω whatever the frequency, it is noted that the input impedance of the rectifier is always lower than that of the antenna. According to Chapter 3 Section 3.2, the most suitable network is the network in T.

The designed adaptation network is shown in Figure 4.4. In order to increase the width of the band and to eliminate unwanted high frequencies, a capacitor C3 with an inductance L3 replaces the capacitor in parallel with the T-filter.

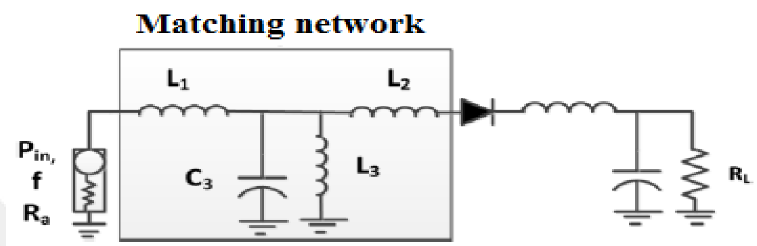

Figure 4.4 Model of the designed RF branch.

The impedance matching network is therefore composed of four components. Practically unlimited combinations of inductance and capacitor values can be used to achieve the desired impedance matching. Thus, an optimization process is necessary to quickly choose different component values.

The objective is to calculate the values of the matching network components such that the maximum power is transferred from the receiving antenna to the load in the selected RF band. Considering the circuit of Figure 4.5, the impedance of the receiving antenna seen by the matching network is equal to R_a . The charge here is the rectifier input impedance modeled by Z_{rect}= R_{rect} + j $*X_{rect}$.

The voltage transfer function, H (ω, Q), can be expressed as a function of the quality factor, Q, (4.1). In addition, network components were expressed as a function of Q (4.6). It should be noted that L3 depends on the bandwidth of the adaptation network, Bwidth, which is another degree of freedom in design.

$$|H(\omega,Q)| = \frac{2(\frac{R_{rect}}{R_a}+1)Q-2(\frac{4\,Q^2R_{rect}}{R_a}-(\frac{R_{rect}}{R_a}-1)^2)}{\left\{4\left[\left(\frac{R_{rect}}{R_a}+1\right)^2Q-\left(\frac{R_{rect}}{R_a}+1\right)\left(\frac{4Q^2R_{rect}}{R_a}-\left(\frac{R_{rect}}{R_a}\right)^2\right)-\left(\frac{R_{rect}}{R_a}-1\right)^2Q\omega_P{}^2\right]^2+..\left[\left(\frac{R_{rect}}{R_a}-1\right)^2(3\omega_P-\omega_P{}^3)+\left(2\left(\frac{R_{rect}}{R_a}+1\right)Q-\frac{8Q^2R_{rect}}{R_a}\right)(3\omega_P-\omega_P{}^3)\right]^2\right\}^{\frac{1}{2}}} \quad \textbf{(4.1)}$$

For $\omega_p = \omega/\omega_c$ and Q= $\frac{1}{2}(\frac{X_{L1}}{R_a} + \frac{X_{L2B}}{R_{rect}})$

$$L_1 = \frac{R_{rect}(2Q_0 - \sqrt{\frac{4{Q_0}^2 R_{rect}}{R_a} - (\frac{R_{rect}}{R_a} - 1)^2}}{\omega_c(1 - \frac{R_{rect}}{R_a})^2} \tag{4.2}$$

$$L_2 = \frac{R_{rect}(2Q_0 \frac{R_{rect}}{R_a} - \sqrt{\frac{4{Q_0}^2 R_{rect}}{R_a} - (\frac{R_{rect}}{R_a} - 1)^2}}{\omega_c(1 - \frac{R_{rect}}{R_a})^2} - X_{rect} \tag{4.3}$$

$$C_3 = \frac{2Q_0}{\omega_c R_{rect}(1 + (\frac{L_1}{R_a})^2)} \tag{4.4}$$

$$L_3 = \frac{B_{width}}{4\pi^2 C_3 {F_s}^2} \tag{4.5}$$

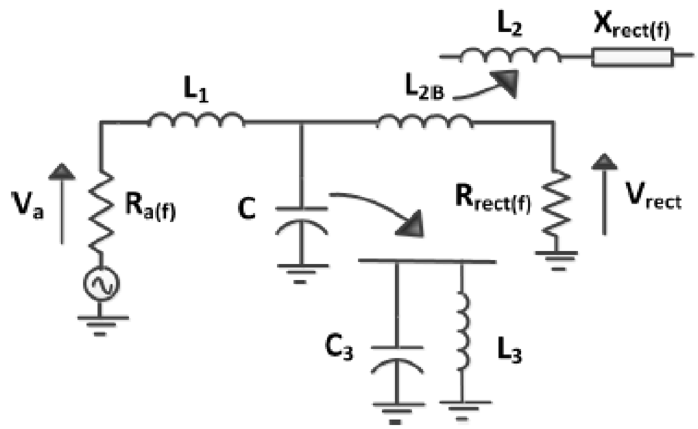

Figure 4.5 Modeling the impedance matching network.

From these equations, two combinations were found and are summarized in Table 3.2. In order to illustrate the degree of freedom over the choice of bandwidth, the scheme of Figure 4.8 was simulated to fit the impedance Z_L = 20 250j Ω at R_a= 50 Ω.

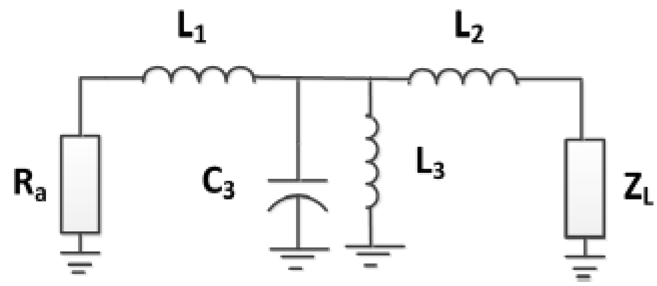

Figure 4.6 Simulated network diagram under ADS.

Table 4.2 Summary of the values of the 2 networks found for the impedance matching of the example

Network name	L1	L2	L3	C3	Bandwidth (MHz)
1	10	12	10.5	0.5	350
2	11	10	12.5	0.5	250

The study of chapter 3 on the insertion losses of an L-shaped network showed us that the efficiency of the network depends on the quality factor of the components. The proposed network, which is the combination of two L-shaped networks, therefore has its effectiveness which depends on the quality factors of its components. The more the impedance to be adapted is moved away from 50 Ω, the higher the insertions losses will be and are estimated at 2.3 dB in simulations (for quality factors of the order of 30). To reduce these losses, it would be necessary to use components with high quality coefficient (such as the use of MEMS for example) and replace where possible some components with distributed elements. The impedance matching network is therefore composed of four components. Practically unlimited combinations of inductance and capacitor values can be used to achieve the desired impedance matching. Thus, an optimization process is necessary to quickly choose different component values. For this, it is possible to use the ADS optimization option.

4.3. Realization of a First Prototype Adapted on Three RF Bands and Experimental Results

4.3.1. Design of the multiband prototype

This prototype has been designed to be adapted to three frequency bands: GSM1800, UMTS and Wi-Fi. The GSM1800 frequency band extends from 1710 to 1880 MHz (including the Down Link and the Up Link), that of UMTS from 1920 to 2170 MHz (including the Down Link and the Up Link) and finally that of Wi-Fi from 2.41 to 2.48 GHz. These bands were selected because they are predominant frequencies in an urban environment (see chapter 3 section 3.1).The schema of simulated rectenna under ADS with Harmonic Balance Mode is shown in Figure 4.10. The selected Schottky diode is the Metelics MSS20-141 diode. The output dc filter is composed of an inductance of 3.3 nH and a capacitor of 68 pF. These values were determined by simulation to obtain a DC output voltage. The antenna impedance, Ra, is set at 50 Ω in the three RF bands. The load is a resistance of 430 Ω.

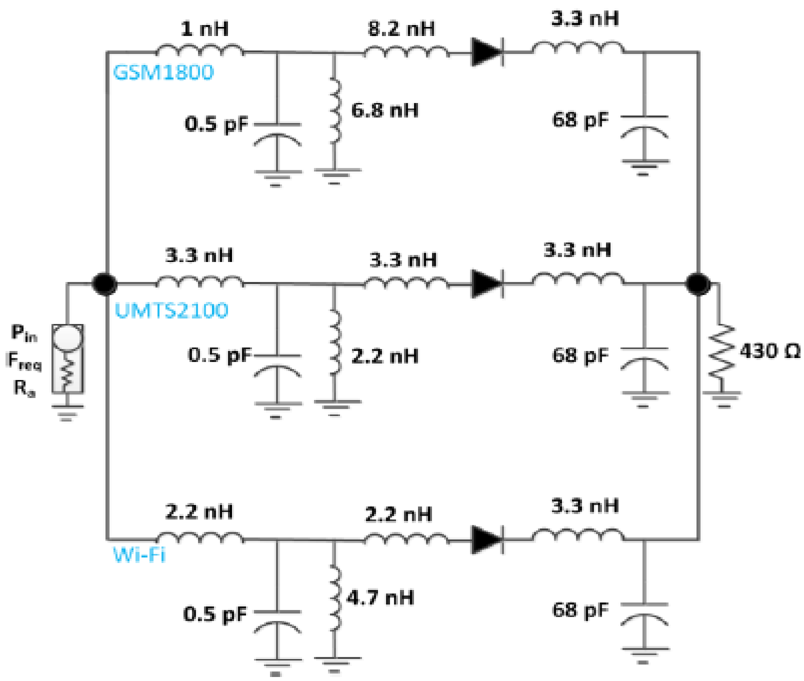

Figure 4.7 Diagram of the rectenna

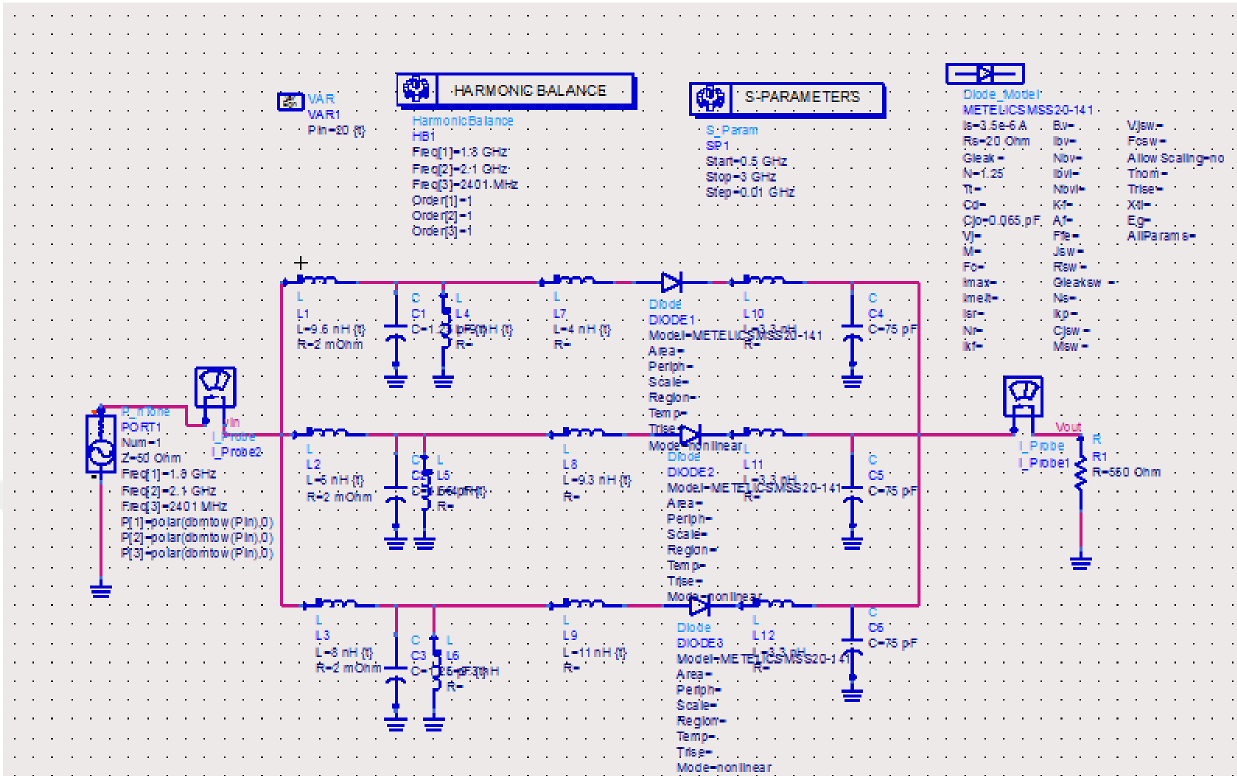

Figure 4.8 Diagram of the rectenna simulated with ADS.

This method therefore makes it possible to obtain a first estimate of the values of the network components. The values found do not necessarily correspond to those of standardized localized elements. A readjustment is therefore necessary, so we used the Tuning in Advanced Design System method. The capability of Advanced Design System (ADS) tuning enables to change one or more design parameter values and quickly see its effect on the output without re-simulating the entire design. The final values of the components of the three networks are shown in Figure 4.9. The output voltage of the rectenna with these component values was simulated as a function of frequency and is also shown in Figure 4.10. The coverage of the frequency band ranges from 1.8 to 2.6 GHz.. The three frequency bands overlap as shown in Figure 4.9 and thus achieve a single broadband.

Inductances and capacitors can be realized in localized or distributed technology. The choice depends on the working frequency and the values of the components. (Boret , 1999).

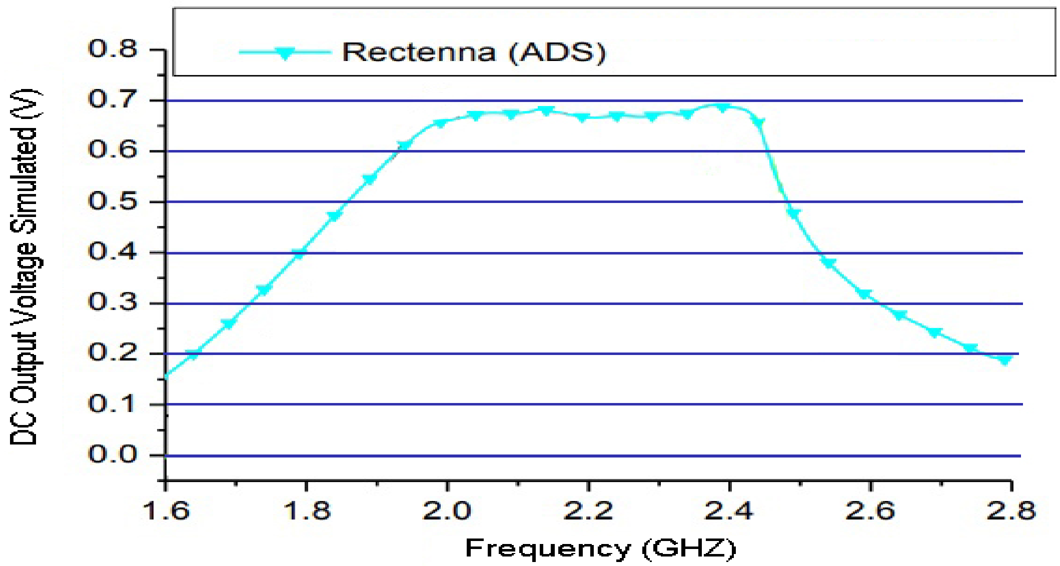

Figure 4.9 Simulated DC Output Voltage

The maximum of 0.6V output voltage is achieved at -20 dbm input power for 430 Ω load value.

The efficiency is calculated from the obtained output voltage using the following equation:

$$\eta(\%) = \frac{V^2{}_{out}}{R_L * P_{in}} \times 100 \quad \textbf{(4.6)}$$

Where P_{in} is the applied RF signal in mW , V_{out} is the obtained output DC voltage and $R_L$is the load value .

The maximum efficiency of 15% is achieved at the operating frequencies 1.8 Ghz , 2.1Ghz and 2.4 Ghz for -20 dbm input power .

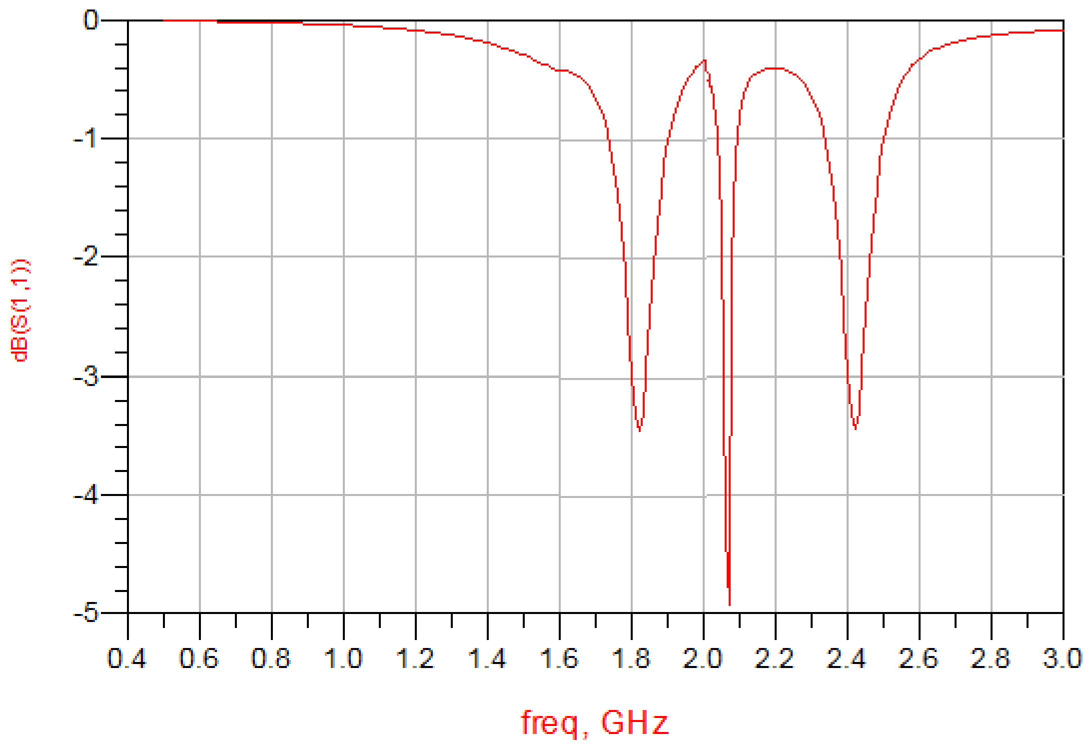

Figure 4.10 Simulated reflection coefficient with respect to frequency

The rectenna radiates best at 1.8 Ghz , 2.1 Ghz and 2.4 Ghz where $S_{11} = -3.5\ db\ and -5\ db$ at other frequencies the rectenna will radiate virtually nothing as S_{11} is close to 0 db so all the power is reflected .

4.3.2. Issues related to the presented architecture

The rectenna thus designed makes it possible to harvest energy from several RF bands and presents satisfactory results for feeding small sensors. Nevertheless, a way of improvement has been studied on the summation of contributions from the three RF branches.

Indeed, the summation of several RF branches can directly affect the overall efficiency of the rectenna (Collado and Georgiadis , 2013). The contributions dc of several rectifiers can be summed in two different ways according to its type of output, either asymmetrical (single ended) or differential. Figure 4.11 shows the two possibilities for summation.

The total power harvested with the "asymmetric type" summation is lower than that of "differential type" (Shinohara and Matsumoto, 1998). This is because a summation of dc outputs of differential rectifiers creates less interference between the RF branches than an "asymmetric type" connection (Miura and Matsumoto , 2001).

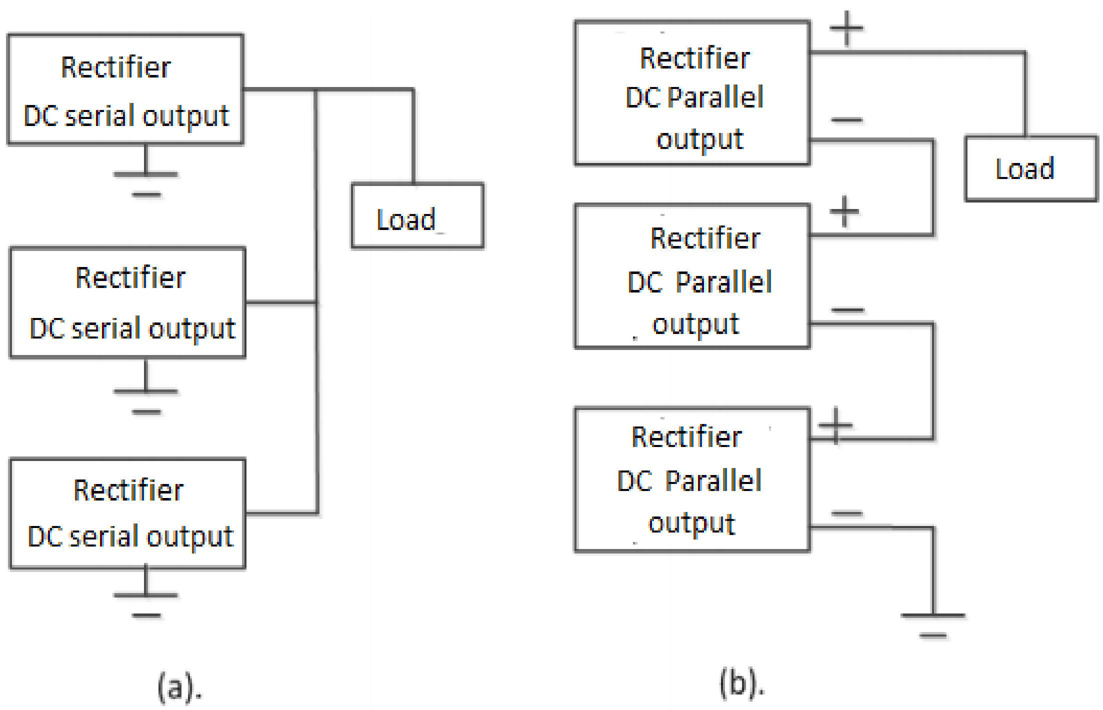

Figure 4.11 Two options for summing DC contributions: (a) with rectifier having asymmetric output, (b) with rectifiers having a differential output.

To illustrate this point, the overall efficiency of the rectenna is studied according to the state of the three RF branches. The objective is to see the impact of an inactive branch and thus to detect possible interferences between branches. The RF circuit shown in Figure 4.12 is used for ADS simulations. Either the Wi-Fi branch, or the UMTS or GSM1800 branch is idle, ie the incident power is -50 dBm. For the other two active branches, the incident power varies between -20 and 0 dBm.

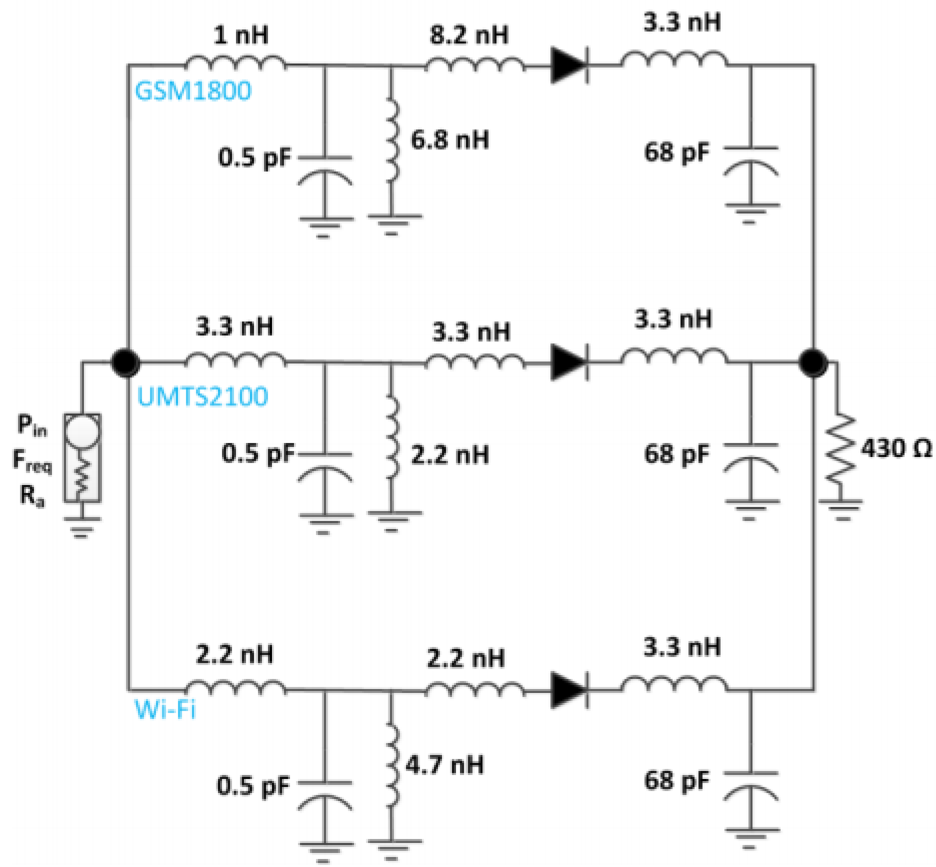

Figure 4.12 ADS diagram of the RF energy harvester

Figure 4.13 shows the RF-dc conversion efficiency as a function of the incident power imposed on each of the two branches. Efficiency differs by a few% depending on the inactive branch (Wi-Fi, UMTS or GSM1800). This result confirms the existence of interference between RF branches.

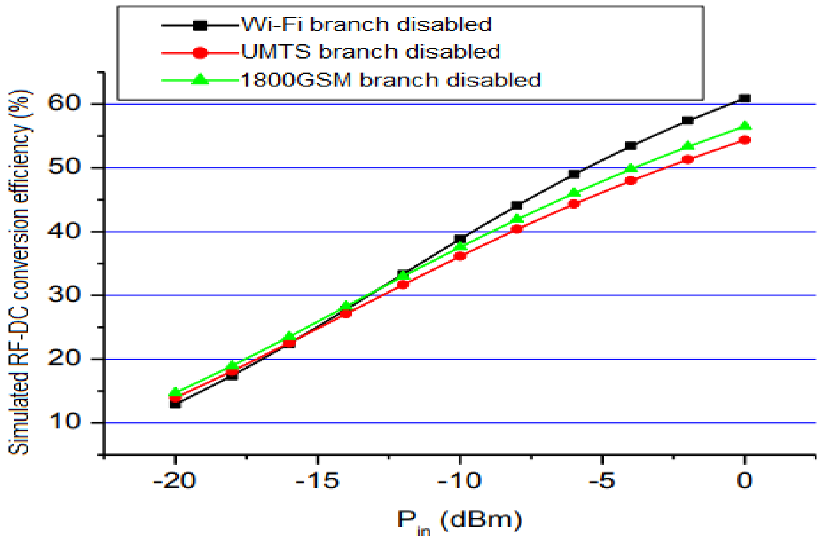

Figure 4.13 Simulated RF-DC Conversion Efficiency versus Power Incident P (in)for a disabled RF branch (Wi-Fi, UMTS or GSM1800).

Thus, because of their asymmetrical output, the series and doubler rectifiers are not necessarily the most suitable for the chosen rectenna architecture. Thanks to its differential output, the Greinacher rectifier is a good candidate. The output voltages of several stacked Greinacher can be summed without creating interference between each RF branch. The inactive RF branch is not seen as a load for the entire circuit. This time, the series rectifiers in Figure 4.12 are replaced by Greinacher rectifiers as shown in Figure 4.14. Either the wireless branch, or UMTS or GSM1800 branch is inactive, ie the incident power is -50 dBm.

For the other two active branches, the incident power varies between -20 and 0 dBm. As shown in Figure 4.13, the RF-dc conversion efficiency is not disturbed if a branch is disabled, regardless of the branch.

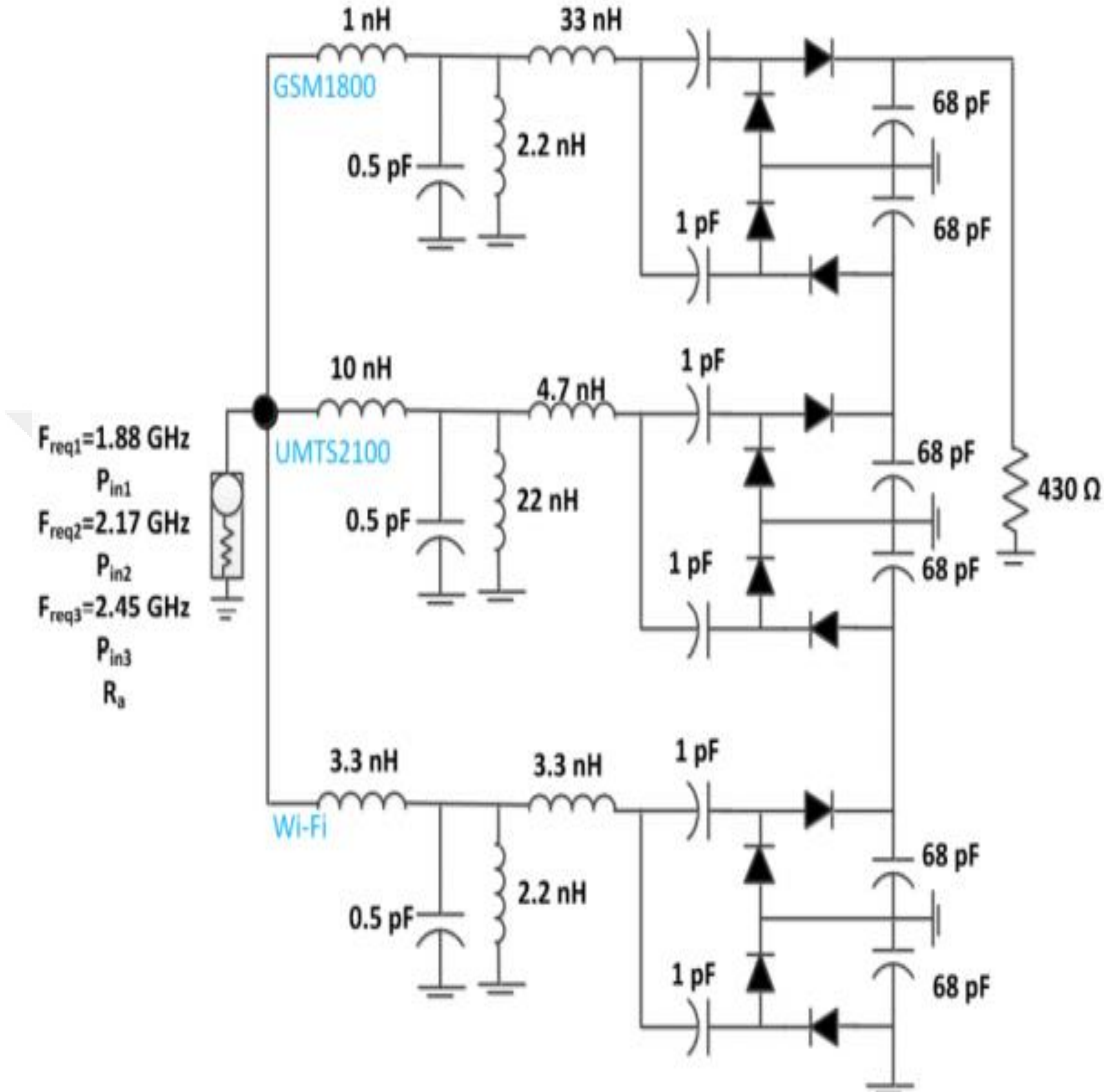

Figure 4.14 Rectenna diagram with Greinacher Rectifiers.

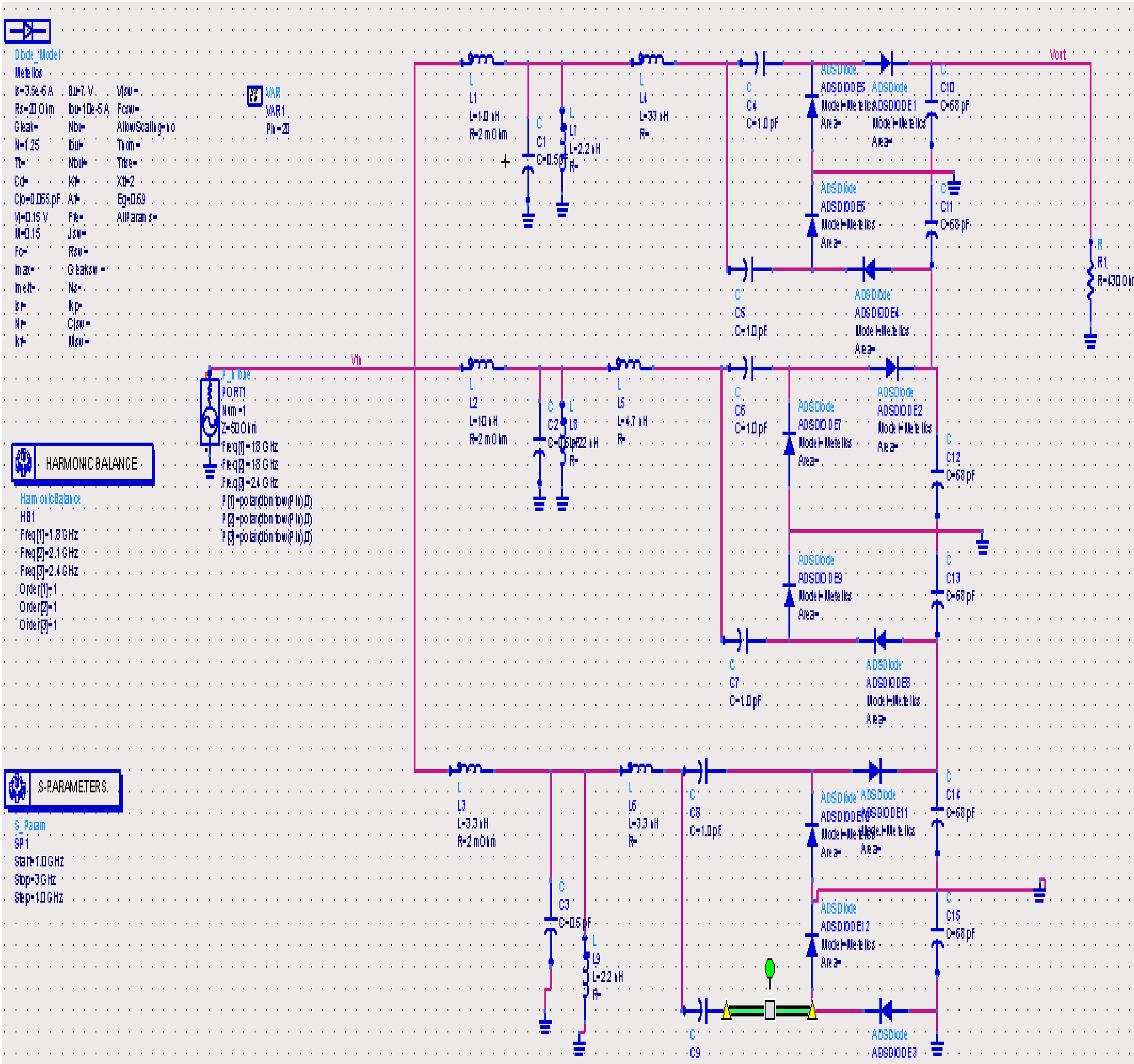

Figure 4.15 Rectenna diagram with Greinacher Rectifiers with ADS.

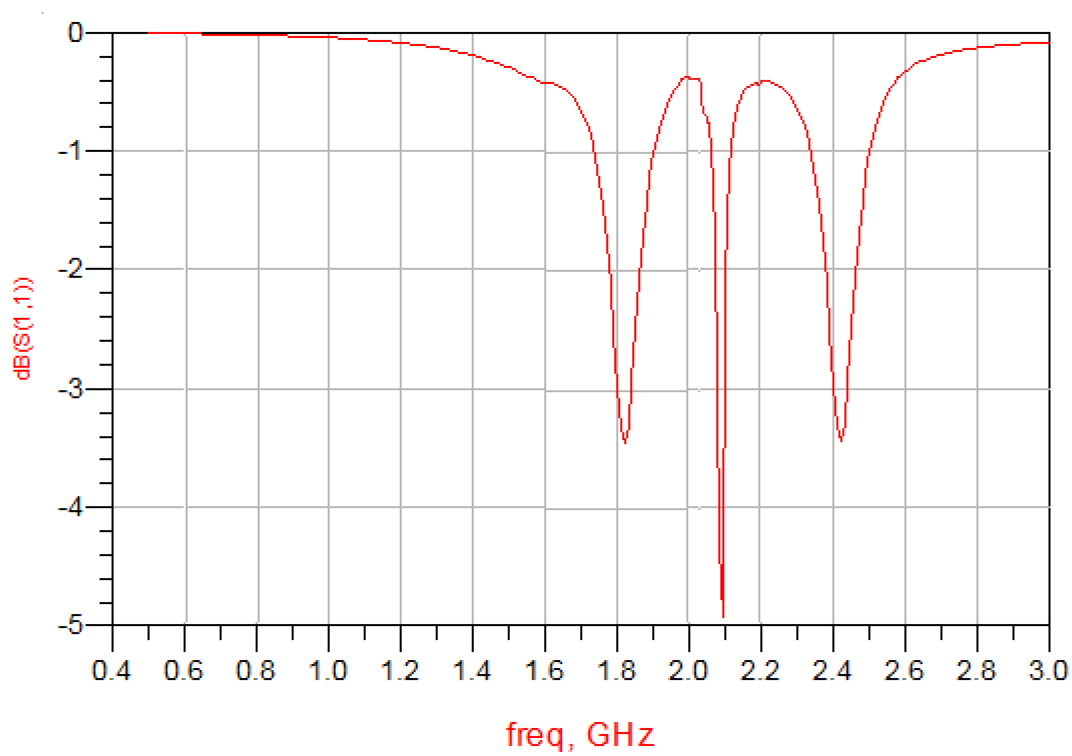

Figure 4.16 Simulated reflection coefficient with respect to frequency

The rectenna radiates best at 1.8 Ghz , 2.1 Ghz and 2.4 Ghz where $S_{11} = -3.5\ db\ and -5\ db$ at other frequencies the rectenna will radiate virtually nothing as S_{11} is close to 0 db so all the power is reflected .

The maximum of 3.51V output voltage is achieved at 10 dbm input power for 430 Ω load value.

The efficiency is calculated from the obtained output voltage using the following equation:

$$\eta(\%) = \frac{V^2{}_{out}}{R_L * P_{in}} \times 100 \qquad \textbf{(4.7)}$$

Where P_{in} is the applied RF signal in mW , V_{out} is the obtained output DC voltage and R_L is the load value .

The maximum efficiency of 70% is achieved at the operating frequencies 1.8 Ghz , 2.1Ghz and 2.4 Ghz for -10 dbm input power .Despite its interesting features, the

Greinacher has twice as many diodes as a voltage doubler and four times more than a series rectifier. The incident power required to exceed the diode thresholds of a Greinacher rectifier is therefore higher than that required for other rectifiers.

Thus, in order to avoid interference between the RF branches, the rectifier must have a differential output. Also, the number of diodes used must be limited so that the rectenna can operate in an environment in which the RF power density is low.

4.4. Realization of a Second Multiband Prototype and Experimental Results

The goal now is to find the optimum rectifier for the selected rectenna architecture.

4.4.1. Improvement of the rectifier stage

4.4.1.1. Presentation of the proposed rectifier

As explained in section 2.2, the rectifier must have a limited number of diodes. The series and doubler rectifiers could therefore be suitable but they have no differential output. However, by removing the ground connection of the doubler, this rectifier has a differential output. The modified voltage doubler is shown in Figure 4.17.

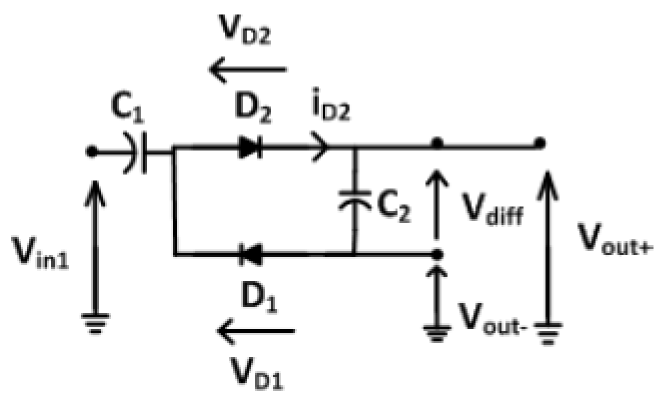

Figure 4.17 Proposed Rectifier Architecture.

The two diodes D_1 and D_2 are connected in parallel, which makes it possible to start the circuit from a single diode threshold. During the negative half-period of Vin1, only the diode D_1 is active. Capacitor C_1 is loaded throughD_1. Similarly, during the positive half ofV_{in1}, D_2 is in turn active and D_1 is blocked. Thus, the capacitor C_2 is charged through D_2 with the charges from V_{in1} and those stored inC_1. Thus, the output voltage V_{diff} is twiceV_{in1}. Given the threshold voltages of the diodes, V_{TH1} andV_{TH2}, V_{diff} is equal to:

$$V_{diff} = V_{out+} - V_{out-} = 2V_{in1} - V_{TH1} - V_{TH2} \quad \textbf{(4.8)}$$

4.4.1.2. Improvement of the obtained DC summation: mathematical formalization

The architecture of the rectenna is shown in Figure 4.18 with i RF branches, each having the rectifier shown above.

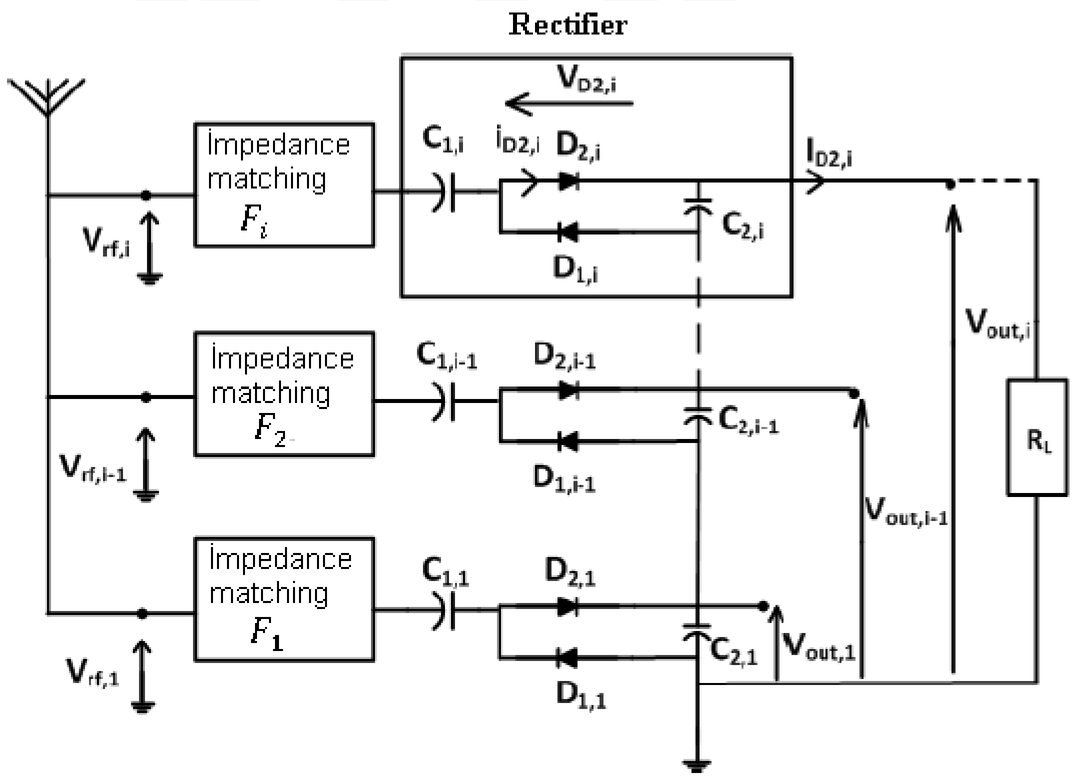

Figure 4.18 Rectenna architecture designed with the proposed rectifier.

The first branch RF is referenced to the ground and the i^{th} branch RF to the $(i-1)^{th}$ branch RF. The load, RL, is connected between the i^{th} RF branch and the circuit ground. In the rest of this section, we will show that the voltage across the load, V_{out}, is the sum of the input voltages, $V_{rf,i}$.

$$v_{D2,i} = -\frac{1}{2}(V_{out,i} - V_{out,i-1}) - R_s I_{D2,i} + |A_{rf,i}| cos\ (\omega t), \tag{4.9}$$

Where R_s is the internal series resistance to the diode, $I_{D2,i}$, i is the dc current at the output of the circuit.

The current in the Schottky diode $D_{2,i}$ polarized is equal to:

$$i_{D2,i} = I_s\, exp\ (\frac{v_{D2,i}}{nV_T}) \tag{4.10}$$

Where V_T is the thermodynamic voltage, I_S is the saturation current of the diode and n the factor of ideality.

From Bessel's function,

$$exp(xcos\ (\omega t)) = B_0 + 2 \sum_{k=1}^{k=m} B_k(x) cos\ (k\omega t) \tag{4.11}$$

The current $i_{D2,i}$, can be expressed by:

$$i_{D2,i} = I_s\, [B_0(\frac{|A_{rf,i}|}{nV_T}) + 2 \sum_{k=1}^{k=m} B_k(\frac{|A_{rf,i}|}{nV_T}) cos\ (k\omega t)\ ] exp\ (y) \tag{4.12}$$

With B_0 and y defined as below:

$$B_0(x) = \frac{exp(x)}{\sqrt{2\pi x}} \tag{4.13}$$

$$y = \frac{-\frac{1}{2}(V_{out,i} - V_{out,i-1}) - R_s I_{D2,i}}{nV_T} \tag{4.14}$$

Then, the DC current of $i_{D2,i}$ can be extracted:

$$i_{D2,i} \approx I_s\,[exp[\frac{-\frac{1}{2}(V_{out,i} - V_{out,i-1}) - R_S I_{D2,i}}{nV_T}]\,\frac{exp[\frac{|A_{rf,i}|}{nV_T}]}{\sqrt{2\pi\frac{|A_{rf,i}|}{nV_T}}}.] \qquad \textbf{(4.15)}$$

From equation (4.9), we can deduce:

$$ln\,(\frac{I_{D2,i}}{I_S}) = -\frac{1}{2nV_T}\,(V_{out,i} - V_{out,i-1}) - \frac{R_S I_{D2}}{nV_T} + \frac{|A_{rf,i}|}{nV_T} - \frac{1}{2}\,ln\,(\frac{2\pi|A_{rf,i}|}{nV_T}) \qquad \textbf{(4.16)}$$

$$(\frac{1}{2} + \frac{R_S}{R_L})V_{out,i} + nV_T\,ln\,(\frac{V_{out,i}}{R_S I_S}) = \frac{1}{2}V_{out,i-1} + |A_{rf,i}| - \frac{nV_T}{2}\,ln\,(\frac{2\pi|A_{rf,i}|}{nV_T}) \qquad \textbf{(4.17)}$$

The characteristics of the chosen Schottky diode make it possible to simplify the equation (4.11). Recall that the Metelics MSS20-141 diode was chosen according to its interesting characteristics (threshold voltage, V_{TH}= 150 mV and junction capacitance C_j= 0.08 pF). The saturation current of the diode, I_S, is 3.5 µA and its internal resistance, R_S, is 20 Ω. The ideality factor, n, typically varies from 1 to 2 depending on the manufacturing process. This factor accounts for the recombination of the charge carriers as they pass through the depletion region. For the Metelics diode, in the depletion region, n is equal to 1. If the diode is biased close to its threshold voltage, then n is 1.3 (Klyukanov ect , 2013).

Under these conditions, assuming that R_L= 11 kΩ, (R_S / R_L) is equal to 1.8 10e-3, which makes (R_S / R_L) negligible in relation to ½. Moreover, $nV_T ln$ ($V_{out,i}$ / (R_S / R_L)) is always negligible compared to $V_{out,i}$ / 2. So equation (3.11) can be simplified as below:

$$\frac{1}{2}V_{out,i} = \frac{1}{2}V_{out,i-1} + |A_{rf,i}| - \frac{nV_T}{2}\,ln\,(\frac{2\pi|A_{rf,i}|}{nV_T}) \qquad \textbf{(4.18)}$$

If the operation is repeated, $V_{out,i}$ can be expressed as a function of the incident RF signals, $|A_{rfj}|$:

$$V_{out,i} = \frac{1}{2}\sum_{j=1}^{j=i}\ (|A_{rf,i}| - \frac{nV_T}{2}\,ln\,(\frac{2\pi|A_{rf,i}|}{nV_T})\,) \qquad \textbf{(4.19)}$$

$V_{out,i}$ is the sum of all input contributions $|A_{rf,i}|$, and $V_{term,i}$ defined by:

$$V_{term,i} = -\frac{nV_T}{2} ln\ (2\pi \frac{|A_{rf,j}|}{nV_T}) \quad \textbf{(4.20)}$$

For high values of $V_{rf,j}$, for example 1 V, n is equal to 1 and $V_{term,i}$ is equal to 0.07 V, therefore negligible in front of $|A_{rf,i}|$. Under these conditions, for values of $|A_{rf,i}|$below 0.2 V, $V_{out,i}$ is expressed as (4.13) and for values above 0.2 V as:

$$V_{out,i} = 2\sum_{j=1}^{j=i} |A_{rf,j}|. \quad \textbf{(4.21)}$$

Thus, $V_{out,i}$ is not disturbed by interference dc between the different branches RF active ($|A_{rf,j}|| \neq 0$) or not ($|A_{rf,j}|= 0$).

From (4.15), it is possible to express $V_{out,i}$ according to $V_{out,i-1}1$ as shown by the two following equations:

$$V_{out,i} = 2\sum_{j=1}^{j=i-1} |A_{rf,j}| + 2|A_{rf,i}|. \quad \textbf{(4.22)}$$

$$V_{out,i}=V_{out,i-1} + 2|A_{rf,i}|. \quad \textbf{(4.23)}$$

Thus, $V_{out,i}$ is the sum of the output voltage $V_{out,i-1}$ and the amplitude of its input voltage $|A_{rf,i}|$. In the particular case where the amplitudes $|A_{rf,j}|$are identical for each of the RF branches, it is possible to deduce that:

$$V_{out,i} = iV_{out,1} \quad \textbf{(4.24)}$$

4.4.1.3. Justification of the mathematical model: Suitability with electric simulations

This rectenna was simulated under ADS. In the simulations, the receiving antenna is modeled by an RF power generator with four frequencies set at 0.9 GHz, 1.8 GHz, 2.1 GHz and 2.45 GHz and an output impedance of 50 Ω. The low-pass filter is a simple 68 pF capacitor. The sensor we wish to self-power is an electronic thermometer with an equivalent impedance of 11 kΩ (supply voltage: 1.5 V). The four networks of impedance adaptations have been designed to transfer the maximum power for this load.

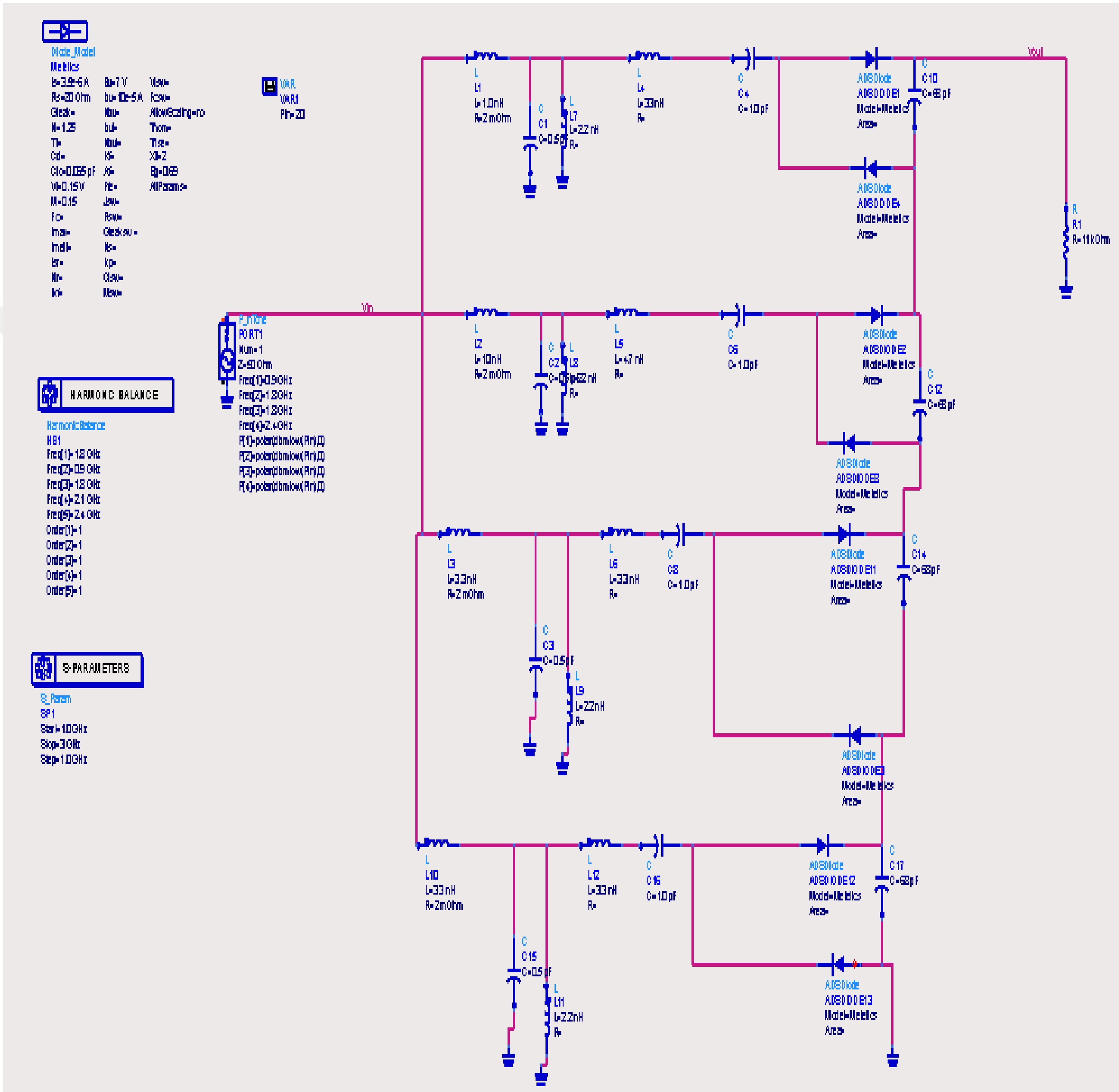

Figure 4.19 Rectenna diagram with proposed Rectifiers with ADS.

The output voltages of $V_{out,i}$, for i = 1 to 4, were simulated as a function of the incident power for each of the four frequencies. In Figure 4.20, the simulation results show that the output voltage dc with the four active RF branches, $V_{out,4}$, is four times higher than the voltage obtained with only one active RF branch. There is little interference between the different outputs. The minimum input power to activate the rectenna is -20 dBm, which is in the power range available in urban environments.

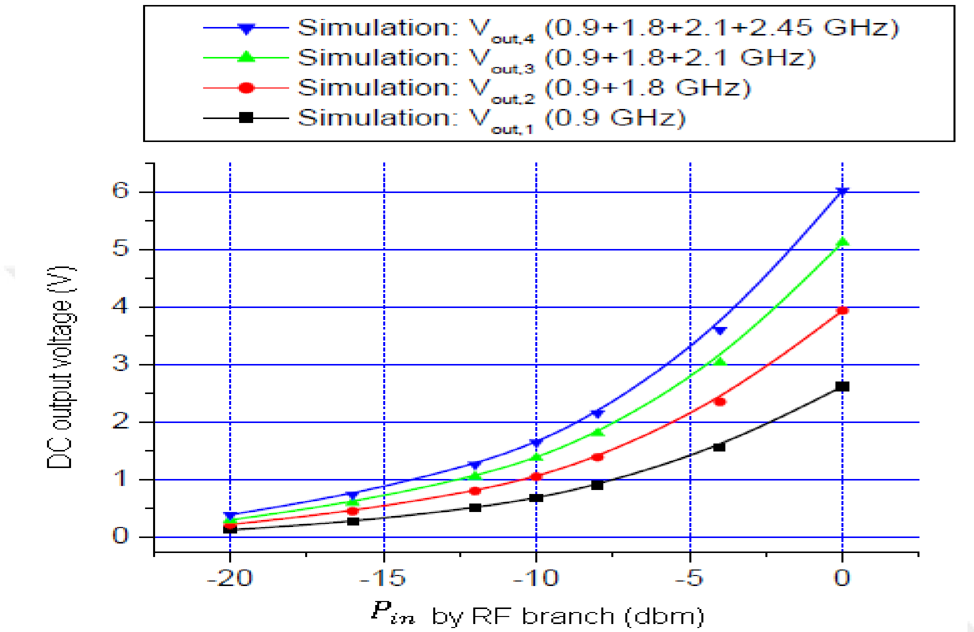

Figure 4.20 DC output voltage simulated as a function of forward power for 1, 2, 3 or 4 branches RF activated.

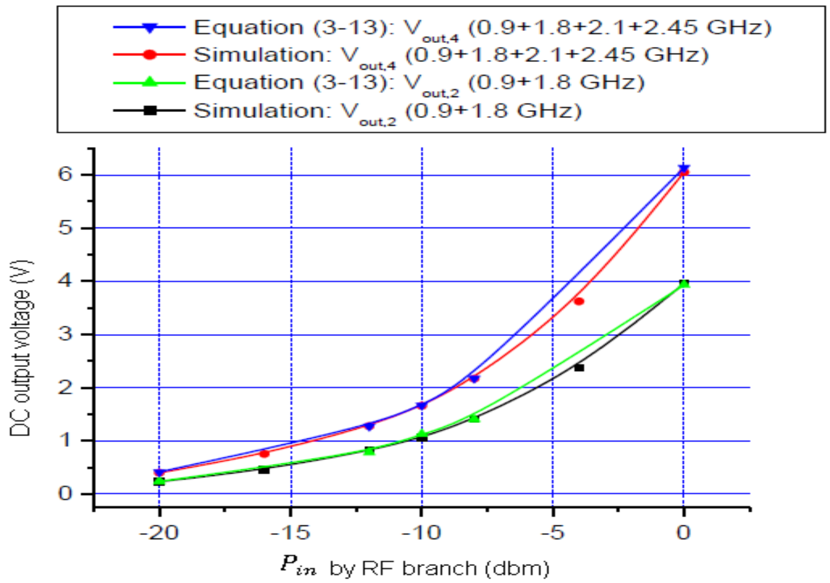

Figure 4.21 Simulated output voltage versus incident power for each frequency compared to the voltage calculated from the mathematical model (4.13) for RL = 11 kΩ.

4.5. Conclusion

In this part, two multiband rectennas have been designed. The first developed rectenna has been optimized to cover three RF bands: GSM1800, UMTS and Wi-Fi. The prototype manufactured has a constant efficiency of 15% on the three RF bands for an input power of -20 dBm for each of the three RF sources. This efficiency reaches 25% in the presence of three RF sources for a total incident power of -20 dBm. The results of the simulation confirm the feasibility of supplying small sensors with RF wave energy. The study on the summation of the different contributions dc of each RF branch of the rectenna has made it possible to design a second multiband rectenna architecture. The rectenna designed this time covers four frequency bands: the GSM900, the GSM1800, the UMTS and the Wi-Fi. Compared to the first conceived rectenna, one branch RF inactive or having an output voltage dc lower than the other branches do not affect the overall efficiency. Each RF branch is independent of each other.

It has been shown in this chapter that an electronic thermometer could be powered by RF waves in an outdoor environment.

5. CONCLUSION AND PRESPECTIVES

The work presented in this manuscript demonstrates the feasibility of converting the electromagnetic energy of Radio Frequency waves to power communicating objects present in any environment.

We first studied several energy sources and energy harvesting techniques for the energy autonomy of sensors. The techniques of energy harvesting from mechanical vibration (piezoelectric, magnetic and electrostatic), thermal, chemical and radiation energy (light waves and Radio Frequencies) vibrations have been analyzed. From this study, we drew up a summary summarizing the advantages and disadvantages of each. With a power density of around 100 mW / m², the solar energy source appears to be the highest. However, RF wave energy is ubiquitous in our urban environment and the efficiency of associated energy conversion systems is greater than that achieved with photovoltaic energy collectors. For these reasons, we have concluded that the power source of Radio Frequency waves can be seen as a promising source for sensor supply.

Thus, the second chapter focused on the techniques of electromagnetic energy recovery of RF waves. As a result of the statistical study of the RF power density level we conducted, it was possible to identify the predominant frequency bands in an urban and rural environment. The GSM900 and GSM1800 are the two predominantly present frequency bands and the power density levels are relatively low. Placed from 50 to 250 meters from a GSM900 antenna, the measured RF power density varies between 1.2 mW / m² and 0.25 mW / m². The variation in the value of the power density also reflects a fluctuation in terms of incident power at the rectenna. Under these conditions, to maintain a constant DC supply voltage for the sensor, it may be necessary to add a dc-dc converter and an energy storage cell to the output of the rectenna.

We then discussed the key points of designing a rectenna. The architectures of the constituent blocks of the rectenna have been analyzed in detail. A judicious choice for the impedance matching network or the rectifier is essential for the correct operation of the harvester in its environment. According to this study, energy harvesting over several frequency bands for sensor power supply has proven to be an interesting solution. In an environment for which RF sources are not controlled, having the ability to harvest energy over a wide band allows more flexibility to harvest energy from the frequency bands present.

The objective of Chapter 3 has been to propose innovative solutions that overcome technological barriers and thus harvest the maximum RF energy present and for low levels of RF power density, of the order of 1 mW / m². Two multiband rectennas have been designed. The first developed rectenna has been optimized to cover three RF bands: GSM1800, UMTS and Wi-Fi. The prototype manufactured has a constant efficiency of 15% on the three RF bands for an input power of -20 dBm for each of the three RF sources. This efficiency reaches 25% in the presence of three RF sources for a total incident power of -20 dBm. Simulation results confirm the feasibility of powering small sensors with RF wave energy.

Then, a study on the summation of the different contributions dc of each RF branch of the rectenna made it possible to design a second multiband rectenna architecture. The rectenna designed this time covers four frequency bands: the GSM900, the GSM1800, the UMTS and the Wi-Fi. Compared to the first conceived rectenna, one branch RF inactive or having an output voltage dc lower than the other branches do not affect the overall efficiency. The simulation results showed the interest of this solution.

Beyond the axes of incremental improvements, more ambitious development prospects can be envisaged such as the realization of a multi-energy harvesting system. There is no single solution that can adapt to all environments, but as many solutions as different environments. As we mentioned in the first chapter, energy can come from a wide variety of sources. In view of their low level of power density, these sources are often too weak to meet current needs but they may be complementary hence the importance of evaluating the interest of soliciting several for the same application. In addition, the implementation of harvested energy management would increase the efficiency of the system by optimizing consumption profiles and achieving better time management according to the production and consumption of energy.

REFERENCES

Agrawal, S. K. Pandey, J. Singh, and M. S. Parihar, « Realization of efficient RF energy harvesting circuits employing different matching technique », in 2014 15th International Symposium on Quality Electronic Design (ISQED), 2014, p. 754-761.

Analog device, « AD7814 | datasheet and product info Temperature Sensor: 10-Bit Digital in 6-Lead SOT-23 | Analog Devices ». http://www.analog.com/en/products/analog-to-digital-converters/integrated-specialpurpose-converters/integrated-temperature sensors/ad7814.html#product-overview.

Ancey, « Ambient functionality in MIMOSA from technology to services », in Proceedings of the 2005 joint conference on Smart objects and ambient intelligence: innovative context-aware services: usages and technologies, 2005, p. 35–38

Basset, D. Galayko, A. M. Paracha, F. Marty, A. Dudka, et T. Bourouina, « A batch-fabricated and electret-free silicon electrostatic vibration energy harvester », J. Micromechanics Microengineering, vol. 19, no 11, p. 115025, 2009.

Bates, N. J. Dudney, B. Neudecker, A. Ueda, and C. D. Evans, « Thin-film lithium and lithium-ion batteries », *Solid State Ion.*, vol. 135, no 1, p. 33–45, 2000. Sanyo, « Sanyo », *http://panasonic.net/sanyo/*, 2012. .

Beeby, M. J. Tudor, E. Koukharenko, N. M. White, T. O'Donnell, C. Saha, S. Kulkarni, and S. Roy, « Design and performance of a microelectromagnetic vibration powered generator », in Solid-State Sensors, Actuators and Microsystems, 2005. Digest of Technical Papers. TRANSDUCERS'05. The 13th International Conference on, 2005, vol. 1, p. 780–783.

Beeby, R. N. Torah, M. J. Tudor, P. Glynne-Jones, T. O'Donnell, C. R. Saha, and S. Roy, « A micro electromagnetic generator for vibration energy harvesting », J. Micromechanics Microengineering, vol. 17, no 7, p. 1257, 2007.

Bergqvist, G. Friedrich, Y. Hamnerius, L. Martens, G. Neubauer, G. Thuroczy, E. Vogel, and J. Wiart, « Mobile telecommunication base stations– exposure to electromagnetic fields », Rep. Short Term Mission COST 244bis, 2001.

Boret, « Monolithic integrated circuits in coplanar technology for reception applications up to 110 GHz », Lille, Lille, 1999.

Breed, « Improving the bandwidth of simple matching networks », *High Freq.Electron*, vol. 7, no 56-60, 2008.

Brown, R. George, N. . Heenan, and R. . Wonson, « Microwave to DC converter », U.S patent 3 434 678, 25-mars-1969.

Brunelli, C. Moser, L. Thiele, and L. Benini, « Design of a Solar-Harvesting Circuit for Batteryless Embedded Systems », IEEE Trans. Circuits Syst. Regul. Pap., vol. 56, no 11, p. 2519 -2528, nov. 2009.

Burch, M. Clark, M. G. Yost, C. T. E. Fitzpatrick, A. M. Bachand, J. Ramaprasad, and J. S. Reif, « Radio frequency nonionizing radiation in a community exposed to radio and television broadcasting », Environ. Health Perspect., vol. 114, n o 2, p. 248-253, febr. 2006.

Camara, « Modeling the storage of photovoltaic energy by supercapacitors », phdthesis, University Paris-Est, 2011. ANFR, « Modeling radio sites and safety perimeters for the public» *http://www.anfr.fr/fileadmin/mediatheque/documents/expace/Guide%20DR17-3.pdf*,18-febr 2009. Supercapacitor, « Supercapacitor Information – Battery

Cartoradio, « ANFR - Cartoradio ». Available in:http://www.cartoradio.fr/cartoradio/web/.C. Haslett, *Essentials of radio wave* *propagation*. Cambridge University Press,2008. H. Kim, R. F. Yazicioglu, S. Kim, N. Van Helleputte, A. Artes, M. Konijnenburg, J. Huisken, J. Penders, and C. Van Hoof, « A configurable and lowpower mixed signal SoC for

Celeste, P. Jeanty, and G. Pignolet, « Case study in Reunion Island », Acta Astronaut., vol. 54, no 4, p. 253.258, févr. 2004.

Chan, P. Paddan, and A. J. Burdett, « A 1V, micropower system-on-chip for vitalsign monitoring in wireless body sensor networks », in *Solid-State Circuits Conference, 2008. ISSCC 2008. Digest of Technical Papers. IEEE International*, 2008, p. 138–602.

Chen, M.-H. Chang, W.-C. Hsieh, andt W. Hwang, « Fully on-chip temperature, process, and voltage sensors », in *Circuits and Systems (ISCAS), Proceedings of 2010 IEEE International Symposium on*, 2010, p. 897–900. Batteryuniversity,*http://batteryuniversity.com/learn/article/is_lithium_ion_the_ideal_battery*, 2010. .

Collado and A. Georgiadis, « Conformal Hybrid Solar and electromagnetic (EM) Energy harvesting rectenna », *IEEE Trans. Circuits Syst. Regul. Pap.*, vol. 60, no 8,p. 10, 2013.

Collado et A. Georgiadis, « Conformal Hybrid Solar and electromagnetic (EM) Energy harvesting rectenna », *IEEE Trans. Circuits Syst. Regul. Pap.*, vol. 60, no 8,p. 10, 2013.

Cook-Chennault, N. Thambi, and A. M. Sastry, « Powering MEMS portable devices—a review of non-regenerative and regenerative power supply systems with special emphasis on piezoelectric energy harvesting systems », Smart Mater. Struct., vol. 17, no 4, p. 043001, août 2008.

Dashevsky, D. Kaftori, and D. Rabinovich, « High efficiency thermoelectric unit within an autonomous solar energy converter », in XVII International Conference on Thermoelectrics, 1998. Proceedings ICT 98, 1998, p. 531.534.

Defosseux, M. Allain, P. Ivaldi, E. Defay, and S. Basrour, « Highly efficient piezoelectric micro harvester for low level of acceleration fabricated with a CMOS compatible process », in Solid-State Sensors, Actuators and Microsystems Conference (TRANSDUCERS), 2011 16th International, 2011, p. 1859 -1862.

Despesse, J. J. Chaillout, T. Jager, F. Cardot, et A. Hoogerwerf, « Innovative Structure for Mechanical Energy Scavenging », in Solid-State Sensors, Actuators and Microsystems Conference, 2007. TRANSDUCERS 2007. International, 2007, p. 895 -898. Citizen, « Eco-Drive: How It Works | Citizen Watch ».

Dieuleveult and O. Romain, *Electronics applied to high frequencies, Dunod, the new factory*. Dunod, l'usine nouvelle, 2008.

Du, H. Li, and T. Gu, « A state of the art review on microbial fuel cells: A promising technology for wastewater treatment and bioenergy », Biotechnol. Adv., vol. 25, no 5, p. 464-482, sept. 2007.

Microelectronic,«EM6607»,http://www.emmicroelectronic.com/products/microcontrollers/multi-io/em6607.International Commission on Non-Ionizing Radiation Protection, « Guidelines for limiting exposure to time-varying electric, magnetic, and electromagnetic fields », Health Phys., vol. 74, no 4, p. 494-522, 1998.

Enz, A. El-Hoiydi, J.-D. Decotignie, A.-S. Porret, T. Melly, et V. Peiris, « WiseNET — An Ultralow-Power Solution for Wireless Sensor Networks », in Analog Circuit Design, J. H. Huijsing, M. Steyaert, et A. van Roermund, Éd. Springer US, 2004, p. 91.122.

Erickson and D. Maksimovic, *Fundamentals of power electronics*, 2nd ed.:Kluwer Academic. Norwell, 2001.ARCEP, « http://www.arcep.fr/>>.

Finkenzeller, RFID Handbook: Fundamentals and Applications in Contactless Smart Cards, Radio Frequency Identification and Near-Field Communication, Third Edition. John Wiley & Sons, 2010.

Fong, and H. C. Luong, « RF energy harvesting circuit with on-chip antenna for biomedical applications », in 2010 Third International Conference on Communications and Electronics (ICCE), 2010, p. 115 -117.

Frei, E. Mohler, G. Neubauer, G. Theis, A. Bürgi, J. Fröhlich, C. Braun- Fahrländer, J. Bolte, M. Egger, and M. Röösli, « Temporal and spatial variability of personal exposure to radio frequency electromagnetic fields », *Environ. Res.*, vol. 109, no 6, p. 779-785, August2009.

Freitas, J.-D. Arnould, and P. Ferrari, « General Expression for Tunable Matching Network Efficiency in the case of complex impedances », in *Microwave Optoelectronics Conference (IMOC), 2013 SBMO/IEEE MTT-S International*, 2013, p. 1-5.

Garrec, I. Roch-Jeune, M. Himdi, R. Sauleau, O. Millet, and L. Buchaillot,« Antenne MEMS à diversité de polarisation », in *Quatorzièmes Journées Nationales Micro-ondes*, Nantes, France, 2005, p. 4 pages.Skyworks,«SMS7630Series»,*http://www.skyworksinc.com/Product/511/SMS7630_Series*. .

Georgiadis, G. Andia, et A. Collado, « Rectenna Design and Optimization Using Reciprocity Theory and Harmonic Balance Analysis for Electromagnetic (EM) Energy Harvesting », *IEEE Antennas Wirel. Propag. Lett.*, vol. 9, p. 444 -446, 2010.

Glynne-Jones, M. J. Tudor, S. P. Beeby, and N. M. White, « An electromagnetic, vibration-powered generator for intelligent sensor systems », Sens. Actuators Phys., vol. 110, n o 1, p. 344–349, 2004.

Guyomar and M. Lallart, « Recent Progress in Piezoelectric Conversion and Energy Harvesting Using Nonlinear Electronic Interfaces and Issues in Small Scale Implementation », Micromachines, vol. 2, no 2, p. 274-294, June 2011.

H. Huang, Y.-T. Ma, et W.-C. Liao, « Design of a Low-Voltage Low- Dropout Regulator », *IEEE Trans. Very Large Scale Integr. VLSI Syst.*, vol. 22, no 6, p. 1308-1313, june 2014.

Han, A. von Jouanne, T. Le, K. Mayaram, and T. S. Fiez, « Novel power conditioning circuits for piezoelectric micropower generators », in *Nineteenth Annual IEEE Applied Power Electronics Conference and Exposition, 2004. APEC '04*, 2004, vol. 3, p. 1541 - 1546 Vol.3.

Harb, « Energy harvesting: State-of-the-art », Renew. Energy, vol. 36, no 10, p. 2641–2654,2011.

Heikkinen and M. Kivikoski, « A novel dual-frequency circularly polarized rectenna», *IEEE Antennas Wirel. Propag. Lett.*, vol. 2, no 1, p. 330-333, 2003.

Hoarau, N. Corrao, J.-D. Arnould, P. Ferrari, and P. Xavier, « Complete Design and Measurement Methodology for a Tunable RF Impedance-Matching Network », *IEEE Trans. Microw. Theory Tech.*, vol. 56, no 11, p. 2620-2627, nov.2008.

Huang, B. Zhang, X. Chen, K.-M. Huang, and C.-J. Liu, « Study on an SBandRectenna Array for Wireless Microwave Power Transmission », *Prog. Electromagn. Res.*, vol. 135, p. 747–758, 2013.

Kanno, K. Morimoto, R. Yokokawa, K. Wasa, H. Kotera, N. Yamauchi, J. Ogawa, T. Matsushima, and K. Aizawa, « High efficiency energy harvester of transferred epitaxial PZT films on stainless steel sheets », in 2010 IEEE 23rd International Conference on Micro Electro Mechanical Systems (MEMS), 2010, p. 152 -155.

Kansal, J. Hsu, S. Zahedi, et M. B. Srivastava, « power Management in Energy Harvesting Sensor Networks », ACM Transactions on Embedded Computing Systems (TECS), vol. 6, no 32, p. 38, sept-2007.

Kawahara, K. Tsukada, and T. Asami, « Feasibility and potential application of power scavenging from environmental RF signals », in *Antennas andPropagation Society International Symposium, 2009. APSURSI'09. IEEE*, 2009, p. 1–4.

Keyrouz, H. J. Visser, and A. G. Tijhuis, « Multi-band simultaneous radio frequency energy harvesting », in *Antennas and Propagation (EuCAP), 2013 7th European Conference on*, 2013, p. 3058–3061.

Kishi, H. Nemoto, T. Hamao, M. Yamamoto, S. Sudou, M. Mandai, and S. Yamamoto, « Micro thermoelectric modules and their application to wristwatches as an energy source », in Eighteenth International Conference on Thermoelectrics, 1999, 1999, p. 301 -307.

Kuhn, F. Seguin, C. Lahuec, and C. Person, « A multi-tone RF energy harvester in body sensor area network context », in *Antennas & Propagation Conference, 2009. LAPC 2009. Loughborough*, Loughborough, 2013, p. 238-241.

Kulkarni, E. Koukharenko, J. Tudor, S. Beeby, T. O'Donnell, and S. Roy, « Fabrication and Test of Integrated Micro-Scale Vibration Based Electromagnetic Generator », in Solid-State Sensors, Actuators and Microsystems Conference, 2007. TRANSDUCERS 2007. International, 2007, p. 879 -882.

Kwon and G. A. Rincon-Mora, « A single-inductor ac-dc piezoelectric energy harvester/battery-charger IC converting$\pm$(0.35 to 1.2 V) to (2.7 to 4.5 V) », in

Solid-State Circuits Conference Digest of Technical Papers (ISSCC), 2010 IEEE International, 2010, p. 494–495.

Kymissis, C. Kendall, J. Paradiso, and N. Gershenfeld, « Parasitic power harvesting in shoes », in Second International Symposium on Wearable Computers, 1998. Digest of Papers, 1998, p. 132 -139.

L. Bullard, H. B. Sierra-Alcazar, H. L. Lee, and J. L. Morris, « Operating principles of the ultracapacitor », *IEEE Trans. Magn.*, vol. 25, no 1, p. 102 -106,jan. 1989.

Le, J. Han, A. von Jouanne, K. Mayaram, et T. S. Fiez, « Piezoelectric micro-power generation interface circuits », IEEE J. Solid-State Circuits, vol. 41, no 6, p. 1411 - 1420, juin 2006.

Leonov and R. J. M. Vullers, « Wearable Thermoelectric Generators for BodyPowered Devices », J. Electron. Mater., vol. 38, no 7, p. 1491.1498, janv. 2009.

Li, G. Dejean, J. Laskar, and M. M. Tentzeris, « Investigation of circularly polarized loop antennas with a parasitic element for bandwidth enhancement »,*IEEE Trans. Antennas Propag.*, vol. 53, no 12, p. 3930-3939, dec. 2005.

Li, S. . Block, D. . Duarte, et L. Changzhi, « A 0.45-V MOSFETs-Based Temperature Sensor Front-End in 90 nm CMOS With a Noncalibrated Relative Inaccuracy From to 105 », *IEEE Trans. Circuits Syst. II Express Briefs*, vol. 60, no 11, p. 771-775, nov. 2013.

Lossec, B. Multon, H. Ben Ahmed, and C. Goupil, « Thermoelectric generator placed on the human body: system modeling and energy conversion improvements », Eur. Phys. J. Appl. Phys., vol. 52, no 1, p. 11103, sept. 2010

Marc Belleville (CEA-LETI, France), « Energy Autonomous Systems: Future Trends in Devices, Technology, and Systems », 2009.

Masotti, A. Costanzo, M. Del Prete, and V. Rizzoli, « Genetic-based design of a tetra-band high-efficiency radio-frequency energy harvesting system », *IET Microw. Antennas Propag.*, vol. 7, no 15, p. 1254-1263, déc. 2013.

Mateu, C. Codrea, N. Lucas, M. Pollak, and P. Spies, « Energy harvesting for wireless communication systems using thermogenerators », in Proceeding of the XXI Conference on Design of Circuits and Integrated Systems (DCIS), Barcelona, Spain, 2006.

Matsumoto, « Research on solar power satellites and microwave power transmission in Japan », IEEE Microw. Mag., vol. 3, no 4, p. 36-45, déc. 2002.

Merabet, F. Costa, H. Takhedmit, C. Vollaire, B. Allard, L. Cirio, and O. Picon, « A 2.45-GHz localized elements rectenna », in *2009 3rd IEEE International Symposium on Microwave, Antenna, Propagation and EMC Technologies for Wireless Communications*, 2009, p. 419 -422.

Merabet, L. Cirio, H. Takhedmit, F. Costa, C. Vollaire, B. Allard, and O. Picon, « Low-cost converter for harvesting of microwave electromagnetic energy », in *IEEE*

Energy Conversion Congress and Exposition, 2009. ECCE 2009, 2009, p. 2592 -2599.

Micropelt, « Micropelt », http://micropelt.com.

Mikeka, H. Arai, A. Georgiadis, and A. Collado, « DTV band micropower RF energy-harvesting circuit architecture and performance analysis », in *RFIDTechnologies and Applications (RFID-TA), 2011 IEEE International Conference on*, 2011, p. 561–567.

Mitcheson, T. C. Green, E. M. Yeatman, and A. S. Holmes, « Architectures for Vibration-Driven Micropower Generators », J. Microelectromechanical Syst., vol. 13, no 3, p. 429-440, juin 2004.

Miura, N. Shinohara, and H. Matsumoto, « Experimental study of rectenna connection for microwave power transmission », *Electron. Commun. Jpn. Part II Electron.*, vol. 84, no 2, p. 27-36, febr. 2001.

Nanver, « Design of an RF power harvester in a silicon-on-glass technology », *http://www.stw.nl/NR/rdonlyres/375B1E7C-F624-43E5-B946 5DF4C3F434FF/0/yan.pdf*, 17-2008.

Nimo, D. Grgic, and L. M. Reindl, « Impedance optimization of wireless electromagnetic energy harvester for maximum output efficiency at µW input power », 2012, p. 83410W-83410W-14.

Nintanavongsa, U. Muncuk, D. R. Lewis, and K. R. Chowdhury, « Design Optimization and Implementation for RF Energy Harvesting Circuits », IEEE J. Emerg. Sel. Top. Circuits Syst., vol. 2, no 1, p. 24-33, mars 2012.

Niotaki, S. Kim, S. Jeong, A. Collado, A. Georgiadis, and M. M. Tentzeris, « A compact Dual-band rectenna using solt-loaded dual band folded dipole antenna », *IEEE Antennas Wirel. Propag. Lett.*, vol. 12, p. 4, 2013.

U. Olgun, C.-C. Chen, and J. L. Volakis, « Design of an efficient ambient WiFi energy harvesting system », *IET Microwaves,2010.*

Nodilo, « RFID Tags: A Step Forward To Changing How We Do Things », InTechWeb Blog.

NXP, « SL3ICS1002/1202 : NXP Semiconductors », 2013. [On line].Available in :http://www.nxp.com/products/identification_and_security/smart_label_and_tag_ics/ucode/series/SL3ICS1002_1202.html.

O'Mathuna, « Super-capacitor and Thin Film Battery Hybrid Energy Storage for Energy Harvesting Applications », *J. Phys. Conf. Ser.*, vol. 476, no 1, p. 012105, dec. 2013.

Paing, J. Shin, R. Zane, and Z. Popovic, « Resistor Emulation Approach to Low-Power RF Energy Harvesting », *IEEE Trans. Power Electron.*, vol. 23, no 3, p. 1494-1501, may 2008.Supercondensateur, « Big case on supercapacitors - Supercapacitor », 2014. [On line]. Available:http://www.supercondensateur.com/dossier-supercondensateurs.

Pavone, A. Buonanno, M. D'Urso, and F. G. Della Corte, « Design Considerations for Radio Frequency Energy Harvesting Devices », *Prog. Electromagn. Res. B*, vol. 45, p. 19–35, 2012.

Phongcharoenpanich, K. Boonying, and S. Kosulvit, « Dual-polarized flat rectenna for 2.45 GHz », in *2013 IEEE-APS Topical Conference on Antennas and Propagation in Wireless Communications (APWC)*, 2013, p. 1433-1436.

Pinuela, P. D. Mitcheson, and S. Lucyszyn, « Ambient RF Energy Harvesting in Urban and Semi-Urban Environments », *IEEE Trans. Microw. Theory Tech.*, vol. 61, no 7, p. 12, 28 2013.

Raghunathan et P. H. Chou, « Design and Power Management of Energy Harvesting Embedded Systems », in Proceedings of the 2006 International Symposium on Low Power Electronics and Design, 2006. ISLPED'06, 2006, p. 369 -374.

Roundy and P. K. Wright, « A piezoelectric vibration based generator for wireless electronics », Smart Mater. Struct., vol. 13, no 5, p. 1131.1142, oct. 2004.

Roundy, « Energy scavenging for wireless sensor nodes with a focus on vibration to electricity conversion », University of California, 2003.

Roundy, P. K. Wright, and K. S. . Pister, « Micro-electrostatic vibration-toelectricity converters », Fuel Cells Methanol, vol. 220, p. 22, 2002. Thermolife, « Thermo Life Energy Corp », http://www.poweredbythermolife.com/.

Roundy, P. K. Wright, et J. Rabaey, « A study of low level vibrations as a power source for wireless sensor nodes », Comput. Commun., vol. 26, no 11, p. 1131.1144, juill. 2003

Sample and J. R. Smith, « Experimental results with two wireless power transfer systems », in Radio and Wireless Symposium, 2009. RWS'09. IEEE, 2009, p. 16– 18.

Sari, T. Balkan, and H. Kulah, « A Wideband Electromagnetic Micro Power Generator for Wireless Microsystems », in Solid-State Sensors, Actuators and Microsystems Conference, 2007. TRANSDUCERS 2007. International, 2007, p. 275 -278.

Schreider, X. Begaud, M. Soiron, and B. Perpere, « Design of a broadband Archimedean spiral antenna above a thin modified Electromagnetic Band Gap substrate », in *First European Conference on Antennas and Propagation, 2006. EuCAP 2006*, 2006, p. 1-4.

Shameli, A. Safarian, A. Rofougaran, M. Rofougaran, and F. De Flaviis, « Power Harvester Design for Passive UHF RFID Tag Using a Voltage Boosting Technique », IEEE Trans. Microw. Theory Tech., vol. 55, no 6, p. 1089 -1097, juin 2007.

Shinohara and H. Matsumoto, « Experimental study of large rectenna array for microwave energy transmission », *IEEE Trans. Microw. Theory Tech.*, vol. 46, no 3, p. 261 268, mars 1998.

Shoaib, W. A. Shah, M. Amin, and N. Shoaib, « Dual Mode Helix Antenna for wideband terrestrial and GPS L2 communications », in *Proceedings of the 5th European Conference on Antennas and Propagation (EUCAP)*, 2011, p. 233-236.

Singh, X. Wang, R. Lafollette, and D. Reisner, « RF-recharged microbattery for powering miniature sensors », in Proceedings of IEEE Sensors, 2004, 2004, p. 349 - 352 vol.1.

Suh and K. Chang, « A high-efficiency dual-frequency rectenna for 2.45- and 5.8-GHz wireless power transmission », *IEEE Trans. Microw. Theory Tech.*, vol. 50, no 7, p. 1784 -1789, juill. 2002.

Sun, Y.-X. Guo, M. He, and Z. Zhong, « A Dual-Band Rectenna Using Broadband Yagi Antenna Array for Ambient RF Power Harvesting », *IEEE Antennas Wirel. Propag. Lett.*, vol. 12, p. 918-921, 2013.

Tentzeris and Y. Kawahara, « Novel Energy Harvesting Technologies for ICTApplications », in *International Symposium on Applications and the Internet, 2008. SAINT 2008*, 2008, p. 373-376.

Torah, P. Glynne-Jones, M. J. Tudor, and S. P. Beeby, « Energy aware wireless microsystem powered by vibration energy harvesting », PowerMEMS Freibg. Ger., p. 323–326, 2007.

Torfs, V. Leonov, K. FLEURY-FRENETTE, and R. J. M. Vullers, « Pulse Oximeter Fully Powered by Human Body Heat », Sens. Transducers J., vol. 80, no 6, p. 1230-1238, 2008.

Union of concerned scientists, « How Solar Energy Works | UCSUSA », Union of Concerned Scientists. [On line]: http://www.ucsusa.org/clean_energy/our-energy-choices/renewable-energy/howsolar-energy-works.html.

Van Bezooijen, M. A. de Jongh, F. van Straten, R. Mahmoudi, and A. H. M. van Roermund, « Adaptive Impedance-Matching Techniques for Controlling L Networks », *IEEE Trans. Circuits Syst. Regul. Pap.*, vol. 57, no 2, p. 495-505, feb. 2010.

Van Rethy, H. Danneels, V. De Smedt, W. Dehaene, and G. Gielen, « A lowpower and low-voltage BBPLL-based sensor interface in 130nm CMOS for wireless sensor networks », in *Proceedings of the Conference on Design, Automation and Test in Europe*, 2013, p. 1431–1435.

Van Sark, N. H. Reich, E. A. Alsema, M. P. Netten, M. Veefkind, S. Silvester, B. Elzen, and M. Verwaal, « A Solar Powered Wireless Computer Mouse: Design, Assembly and Preliminary Testing of 15 Prototypes », 2007.

Visser, A. C. F. Reniers, and J. A. C. Theeuwes, « Ambient RF Energy Scavenging: GSM and WLAN Power Density Measurements », in Microwave Conference, 2008. EuMC 2008. 38th European, 2008, p. 721 -724.

Visser, A. C. F. Reniers, and J. A. C. Theeuwes, « Ambient RF Energy Scavenging: GSM and WLAN Power Density Measurements », in *Microwave Conference, 2008. EuMC 2008. 38th European*, 2008, p. 721 -724.

Vullers, R. van Schaijk, I. Doms, C. Van Hoof, and R. Mertens, « Micropower energy harvesting », Solid-State Electron., vol. 53, no 7, p. 684-693, juill. 2009.

Waltisperger, C. Condemine, et S. Basrour, « Photovoltaic energy harvester for micro-scale applications », in NEWCAS Conference (NEWCAS), 2010 8th IEEE International, 2010, p. 177 -180.

Wang, N. Wang, A. Vinco, R. Siddique, M. Hayes, B. O'Flynn, et C. O'Mathuna, « Super-capacitor and Thin Film Battery Hybrid Energy Storage for Energy Harvesting Applications », J. Phys. Conf. Ser., vol. 476, no 1, p. 012105, déc. 2013.

Wanotayan and D. Torrungrueng, « Design of L-type impedance matching networks for lossless metamaterial transmission lines using Meta-Smith charts », in *2011 8th International Conference on Electrical Engineering/Electronics,Computer, Telecommunications and Information Technology (ECTI-CON)*, 2011, p.240-243.

Williams and R. B. Yates, « Analysis of a micro-electric generator for microsystems », in Proceedings of the Transducers, 1995, vol. 95, p. 369–372.

Win, X. Wu, S. Dasgupta, W. J. Wen, R. Kumar, and S. K. Panda, « Efficient solar energy harvester for wireless sensor nodes », in 2010 IEEE International Conference on Communication Systems (ICCS), 2010, p. 289 -294.

Yan, Joonsung Bae, S. Lee, T. Roh, K. Song, and H.-J. Yoo, « A 3.9 mW 25- Electrode Reconfigured Sensor for Wearable Cardiac Monitoring System », *IEEE J. Solid-State Circuits*, vol. 46, no 1, p. 353-364, janv. 2011.

Yang and H. Yin, « Energy Conversion Efficiency of a Novel Hybrid Solar System for Photovoltaic, Thermoelectric, and Heat Utilization », IEEE Trans. Energy Convers., vol. 26, no 2, p. 662.670, juin 2011.

Yang and K.-S. Yun, « Piezoelectric shell structures as wearable energy harvesters for effective power generation at low-frequency movement », Sens. Actuators Phys., vol. 188, p. 427-433, déc. 2012.

Yang, Y. Qin, C. Li, G. Zhu, and Z. L. Wang, « Converting Biomechanical Energy into Electricity by a Muscle-Movement-Driven Nanogenerator », Nano Lett., vol. 9, no 3, p. 1201.1205, mars 2009.

Yo, C.-M. Lee, C.-M. Hsu, and C.-H. Luo, « Compact Circularly Polarized Rectenna With Unbalanced Circular Slots », *IEEE Trans. Antennas Propag.*, vol.56, no 3, p. 882 -886, mars 2008.

Yoo, L. Yan, S. Lee, Y. Kim, and H.-J. Yoo, « A 5.2 mW Self-Configured Wearable Body Sensor Network Controller and a 12 W Wirelessly Powered Sensor for a Continuous Health Monitoring System », *IEEE J. Solid-State Circuits*, vol. 45, no 1, p. 178-188, jan. 2010.

Zuo, « Survivable RFID Systems: Issues, Challenges, and Techniques », IEEE Trans. Syst. Man Cybern. Part C Appl. Rev., vol. 40, no 4, p. 406-418, juill. 2010.

CURRICULUM VITAE